



TECHNISCHE  
UNIVERSITÄT  
WIEN  
Vienna University of Technology

## Diploma thesis

# Characterization and development of biocompatible and -degradable photopolymers for lithography- based additive manufacturing

completed to attain the academic degree of

## Diplom-Ingenieur

under the supervision of

**Univ.-Prof. Dr. mont. Jürgen Stampfl**

(E308 Institute of Materials Science and Technology, Functional non-metals)

**Dipl.-Ing. Christoph Hofstetter**

(E308 Institute of Materials Science and Technology, Functional non-metals)

submitted to TU Wien

**Faculty of Mechanical and Industrial Engineering**

by

**Adham Rizk, BSc**

[Redacted]

[Redacted]

[Redacted]

[Redacted]

Vienna, January 2019

Adham Rizk



TECHNISCHE  
UNIVERSITÄT  
WIEN  
Vienna University of Technology

I note that, at the time of printing, my study was entitled

## Diploma thesis

with the approval of the examining board.

I further declare that I have carried out my diploma thesis independently according to the accepted principles of scientific treatises and that I have explicitly referenced all aids and literature used.

Furthermore, I declare that the work presented here is completely original, has not been presented in Austria or abroad and is in accordance with the appraised work by the reviewer.

Vienna, January 2019

  
Adham Rizk

---

*“The role of the infinitely small in nature is infinitely great.”*

— Louis Pasteur

---

## Note of thanks

I would first like to thank my thesis advisor, Univ.-Prof. Dr. mont. Jürgen Stampfl of the Institute of Materials Science and Technology at Vienna University of Technology. He encouraged me to work in this interdisciplinary field and consistently supported me in making this work my own, while also steering and guiding me in the right direction when needed.

I would also like to thank my second thesis advisor, Dipl.-Ing. Christoph Hofstetter, for his constructive support throughout. The door to Hofstetter's office was always open whenever an obstacle arose or I had a question about my research.

I would also like to thank the experts who were involved in the validation review for this research project: Edith Asiemo, Stefan Zellhofer, and Dipl.-Ing. Dr. techn. Thomas Koch. Without their dedicated participation and fruitful input, the validation review could not have been successfully conducted.

I would also like to acknowledge the second reader of this thesis, Univ.-Prof. Dipl.-Ing. Dr. techn. Robert Liska of the Institute of Applied Synthetic Chemistry at Vienna University of Technology, to whom I am extremely grateful for his very valuable comments and feedback.

I would also like to thank my friends Aly, Benedikt, Nadine, Hassan and Matthias, my cousin Elias, my grandmother Lieselotte and my siblings Dana and Malek, who have always believed in me and supported all my endeavours.

Finally, I must express my very profound gratitude to my parents, Lubna and Akmal, for providing me with unfailing support and continuous encouragement throughout my years of study and especially throughout the process of researching and writing this thesis. This accomplishment would not have been possible without them. Thank you.

---

## Abstract

Stereolithography based on bottom-up digital light processing has become an established lithography-based additive manufacturing technology to produce parts with high precision and resolution for biomedical applications. Vinyl ester-based photopolymers show good biocompatibility and biodegradation performance. However, they must be developed towards better mechanical properties to function as viable bone replacement material. Therefore, in this study, vinyl ester-based monomers are mixed with the additive divinyl carbonate to form bio-photopolymers with higher toughness. Moreover, the base matrix of the compound was tuned along with post-curing to further enhance the mechanical properties. The assessment of these polymer networks was done via a tensile and impact test along with a dynamic mechanical analysis showing that the developed formulations exhibited considerably higher levels of strength and toughness compared to previously developed formulations without such additives.

The mechanical properties suggest that these formulations are suitable for biomedical applications. The print performance of the developed resin is demonstrated on a vat photopolymerized bone scaffold as well. Resulting from the improvement of mechanical properties, vinyl ester- and carbonate-based bio-photopolymers display lower curing speeds compared to highly crosslinked acrylate resins. The slow structuring of the polymer network ends in layer heterogeneities during printing. Thus, a novel way to characterize this assumed inhomogeneity was found in nanoindentation, by testing the cross-sections of printed parts. Moreover, the influence of the light absorber on the penetration depth dependent mechanical properties at the post-curing process was investigated. It was discovered that a high amount of light absorber is crucial for good mechanical properties of the green part at constant cure depth. One could observe the layer heterogeneity, which could not be removed with post-curing. Furthermore, gamma sterilization did not result in more homogenous global mechanical properties, independent of sample thickness. The layer heterogeneity was still present.

**Keywords:** vinyl ester, bio-photopolymer, cure depth, nanoindentation, vat photopolymerization

---

## Kurzfassung

Lithographie-basierte additive Fertigung, genauer das sogenannte Digital Light Processing (DLP), ist zu einer etablierten additiven Fertigungstechnologie geworden, um Teile mit hoher Präzision und Auflösung für biomedizinische Anwendungen herzustellen. Photopolymere auf Basis von Vinylester weisen eine gute Biokompatibilität und –Abbaubarkeit auf. Die mechanischen Eigenschaften solcher Bio-photopolymere müssen jedoch verbessert werden, um als Knochenersatzmaterial einsetzbar zu werden. Daher werden in dieser Arbeit Monomere auf Vinylesterbasis mit dem Co-Monomer Divinylcarbonat zur Bildung zäher Photopolymere vermischt. Zusätzlich wird das Polymernetzwerk durch einen kontrollierten Nachhärtungsprozess optimiert. Die mechanischen Eigenschaften dieser neuartigen Photopolymere wurden mittels Zugversuch, Schlagprüfung und dynamisch-mechanischer Analyse analysiert mit dem Ergebnis, dass die entwickelten Formulierungen bessere Werte in Festigkeit und Zähigkeit aufzeigen konnten und sich somit für biomedizinische Anwendungen eignen. Weiters wurde mit einem erfolgreichen Druckversuch einer Gerüststruktur aus dem entwickelten Harz die Verbaubarkeit via Hot-Lithography des entwickelten Biophotopolymers demonstriert. Biophotopolymere auf Vinylester- und Carbonatbasis zeigen aufgrund der Verbesserung der mechanischen Eigenschaften im Vergleich zu hochvernetzten Acrylharzen eine niedrigere Härtungsgeschwindigkeit. Die langsame Strukturierung des Polymernetzwerks endet beim Drucken in Schichtheterogenitäten. So wurde mit der Analyse via Nanoindentation ein neuer Weg gefunden, um diese Inhomogenität zu charakterisieren. Darüber hinaus wurde der Einfluss von Lichtabsorber auf die, von der Eindringtiefe abhängigen, mechanischen Eigenschaften beim Nachbelichtungsprozess untersucht. Es wurde entdeckt, dass eine große Menge an Lichtabsorber bei konstanter Durchhärtungstiefe für gute mechanische Eigenschaften des Grünkörpers entscheidend ist. Die Schichtheterogenität konnte erfolgreich detektiert werden. Ein Nachhärten der Probe konnte diese Schichtheterogenität nicht entfernen. Eine Behandlung mit Gammastrahlung im Zuge der Gamma Sterilisation führte nicht, unabhängig von der Bauteilhöhe, zu homogeneren globalen mechanischen Eigenschaften. Die Schichtheterogenität wurde auch dabei nicht vollständig eliminiert.

**Schlüsselwörter:** Vinylester, Biophotopolymer, Durchhärtungstiefe, Nanoindentation, Wannen-Photopolymerisation

## Abbreviations

$a_n$	Dynstat impact strength [ $\frac{\text{mJ}}{\text{mm}^2}$ ]
A	Area [mm]
$A_n$	Dynstat impact strength [kJ]
ppC <sub>d</sub>	Post-processing curing depth
C <sub>d</sub>	Cure depth [ $\mu\text{m}$ ]
D <sub>p</sub>	Penetration depth [ $\mu\text{m}$ ]
E*	Complex Modulus [MPa]
E'	Storage Modulus [MPa]
E''	Loss Modulus [MPa]
E <sub>c</sub>	Critical exposure [ $\frac{\text{mJ}}{\text{cm}^2}$ ]
E <sub>max</sub>	Maximum exposure [ $\frac{\text{mJ}}{\text{cm}^2}$ ]
E <sub>r</sub>	Reduced Young's Modulus / Indentation Modulus [GPa]
$\Delta E_r$	Gradient of Reduced Young's Modulus [GPa]
$\varepsilon$	Strain [%]
$\varepsilon_B$	Elongation at Break [MPa]
F <sub>n</sub>	Normal force [N]
T <sub>g</sub>	Glass Transition Temperature [°C]
$\sigma$	Stress [MPa]
$\sigma_B$	Strength at Break [MPa]
3D	Three-dimensional
AM	Additive Manufacturing
AMT	Additive Manufacturing Technology
CAD	Computer Aided Design
CT	Computer Tomography
DLP	Digital Light Processing
DLP L-AMT	Digital Light Processing Lithography-based Additive Manufacturing Technologies
DLP SLA	Digitally Light Processed Stereolithography
DMA	Dynamic Mechanical Analysis
DTM	Desk Top Manufacturing
DVA	Divinyl Adipate
DVC	Divinyl Carbonate
EGDVA	Ethoxylated Glycerol modified with Divinyl Adipate
FDM	Fueled Deposition Modeling
GDVA	Glycerol modified with Divinyl Adipate

LA	Light Absorber
L-AMT	Lithography-based Additive Manufacturing Technologies
LED	Light-emitting diode
M3_DVC	Compound batch for material development study
M3_DVCx	Compound with x weight percent of divinyl carbonate
M3_DVCx_y	Variation y of compound with x weight percent of divinyl carbonate
M3_TS_DVCx_y	Variation y of compound with x weight percent of divinyl carbonate from full factorial design
MP3_LA	Compound batch for material characterization study
MP3_xLA_ys	Compound with x light absorber weight percent and y seconds of post-curing
MRI	Magnetic Resonance Imaging
PCL	Polycaprolactone
PGA	Poly(glycolic acid)
PLA	Poly(lactic acid)
SLA	Stereolithography
SLS	Selective Laser Sintering
Steri	Gamma-Sterilization
TMPMP	Trimethylolpropane tris(3-mercaptopropionate)
UV	Ultra Violet
wt%	Weight percent

---

# Table of Contents

1	Introduction.....	1
1.1	Background .....	1
1.2	Aim of the work.....	3
1.3	Outline .....	4
2	State-of-the-Art.....	6
2.1	Mechanical properties and application of biomaterials .....	6
2.2	Metal replacements for bone fractures .....	8
2.3	Criteria for biocompatible –and degradable photopolymers .....	8
2.4	Synthetic polymers .....	10
2.5	Additive Manufacturing Technologies for tissue engineering .....	12
3	Theoretical background .....	13
3.1	Bone replacement.....	13
3.2	Tissue engineering.....	16
3.3	Additive Manufacturing Technologies.....	17
3.3.1	Material extrusion with FDM.....	19
3.3.2	Vat photopolymerization with laser or DLP.....	20
3.3.3	Powder bed fusion with SLS .....	21
3.4	Material paradigm and mechanical properties .....	22
3.4.1	Material paradigm.....	22
3.4.2	Definition of mechanical properties.....	23
3.5	Photopolymers.....	24
3.5.1	Photopolymerization .....	25
3.5.2	Reactivity of photopolymers .....	28
4	Materials and methods.....	29
4.1	Material components.....	29
4.1.1	Divinyl Carbonate .....	29
4.1.2	Divinyl Adipate .....	29
4.1.3	(Ethoxylated) Glycerol modified with Divinyl Adipate .....	30
4.1.4	Pyrogallol® .....	30
4.1.5	Trimethylolpropane tris(3-mercaptopropionate) .....	30

---

4.1.6	Quinoline Yellow .....	31
4.1.7	Ivocerin®.....	31
4.1.8	10MV .....	32
4.2	Applied Methods.....	32
4.2.1	Blueprinter 6 .....	32
4.2.2	UV-oven.....	33
4.2.3	$\gamma$ -sterilisation of cured photopolymers.....	33
4.2.4	Tensile test.....	34
4.2.5	Dynamic mechanical analysis .....	36
4.2.6	Dynstat impact test .....	39
4.2.7	Nanoindentation .....	40
5	Material development of tough photopolymers .....	43
5.1	DVC as toughness modifier .....	44
5.1.1	Compound preparation.....	44
5.1.2	Mechanical properties of M3_DVC with varying molar mass.....	45
5.2	Base matrix analysis with factorial design .....	48
5.2.1	Full factorial experiment .....	50
5.2.2	M3_TS_DVC80_6 .....	52
5.3	Application perspective of developed material.....	55
5.3.1	Material preparation.....	56
5.3.2	Mechanical properties of gamma-sterilized material .....	56
5.3.3	Printability of tough photopolymers with hot lithography.....	59
5.4	Conclusions for results of material development .....	60
6	Material characterization via nanoindentation.....	62
6.1	Material preparation .....	62
6.1.1	Material blending .....	63
6.1.2	Cure depth .....	63
6.1.3	Defining Cd via working curve.....	65
6.1.4	3D-printing of test structure .....	67
6.1.5	Post-processing.....	68
6.1.6	Microscopic images .....	70
6.2	Layer heterogeneity of cross-section.....	71

---

---

6.2.1	Principal of the nanoindentation measurement .....	72
6.2.2	Global layer behaviour .....	73
6.2.3	Post-processing curing depth.....	76
6.2.4	Local layer behaviour .....	78
6.2.5	Sterilization effect on layer heterogeneity.....	80
6.3	Conclusions for results of material characterization .....	82
7	Conclusions.....	84
7.1	Conclusions for material development of tough photopolymers.....	84
7.1.1	Limitations of approaches and results .....	84
7.1.2	Outlook.....	84
7.2	Conclusions for material characterization via nanoindentation .....	85
7.2.1	Limitations of approaches and results .....	85
7.2.2	Outlook.....	86
8	References .....	87
9	Table of Figures .....	92
10	List of Tables.....	95
11	List of Equations .....	96
12	Appendix .....	97
12.1	Appendix for material development of tough photopolymers .....	97
12.2	Appendix for material characterization.....	98

# 1 Introduction

A critical issue facing medical sciences is the aging population. The longevity achieved in the last century as a product of advancements in public health, socioeconomic development and medical technology marks an enormous achievement for humankind. The majority of people born today will live beyond the age of 65 years, and many will even survive past the age of 85 years (Rowe, Fried, Jackson, Novelli, & Stone, 2016). This dramatic extension of life has numerous ramifications we have yet to fully comprehend. It is, however, very clear that healthcare is of utmost importance.

Fortunately, new strides are consistently being made in biomedicine in order to improve healthcare. One of the most important fields in biomedicine is tissue engineering. Globally, millions of people would greatly benefit if tissues and organs could be replaced on demand. Traditionally, the foundation for treating injured and contaminated parts of the body has been their replacement with intact tissues and organs. The sole dependence on transplantation has created a waiting list of people in need of donated tissues and organs, and usually, supply cannot meet the demand. The price this gap has on our ability to provide patient care to patients with deteriorating organs and destructive diseases is massive. Scientists and clinicians, motivated by the need to develop safe and reliable sources of tissues and organs, have been improving therapies and technologies that can restore tissues and, in some cases, produce new tissues altogether. (Dzobo et al., 2018)

An aging society inevitably falls victim to age-related chronic diseases, one being those of joints and bones. Suitable (temporary) substitutes are necessary in the treatment of those diseases to support the healing process. Bone fracture is a very common medical condition and thus the biomedical field has long been optimising different kinds of materials to treat patients by implanting artificial bone.

## 1.1 Background

Bone tissue engineering is concerned with creating implantable bone substitutes for critical skeletal defects that cannot heal on their own. Typically, human bone can regenerate itself by cycle of bone resorption and bone formation. This means that the human body can heal bone fractures. But if bone damage is triggered by a disease or severe injury, the body struggles to repair its bone structures. These defects are common clinical scenarios in orthopaedics and craniofacial surgery, for the treatment of bone loss due to trauma, infection, and tumour resection. In this case, combinations of cells and bioactive molecules are seeded onto three-dimensional biomaterial scaffolds to create an implantable 'osteogenic' implant in the bone tissue engineering paradigm. This means that the substitute biomaterial acts as a scaffold for the

surrounding cells or tissue to invade, grow and consequently guide tissue regeneration towards new bone formation. (Xu, Imamura, & Nakagawa, 1997a)

Intervention in a complex and sensitive biological system such as the human body necessitates that several pre-requisites be fulfilled to ensure the successful replacement of fractured bone. (Mautner, Steinbauer, Orman, et al., 2016) In Figure 1, the three requirements for bone tissue engineering are illustrated: a biomaterial for bone scaffolds should be biocompatible, –degradable and mechanical properties should ideally mirror those of the replaced tissue both initially and during degradation.

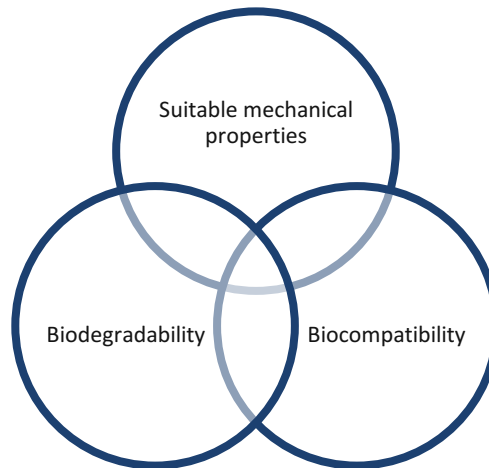


**Figure 1: Criteria for material in bone tissue engineering**

Biocompatibility refers to the reaction in the body upon implantation. The implant must show inflammation immunity and no cytotoxic response but osteoinductivity (scaffold to promote bone apposition) and osteoconductivity (signals to induce osteogenic differentiations of local stem cells) are desired as well. (Awad, O’Keefe, Lee, & Mao, 2014) While not necessarily a pre-condition, biodegradability has two major advantages over conventional implants like metal plates, rods or screws, namely:

- A gradual load transfer to the healing bone
- No need for surgical removal

Biodegradability can mean degradable, absorbable or resorbable, which all describe degradation in the human body but differ merely in the degradation process. Degradability refers to a biologically mediated degradation process, such as enzymatic or cellular process. Absorbability refers to a chemically mediated degradation, but the degradation products are generally excreted through one of the body’s organ systems. Resorption also signifies a chemically mediated degradation process such as hydrolysis where the degradation products are then incorporated into normal metabolic pathways like the citric acid cycle. Known as the Krebs cycle, it is a sequence of reactions by which most living cells generate energy during the process of aerobic respiration.

Ultimately, the material should not trigger a continuous inflammatory or toxic response upon embedding in the body. Degradation times must match the healing and regeneration process of the replaced tissue. Secondly, it should lead to non-toxic degradation products, which are able to be metabolized and cleared from the body. Thirdly, biocompatible implants must be sterilisable (Raposo-Amaral et al., 2014) Such synthetic graft implants should meet basic design criteria, including the capability for intraoperative reshaping (where needed), and sufficient initial strength and toughness.

A rather novel method to retain such bone scaffolds is through additive manufacturing technologies (AMTs). Bone tissue engineering has the potential to profit a great deal from advantages in scaffold fabrication, as demands for complex structures and defined porosity can be met. It has demand for scaffolds that provide mechanical support in cases where bone is removed from an injured site. Therefore, the employment of AMTs provides obvious advantages. Medical imaging coupled with computer-aided design (CAD) can be used to create a perfect-fit blueprint for bones to replace fractured bone. The blueprint can then be fed into a so-called 3D printer to build up an exact replica using a material that adheres to the prerequisites for bone tissue engineering. (Bak, 2003) To date and despite numerous exciting advances in preclinical models, regulatory approval barriers, business challenges, and related intellectual property lifecycle issues have impeded clinical translation from the bench to the bedside of such printed bone scaffolds. (Awad et al., 2014) In recent years, however, the number of reports dealing with its use for fracture repair in both animals and humans has increased dramatically and progress in viable printed biomaterials has been achieved.

## 1.2 Aim of the work

In this study, the aim is for novel biocompatible and -degradable resin formulations – including monomers, additives and stabilizers – that are processable with lithography based additive manufacturing (L-AMT) to fabricate patient-specific bone implants. State-of-the-art resins for L-AMTs are (meth)acrylates, and although currently in use as biomaterials for various applications, they have several disadvantages. (Meth)acrylates exhibit rather poor reactivity towards photo-polymerisation and acrylates are prone to cause irritation or result in high cytotoxicity. (Orman, 2018) Furthermore, the networks that are formed upon irradiation have a high crosslink density, which leads to brittleness. This is especially unfavourable when aiming to construct bone replacements, where a certain material toughness is required.

Instead, bone scaffolds that are printed via L-AMTs should have adequate mechanical properties and show high accuracy and quality that enable porous structures. High toughness and elongation at break as well as a suitable storage modulus at body temperature are essential. Furthermore, they are required to have low cytotoxicity

values for both the formulations with all its components, as well as the implant and its degradation products. The degradation should preferably follow a surface erosion mechanism, preventing premature failure of the implant.

From these reasons, it is clear that there is a need to develop new photopolymers that meet all the pre-requisites of biomaterials. Previous research shows vinyl ester-based photopolymers to be a promising alternative to common (meth)acrylate systems. They show significantly lower cytotoxicity and good mechanical properties which can be further improved using toughness modifiers like monomers with high molecular weight. Based on previous research, a mixture of multifunctional vinyl ester-based monomers and toughness enhancing modifiers were investigated, to create a novel photopolymer with good mechanical properties, biocompatibility and -degradation behaviour.

Therefore, a material characterization and development of vinyl ester-based photopolymers was conducted in this study. The research question focuses on two areas of study on printed bone scaffolds.

The first area discusses the development of vinyl ester-based biomaterials in terms of toughness. This can be achieved by incorporating toughening long-chain additives, optimising the base matrix and improving post-processing of the biomaterial. Such an additive is diluted in an existing formulation and is optimised along with the base matrix and post-curing accordingly via material testing. Furthermore, the effect of  $\gamma$ -sterilisation on the compound and the printability of the material via digitally light processed L-AMT is investigated as well.

The second area focuses on material characterization of printed compounds on a layer basis. The printability is dependent on the parameter setting of the printer and the adhesiveness of the resin. Cure and penetration depth aid the understanding of interlaminar bonding between the printed layers. Moreover, the layer hardness varies over the printed model due to different light absorber concentration and post-curing intensity and duration. This assumed layer heterogeneity is investigated by nanoindentation measurements on printed cross-sections. Specifically, this research assesses the hardness of cured samples by investigating whether a local (within layer) and a global gradient (from the surface to the inner of a part) due to post-curing are observable. This post-treatment includes post-curing with visible and UV light, as well as parts that are treated with  $\gamma$ -irradiation.

### 1.3 Outline

This thesis topic is interdisciplinary in nature in that it combines several major fields such as biomedicine, material science and additive manufacturing technology. In the following chapter, a literature review of the state-of-the-art research in bone tissue engineering within these different fields was conducted. Next, fundamental theory in

related fields of the research that gives an overview on basics in bone tissue engineering, photopolymers and additive manufacturing technologies is touched upon. Thereafter, the structural formula of major chemical compounds used for material characterization and development is examined, with a presentation of the most significant measurement methods used to identify the mechanical properties of the compounds. The results of the two research areas, namely material development and characterization, will be analyzed in sections 5 and 6, respectively. Here the material preparation, post-processing and measurements will be discussed comprehensively. Subsequently, these results will be critically situated in the greater context of the field of research. Lastly, attachments that complement the retrieved results will be presented for full disclosure.

## 2 State-of-the-Art

In this chapter, currently used materials for bone tissue engineering are discussed in terms of their functionality and mechanical properties to compare them to the printed biomaterials that are developed in this thesis. Therefore, metals and synthetic polymers are discussed in terms of their capacity to function as bone replacement material.

### 2.1 Mechanical properties and application of biomaterials

A comparative analysis of currently used materials is helpful as it allows for a better understanding of the mechanical properties aimed at by characterizing and developing biomaterials. Therefore, Table 1 presents distinctive materials with their mechanical properties and area of application.

NBR: Natural bone remodeling; PGA: Poly glycolic acid; PCL: Poly caprolactone; PLA: Poly lactic acid; BMP: bone morphogenetic proteins; GBR: guided bone regeneration; HA: hydroxyapatite

**Table 1: Natural bone tissue compared to other degradable and non-degradable materials and their application (Sheikh et al., 2015)**

Material	Compressive strength (MPa)	Tensile strength (MPa)	Young's modulus (GPa)	Elongation (%)	Degradation time (months)	Loss of total strength (months)	Applications or bone repair and regeneration
<b>A. Bone</b>							
Human cortical	131-224	35-283	17-20	1.07-2.10	NBR	None	Autograft and allograft used for defect filling, alveolar ridge augmentation, sinus
Human cancellous	5-10	1.5-38	0.05-0.1	0.5-3	NBR	0.5-1	Augmentation, dental ridge preservation
<b>B. Degradable</b>							
Collagen	0.5-1	50-150	0.002-5	3	2-4	1-4	Carriers (sponges) for BMP, composite with HA, membranes for GBR, scaffolds
Chitosan	1.7-3.4	35-75	2-18	1-2	4-6	<3	Scaffolds, microgranules, composite materials, VBA, membranes, xerogels
PGA	340-920	55-80	5-7	15-20	3-4	1	Internal fixation, graft material, scaffold, composite
PCL	20-40	10-35	0.4-0.6	300-500	>24	>6	Scaffolds and composites with HA fillers
PLA	20-30	100-150	1.5-5	5-10	>24	3	Fracture fixation, Interference screws, scaffolds, bone graft material
Hydroxyapatite	500-1000	40-200	80-110	0.5-1	>24	>12	Scaffolds, composites, bone fillers (granules and blocks), pastes, vertebroplasty, drug delivery, coatings
Magnesium	65-1000	135-285	41-45	2-10	0,25	<1	Implants, osteosynthesis devices, plates, screws, ligatures, and wires
<b>C. Non-degradable</b>							
Titanium alloy	900	900-1000	110-127	10-15	No	None	Implants, plates, screws, BMP carriers, orthognathic surgery, mid-facial fracture treatment
Bioglass	40-60	120-250	35	0-1	No	None	Bone defect fillers
Stainless Steel	500-1000	460-1700	180-205	10-40	No	None	Implants, plates, mini-plates, screws

## 2.2 Metal replacements for bone fractures

Why are biodegradable and –compatible materials preferred over metallic implants in bone tissue engineering? Today, metal plates, pins, rods, and screws are used for rigid internal repair of bone, which has been damaged by trauma or reconfigured surgically to correct defects occurring congenitally, developmentally, or because of disease. These devices align bone fragments, bring their surfaces into proximity, and, due to device structural stiffness, control relative motion to allow bone union. For healing, this stabilization must persist for several weeks or months without device breakage or loosening. The level of relative motion that can be tolerated has not been determined, but gross motion at a fracture site is known to result in non-union. Conversely, many studies have shown that completion of healing is prevented by highly rigid fixation since much of the load that is normally carried by the bone is transferred across the fracture spot by the graft. This is due to the elastic modulus mismatch between bone and metal ( $E_{bone} = 6 - 20 \text{ GPa}$ ;  $E_{metal} = 100 - 200 \text{ GPa}$ ), which is termed stress-shielding. (Sheikh et al., 2015) This means that the bone heals incompletely or may even remodel in accordance with Wolff's law<sup>2</sup>, so the shielded area is susceptible to re-fracture if the implant is removed. Furthermore, all non-stainless-steel systems share the problem that they cannot be as easily twisted or bent into a permanent new shape at room temperature. (Daniels, Chang, Andriano, & Heller, 1990) Moreover, concerns over bio-inert materials like metals and ceramics include limited supply, anatomical, structural and surgical limitations and increased bone resorption during healing. (Sheikh et al., 2015)

Metallic implants are removed in a second surgery to eliminate pain (which can be triggered by tissue pressure, infection, local corrosion or friction related to loosening), or at the demand of the patient for broad reasons or at the recommendation of the surgeon, should it be in the patient's best interests in the long run. (Daniels et al., 1990) Finally they exhibit poor overall integration with the tissue upon implantation. On the other hand, ceramics are brittle which makes them impractical in areas of increased torsion, bending or shear stress. (Salgado, Coutinho, & Reis, 2004)

## 2.3 Criteria for biocompatible –and degradable photopolymers

Firstly, what is a photopolymer? Photopolymers are macromolecules that are composed of covalently bonded repeating monomers that can be either the same or different, hence the terms homopolymers or copolymers. These materials can be

---

<sup>2</sup> Developed by German anatomist and surgeon Julius Wolff in the 19th century, it states that bone in a healthy person or animal will adapt to the loads under which it is placed. If loading on a bone increases, the bone will remodel itself over time to become stronger to resist that sort of loading.

amorphous and crystalline with chains being linear, branched or cross-linked with other chains. Moreover, photopolymer properties are affected by temperature and it is important to synthesize biodegradable polymers with the glass transition temperature ( $T_g$ ) above the body temperature, because they become too flexible above their  $T_g$  and thus inadequate for bone tissue engineering. (Daniels et al., 1990)

Secondly, what makes a photopolymer not biocompatible? Studies show that the main component of leachable substances out of a cured photopolymer are, to a large extent non-cured residual monomers, which has the utmost effect on biocompatibility. This is done most commonly by cyto- and genotoxicity tests according to DIN EN ISO 10993. For example, cytotoxicity tests revolve around the cell-viability after contact with photopolymer extracts. In contrast, genotoxicity can, for instance, be determined by bacteria growth on agar plates. Immunogenicity is important, as these grafts are implanted for a significant amount of time. Current metal implants such as hip joints have a durability of around 15 years, for example. Synthetic grafts are expected to exceed this duration without toxic reaction in the patient. (Leonhardt et al., 2016) To reduce cytotoxic effects, a post-processing of the cured photopolymer needs to occur, such as the extraction of residual monomers with supercritical  $CO_2$  or a chemical modification of the chain length of the monomers to reduce water uptake and consequently dissolve excessive elements. (Orman, 2018)

Thirdly, what makes a photopolymer biodegradable? It is a material that completes the surface erosion mechanism and dissolves in a metabolic process. Its measured biodegradation rate is very useful for clinical applications as it can be altered by changing the structural composition and fabrication techniques. Unfortunately, the degradation of implant materials is accompanied by an unwanted decrease in mechanical properties. Nonetheless, if the degradation is controlled and gradual, then the loads will transfer from the implants to bone or soft tissue to avoid the stress shield effect. The degradation process and rate is affected by various factors such as the molecular composition, molecular weight  $M_w$  and crystallinity. (Mautner, Steinbauer, Orman, et al., 2016) Additionally, biodegradation is dependent on the polymer chain length, because the longer they are the more hydrolytic chain scissions need to occur. More crystalline polymer networks show stronger inter- and intra-molecular bonding and hence degrade slower than amorphous networks. (Sheikh et al., 2015) Eventually, the ideal biomaterial should degrade in roughly the same amount of time the respective tissue needs to rebuild itself as shown in Figure 2.

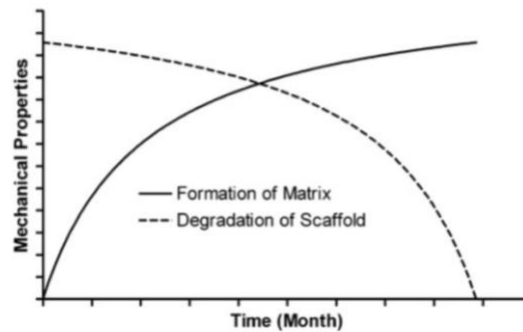


**Figure 2: Ideal degradation time of a scaffold in relation to regenerative tissue (Raghunath, Rollo, Sales, Butler, & Seifalian, 2007)**

Eventually, functional tissue needs an optimal interaction on cellular and biochemical levels. There are a few more specific criteria that ought to be met for biocompatible and -degradable photopolymers to be used successfully for bone repair and tissue engineering applications:

- The polymer surface should permit cell adhesion and growth to follow
- There should be no inflammatory or toxic response regarding the polymer or its degradation products post-implantation in vivo
- Interconnected high porosity
- High surface area and adequate space for extracellular matrix
- Entirely degradable with controlled resorption timing of the scaffold matrix (degradation rate ideally matching the regenerating bone tissue like Figure 2)
- Printability with L-AMTs

## 2.4 Synthetic polymers

Based on their origin, polymers can be classified as natural or synthetic. Due to their innate low strength compared to metals, natural polymers are mostly used as grafts for small bone fractures that do not bear high loads. The mechanical properties of these polymer grafts can be improved by adjusting the design and synthesis process. Synthetic polymers also have the advantage of having a well-controlled and reproducible molecular structure and are non-immunogenic. (Sheikh et al., 2015) Immunogenicity is the ability to induce a cell-mediated or humoral immune response in the body. To characterize and develop photopolymers for L-AMTs, synthetic polymers function as references in terms of mechanical properties and bio-adaptability. These features are discussed in the following.

There are synthetic polymers that can be manufactured under specific conditions and have the advantage of overall predictable and tuneable properties while maintaining low risk of immunogenicity. Polycaprolactone (PCL), poly(glycolic acid) (PGA) and poly(lactic acid) (PLA) are thermoplasts that fulfil the requirements for their use as bone replacement material:

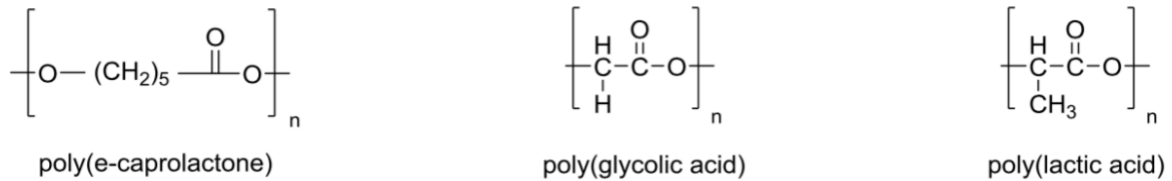


**Figure 3: Chemical structures of biocompatible and -degradable polymers**

For example, PLA polymers range from amorphous glassy polymer to semi-crystalline and highly crystalline polymer. This means that its properties can be modified and adjusted rather broadly. It is soluble by a variety of organic solvents and, thus, can be handled by numerous solvent and thermal-based methods. Biodegradation is done via hydrolytic degradation through the process of de-esterification. The elimination of monomeric by-products is prepared by natural excretory pathways. (Sheikh et al., 2015)

A range of its mechanical properties can be summed up as follows: PLA has a glass transition temperature of 60–65 °C, a melting temperature of 170–178 °C and a Young's modulus of 1.5–5 GPa. Heat-resistant PLA can withstand temperatures of 110 °C long term. Ultimately, the basic mechanical properties of PLA are between those of polystyrene and polyethylene terephthalate (PET). (Garlotta, 2001) The high Young's modulus makes it suitable for long-bearing applications in orthopaedics. In the 1960s the first sutures were approved by the US food and drug administration (FDA) and since then, many other degradable implants made from this polymer have been introduced to the market. However, PLA suffers from bulk erosion. This phenomenon is caused by the release of acidic degradation products leading to pH-related tissue necrosis. (Sheikh et al., 2015) Furthermore, premature failure of the implant is a major problem, as heterogeneous degradation often causes the interior of bulkier scaffolds or parts to degrade faster than the shell. Degradation products are trapped inside, leading to auto-catalysed degradation, eventually causing the implant to fail. (Orman, 2015)

PLA and other thermoplasts first generated interest three decades ago when polyesters were employed for suture materials. To this day, they remain one of the most widely used synthetic biodegradable materials. However, properties of highly porous scaffolds are weak for bone tissue engineering. They also lower local pH value in vivo due to degradation products that, in turn, accelerate the degradation rate of the implants to a degree that limits their clinical usefulness because of potential inflammatory reactions. (Sheikh et al., 2015) The earliest reported use of a biocompatible and -degradable polymer for fracture repair was described in 1971 by Kulkarni et al. He effectively used extruded rods of PLA to decrease jawbone fractures in dogs. However, he did not achieve consistent strength in his rods. (Daniels et al., 1990)

## 2.5 Additive Manufacturing Technologies for tissue engineering

Plenty of research has been invested towards bio-inert scaffolds made from ceramics or metals using selective laser sintering (SLS) or L-AMTs. Currently, L-AMTs are used for the printing of bone scaffolds due to the high precision. The significant advantages of degradable scaffolds made by additive manufacturing technologies are clear, but establishing working systems or their introduction into clinical trial is still a work in progress within academia. The challenge of such fabrication techniques is the problem of delamination during printing along with the lack of suitable materials in terms of biocompatibility, -degradability and mechanical properties - one of the main reasons why the printing of customized, degradable scaffolds is still in its early stages. (Gibson, Rosen, & Stucker, 2010)

### 3 Theoretical background

This chapter provides background knowledge about the different fields this interdisciplinary research engages with. To understand bone tissue engineering, we review the biomechanical and –chemical aspects of it as well as different technologies in additive manufacturing. Moreover, important material parameters are discussed.

#### 3.1 Bone replacement

Even though natural human bone comes in all shapes, sizes and forms, it has the same overall structure. It is a natural composite consisting in interval parts of collagen nanofibers strengthened with nanocrystalline hydroxylapatite. Generally, bones can be divided into two types according to their architecture: cortical (or compact) bone and cancellous (or trabecular) bone. Cancellous bone comprises 20 %, while cortical bone comprises 80 % of the total skeleton. Both have approximately the same material density, but cancellous bone is macroscopically porous with a relative density of less than 0.7 in comparison, making its modulus and ultimate compressive strength approximately 20 times smaller than that of cortical bone. A healthy human body contains 206 bones of various shapes and sizes. Inside this spongy structure lies the bone core which is constantly reproducing our blood cells. To achieve cell propagation and nutrition flow, spongy bone has discrete porosity in a size range between 50 and 100  $\mu\text{m}$  of interconnected pores. (Bose, Roy, & Bandyopadhyay, 2012) In a whole bone, such as the femur depicted in Figure 4, both types of bone are existent, with cortical bone being a protective shell around the porous cancellous bone.

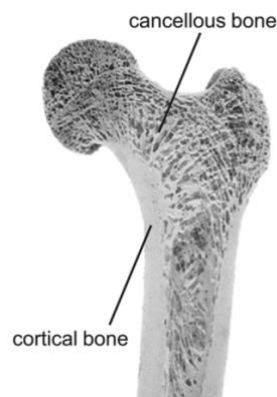


**Figure 4: Cortical and cancellous bone in human femur (Willems, Everts, Langenbach, & Zentner, 2013)**

Bone is a dynamic tissue with a unique capacity to heal and remodel without leaving a scar. It performs several integral functions in the maintenance of body systems, such as protecting vital organs, providing support and site for muscle attachment for locomotion, generating red and white blood cells for immunoprotection and oxygenating other tissues, retaining reserve stores of calcium, phosphate, and other

important ions, and providing housing to hematopoietic stem cells in the bone marrow. (Oyen, 2008) Therefore, pathologies of bone can be very serious, affecting a wide range of body functions. Bone deficiencies can result from abnormal development, tumours or general trauma.

Tissues overall are not merely made up of cells, but rather are a combination of specific cells and extracellular matrix. (Sikavitsas, Temenoff, & Mikos, 2001) They can be categorized as epithelial, muscle, nervous, and connective tissues. Together with cartilage, ligament, and tendon, bone belongs to the group of connective tissues, which have relatively small numbers of cells and much more extracellular matrix than other tissues. Most of the outstanding properties of bone are related to its extracellular matrix constitution and its hierarchical organization. (Orman, 2018)

As previously mentioned bone has a very high regeneration capability and can restore itself without forming scar tissue. This can be astoundingly observed in embryonal and infant growth. The skeleton of an embryo is mostly made up of cartilage and at birth the body consists of about 270 bones which further grow together during adulthood. The transformation or replacement of cartilage with bone is carried out by osteoblasts. (Kawamura et al., 2007) When they are triggered they start to form the organic bone component, called osteoid, mainly containing collagen, while present calcium phosphate leads to gel and form hydroxyl apatite. Most of those osteoblasts perish along this process while some get embedded into the bone tissue and transform into osteocyte. While the formation of new bone tissue mostly takes place during early adolescence and after injuries, bone remodelling is a constant process of optimization also taking place in adults. Bone tissue undertaking this development is split by osteoclasts and then rebuilt. This mechanism is activated by hormones adjusting the bloods calcium levels. The osteoclasts generate acidic conditions after conferring to the bone tissue and consequently degrade it while releasing minerals and other molecules stored in the bone matrix into the blood. Afterwards osteoblasts start to form new bone tissue. (Fan et al., 2011)

Because of these two mechanisms a healthy human skeleton can typically heal well. But after major injuries bone replacements must be done to substitute damaged natural bone in both structure and function. Depending on their source, replacements are categorized into auto-, allo-, iso-, syntho- and xenografts.

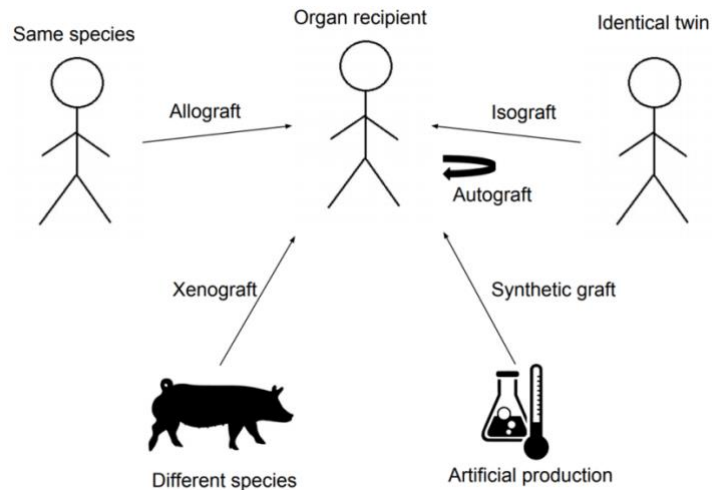


**Figure 5: Types of transplants**

Autografts are considered the golden standard in that they originate from the patient's own body and, thus, do not pose a risk of an immune response. The key drawback is the requirement of another surgical spot. Moreover, many patients suffering from bone-related diseases do not have sufficient material to be used. Furthermore, risks like blood loss, infections and nerve damage need to be considered. Replacements taken from other human donors are termed allografts. There is no second surgical spot needed but the graft instigates an immune reaction forcing the patient to take suppressing medication. Transplants from a monozygotic twin are called isografts. These grafts are very likely to be received favourably due to them being genetically identical. Xenografts are transplantations taken from animals like pigs or monkeys, evidently also having the issue of causing an immune response.

If none of those are accessible or appropriate, synthetic grafts are utilized. Such artificial bone replacements can either be non-degradable, like many ceramics and metals/alloys or they can degrade during the regeneration of the natural bone. Non-degradable parts like plates, pins and screws frequently linger in the patient after bone healing which may cause problems and further surgeries. (Salgado et al., 2004) Hence, degradable implants that can be personalized in terms of structure and properties are favourable.

Still autologous bone transplants are usually the golden standard when it comes to bone replacements with it being the second most transplanted tissue (after skin grafts). (Schnürer, Gopp, Kühn, & Breusch, 2003) Recent developments, though, are showing promising alternatives to natural bone without the earlier disadvantages of additional surgical sites, availability and negative reactions.

### 3.2 Tissue engineering

The interdisciplinary field of tissue engineering brings together biology, medicine, material science, chemistry and others to advance artificial grafts that can be used to substitute or restore impaired tissue like bone, skin, blood vessels or tendon. (Raposo-Amaral et al., 2014) What started in the 1950s as inert materials that are principally not repelled by the body is now so-called third-generation biomaterials that are believed to prompt tissue regeneration. (Vallet-Regí, Colilla, & González, 2011) A more precise term that is often used in literature is Tissue Engineering and Regenerative Medicine (TERM). (Pina, Oliveira, & Reis, 2015) Figure 6 depicts the three pillars of tissue engineering that revolve around cells, scaffolds and signals.

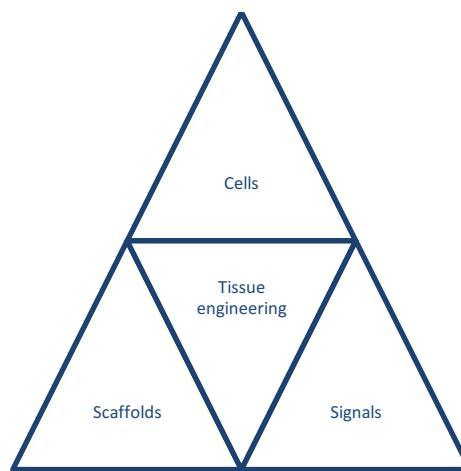


**Figure 6: Pillars of tissue engineering**

There are generally two feasible ways to achieve tissue regeneration. One could either grow the needed tissue outside a biological environment prior to implantation, which is termed the *in vitro* approach, or directly implant a degradable scaffold into the damaged tissue of the patient ensuing the *in vivo* approach. The *in vitro* pathway has the disadvantage of rather low “off-the-shelf” availability, which might be life-threatening for patients in emergency situations. To use this *in vivo* approach, a biocompatible and -degradable scaffold material is needed which is structured via suitable manufacturing techniques. Any tissue consists of a matrix and one, or usually, many cell types. The matrix works as a three-dimensional scaffold for cells and provides them with a tissue specific environment and architecture. Furthermore, it serves as a reservoir of water, nutrients and growth factors. To restore function or regenerate tissues one needs a template (scaffold) that will act as a provisional matrix for cell proliferation and extracellular matrix deposition, with resulting bone growth until new bony tissue is completely restored. Moreover, the scaffold would act as a template for the vascularization of the novel tissue. (Salgado et al., 2004)

These scaffolds are rather difficult to fabricate because they should not only be direct contact with living cells and bio-factors, but should also offer suitable mechanical

properties and degradation behaviour. (Bose et al., 2012) Consequently, utilizing the right engineering method is critical. Because the porosity has an enormous influence on cell-ingrowth and nutrition transport, the fabrication technique must be able to make such structures with sufficient resolution.

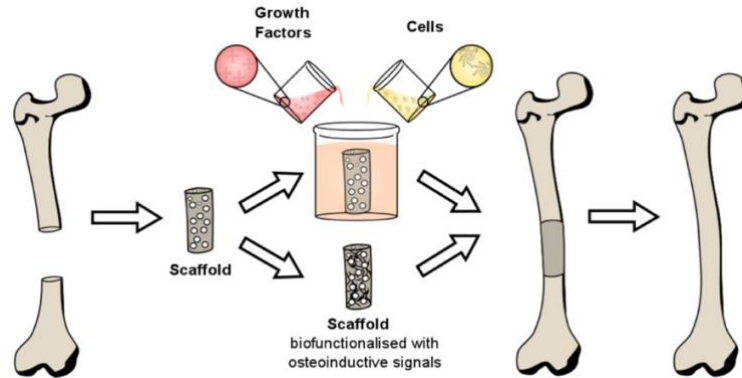


**Figure 7: Schematic process of bone tissue engineering (Redl, 2016)**

When it comes to manufacturing bone grafts there is always a balance that has to be struck between smaller pores, providing a bigger surface for cell proliferation and bigger pores that enable vascularization, flow of nutrients, oxygen and degradation products of the scaffold. (Feng et al., 2011) An optimal pore size of 325  $\mu\text{m}$  is suggested for the matters of bone tissue engineering. (Murphy, Haugh, & O'Brien, 2010) Evidently, this has a substantial impact on mechanical properties. Thus, materials must be found that display adequate mechanical stability and still have the anticipated degradation behaviour and porosity. (Orman, 2018)

### 3.3 Additive Manufacturing Technologies

Materials can be divided into:

- Metals & alloys
- Ceramics
- Polymers

For every form of material there is an additive manufacturing technology. This chapter discusses some relevant technologies.

Manufacturing technology can be categorized into three groups, when based solely on geometry (Gibson et al., 2010):

- Subtractive manufacturing technology
- Formative manufacturing technology
- Additive manufacturing technology

With subtractive manufacturing technology, the desired geometry is obtained by the defined removal of material, for example, by milling or turning. Formative manufacturing means to alter the geometry in a defined way by applying external forces or heat, for example, by bending, forging, or casting. Crucially, formative manufacturing does not change the volume of the part. Additive manufacturing creates the desired shape by adding material, preferably by staggering contoured layers on top of each other. Therefore, it is also called layer technology. The principle of layer technology is that any object can be divided into layers and reconstructed using these layers, regardless of geometric complexity, like in Figure 8. (Gibson et al., 2010)



Figure 8: Principle of layer technology (Gebhardt & Hötter, 2016)

Before an object can be printed, its CAD file must be converted to a format that is readable by a 3D printer— usually STL format. AMTs use computer generated data like Computer Tomography (CT), Magnetic Resonance Imaging (MRI) or Computer Aided Design (CAD) data to create objects with arbitrary structures. The process from CAD file to 3D part is illustrated in Figure 9.



Figure 9: Schematic process<sup>3</sup>

What AMTs have in common is that they work without tools or moulds and the parts are built using a layer-by-layer approach. (Gebhardt & Hötter, 2016) In this chapter, we will examine some of the different AMTs. The selection of AMTs has been made based on what are considered the most common technologies currently utilised in different industries.

<sup>3</sup> [http://www.3dstuffmakers.com/?page\\_id=2096](http://www.3dstuffmakers.com/?page_id=2096) ; last visited 2018-10-18

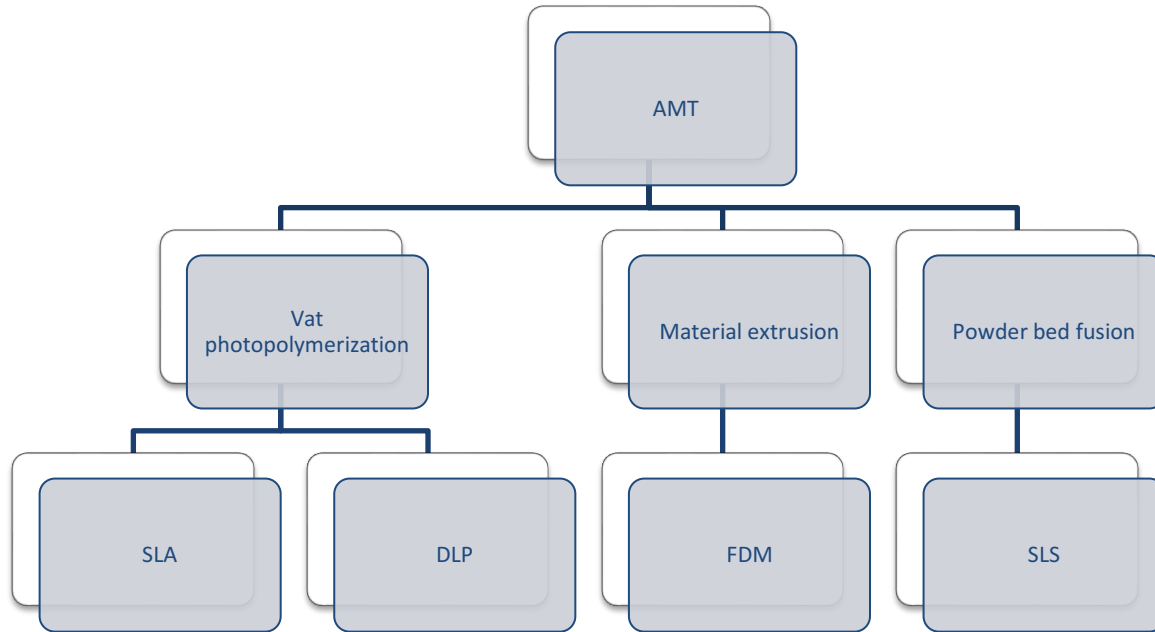


Figure 10: Selection of AMTs

Generally, AMTs lower costs, save time, and surpass the limits of building processes for product development. From conception and functional prototypes in rapid prototyping to springs, fixtures, or even end-use parts in manufacturing, AMTs offer flexible solutions in a broad range of applications. Over the last few years, high-resolution 3D printers have become more affordable, easier to use, and more reliable. (formlabs, 2018)

### 3.3.1 Material extrusion with FDM

There are several different AMTs, but the most commonly used is Fused Deposition Modeling (FDM). FDM uses a thermoplastic filament, which is heated to its melting point and then extruded, layer by layer, to build a 3D object. FDM printers use two types of materials: a modelling material, which comprises the finished object, and a material that supports the object during printing. (Palermo, 2013a) While the object is printed, these materials take the form of plastic strands or filaments, which are unwound from a coil and pressed through an extrusion nozzle. The nozzle melts the filaments and extrudes them onto a build platform. Both the nozzle and the build platform are controlled by a computer that renders the proportions of an object into cartesian coordinates for the nozzle and build platform to follow during printing. In a standard FDM printing method, the extrusion nozzle moves over the build platform horizontally and vertically, drawing a cross-section of an object onto the platform. This thin layer of polymer cools-off and solidifies, closely binding to the layer beneath it. Once a layer is completed, the base is lowered to make room for the next layer. Printing time depends on the volume of the printed object. Small pieces and tall, thin pieces print quickly, while larger, complex pieces take longer to print. FDM is a rather slow

method in comparison to other AMTs. When a piece is finished, its support materials are detached either by soaking the piece in a water and detergent solution or manually cracking the support material in the case of thermoplastic supports, for example. Pieces may also be smoothed, milled, painted or coated to advance their function and appearance. (Gibson et al., 2010)

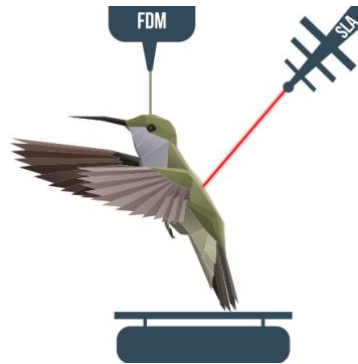


Figure 11: FDM vs. SLA (“FDM vs SLA: Direct Comparison Guide,” 2018)

### 3.3.2 Vat photopolymerization with laser or DLP

The stereolithography apparatus (SLA) selectively irradiates the transparent bottom by laser or digital light processor through the surface of a liquid pool of photocurable resin. Figure 11 emphasizes the essential difference when compared to FDM. (Lee, Aksay, & Prud’homme, 2001) If the resin cannot be processed at room temperature due to its composition and high viscosity, the vat must be heated constantly and distributed evenly to guarantee buildability by a sweeper. SLA systems operating at elevated temperatures are referred to as “hot-lithography”.

SLAs consist of four main segments: a perforated platform that is lowered into the vat, a vat that can be filled with photopolymer, an UV laser and a computer regulating the platform and the laser. In the first step of the SLA process, a thin layer of photopolymer (typically between 0.025-0.15 mm) is exposed above the pricked platform. The UV laser irradiates the pricked platform, drawing the shape of the piece being printed. The UV-curable liquid solidifies promptly upon irradiation, forming the first layer of the piece. When the initial layer of the piece is solidified, the platform is lowered or raised - depending on machine setup - exposing a new surface layer of liquid polymer. The laser once again traces a cross-section of the piece being printed, which instantly bonds to the hardened section beneath (or above) it. This process is repeated multiple times until the entire piece has been printed. The platform is then raised to expose a three-dimensional object. After it is cleaned with a liquid solvent to free it of left-over resin, the object is seared in an ultraviolet oven to cure the plastic even further. Pieces of SLA mostly have smooth surfaces, but the quality of a piece depends on the quality of the machine used. Naturally, procedure time depends on piece size. Small pieces are typically manufactured with smaller machines and normally take between six to

twelve hours to print. Larger objects, which are several meters in three dimensions, take days. (Palermo, 2013c)

The main disadvantage of this method is that the resulting photopolymers have rather poor mechanical properties compared to thermoplastics. (Van de Velde & Kiekens, 2002) Also, the presence of air on the surface during the polymerization can cause problems due to oxygen inhibition.

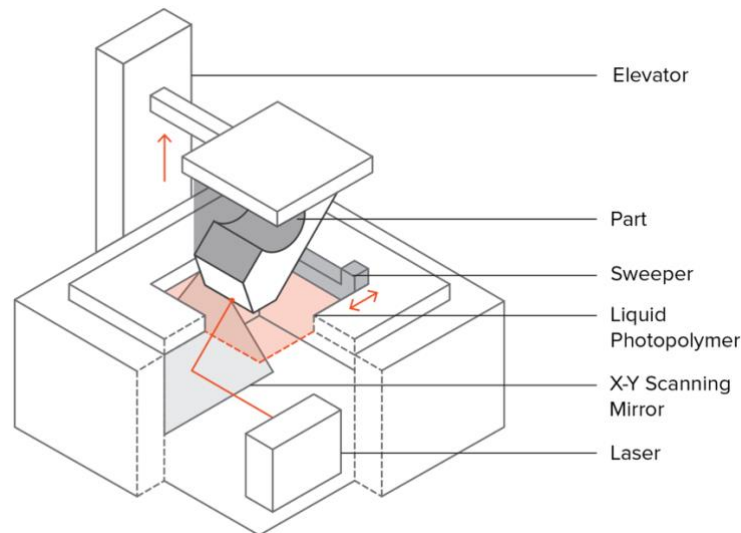


Figure 12: Schematic principle of SLA printer (Varotsis, 2016)

Bottom-up DLP functions like SLA are considered part of L-AMTs. It cures a whole layer using a digital light processor instead of a laser beam. Also, the irradiation takes place at the bottom of the resin-filled tub, excluding ambient oxygen. Compared to SLA it is faster and more economic regarding cost of the equipment and material consumption. DLP is a display based on optical micro-electro-mechanical technology that uses a digital micromirror device. Unfortunately, it has difficulty in resolution and surface quality in comparison to SLA. Also, like all L-AMTs, the achievable mechanical properties are limited. In this study, an analysis of layer hardness was conducted on photopolymers that were fabricated using this method.

### 3.3.3 Powder bed fusion with SLS

Another important technology is called selective laser sintering (SLS). During SLS, small particles of plastic, ceramic or glass are bonded together by heat from a high-power laser to form a solid, three-dimensional object. Sintering is an ancient technology that has been used for thousands of years to make everyday items like bricks, porcelain and jewellery.

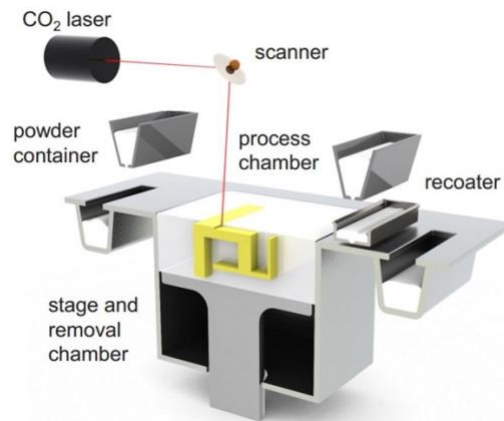


Figure 13: Schematic principle of SLS (Palermo, 2013b)

Objects printed with SLS are created with powder materials, frequently plastics, such as nylon, which are dispersed in a thin layer on top of the build platform inside an SLS machine. A laser, which is rendered by a computer, pounds down on the platform, tracing a cross-section of the object onto the powder. (Palermo, 2013b) The laser heats the powder either to just beneath its boiling point (sintering) or over its boiling point (melting), which fuses the particles in the powder together into a solid form. Once the primary layer is created, the platform of the SLS machine descends — typically less than 0.1 mm — revealing another layer of powder that is traced by the laser and fused together. This is repeated several times until the entire piece has been printed. When the piece is completed, it is left to cool in the machine before being removed. In contrast to other AMTs, SLS requires very little additional tooling when a piece is printed, meaning that pieces are usually not smoothed after printing. No additional support scaffolds are needed in SLS, which means that SLS is relatively faster than other technologies. (Gebhardt & Hötter, 2016)

### 3.4 Material paradigm and mechanical properties

In this section, we will briefly discuss the fundamental science of material study and what it entails. Moreover, the most important mechanical properties used to characterize photopolymers are presented in the following.

#### 3.4.1 Material paradigm

The basis of materials science involves the characterization of materials. This comprises the four important examinations: structure, properties, performance and processing. It is an interdisciplinary field of chemistry, physics and engineering, and focuses on the comprehension of the materials paradigm in Figure 14: the foundation of materials science includes examining the structure of materials and linking them to their properties. When a structure-property correlation is identified, it is possible to analyze the relative performance of a material in a task. The main causes that lead to the structure of a material and thus to its properties are its essential chemical elements

and the way in which they have been processed into its final form. Moreover, the processing of the developed material is crucial for performance. (Orman, 2018)

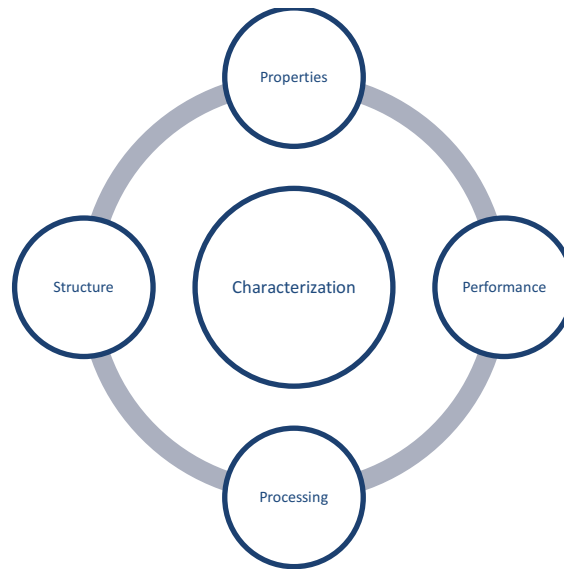


Figure 14: Materials paradigm

### 3.4.2 Definition of mechanical properties

The most important properties that determine the mechanical behavior of a material or component are rigidity, brittleness, strength, toughness and hardness. A definition of these properties is rather difficult, because they are not physical quantities. In contrast to physical quantities such as length or time, we often cannot assign a unique physical unit (such as m or s) to the associated technical quantities, since the same variables are used in technical terms for different variables. Material testing methods can be used to determine material characteristics that can be assigned to these technical quantities. Hence, a qualitative definition of these properties is presented as follows (Stampfl & Degischer, 2010):

- Rigidity is the resistance of a component to elastic deformation. Depending on the type of load one speaks of, for example, bending or torsional rigidity. For the overall rigidity of the component, the respective elastic characteristics of the material and the component geometry are responsible.
- Strength is resistance to plastic deformation or breakage. Plastic deformation is a permanent strain or bending after relieving the sample. The strength is measured in units of stress (force per surface).
- Toughness is the resistance to crack growth. Tough materials can dissipate a lot of energy during crack growth, and are therefore more resistant against crack propagation than brittle materials. Toughness is usually closely related to the material's ability to deform plastically.
- Hardness is the resistance to surface indentation by a foreign body and thus depends on the test procedure used.

Characteristic values of these properties include Young's modulus, tensile strength, Vickers hardness and Dynstat impact strength for example. Characteristic values can be obtained through many different testing procedures. For example, the Young's Modulus of a material can be determined by tensile testing, dynamic mechanical analysis (DMA) or nanoindentation.

The most important methods that are used in this study include: tensile testing, DMA, impact test with Dynstat configuration and nanoindentation. It should be noted that several characteristic values can be retrieved from one testing procedure. The following table presents the most important parameters of material testing utilized in this study:

**Table 2: Sample of characteristic values of materials**

Parameter	Symbol	Unit
<i>Elastic parameters</i>		
<b>Young's modulus</b>	$E$	$GPa$
<b>Shear modulus</b>	$G$	$GPa$
<i>Strength parameters</i>		
<b>Yield strength</b>	$\sigma_{eH}, \sigma_{eL}$	$MPa$
<b>Tensile strength</b>	$\sigma_m$	$MPa$
<b>Break strength</b>	$\sigma_B$	$MPa$
<i>Toughness parameters</i>		
<b>Dynstat impact strength</b>	$a_n$	$\frac{mJ}{cm^2}$
<b>Charpy impact strength</b>	$a_{cU}$	$\frac{mJ}{cm^2}$
<i>Hardness parameters</i>		
<b>Vickers' hardness</b>	$HV$	-
<b>Brinells' hardness</b>	$HB$	-
<b>Rockwells' hardness</b>	$HR$	-

### 3.5 Photopolymers

Photo-initiated resins follow a different initiation process than thermally treated polymerization does. Light curing has greatly expanded in industrial processes over the past several decades. Many conventionally thermally cured and solvent-based technologies can be substituted by photopolymerization technologies. The advantages of photopolymerization over thermally cured polymerization include high rates of polymerization (Gibson et al., 2010) In some occurrences, a resin may cure in a fraction of a second when exposed to light, as opposed to thermally cured resins which can require half an hour or longer. (Gebhardt & Hötter, 2016) Most commonly, photopolymerized systems are cured through UV radiation, since it is more energetic. Still, the improvement of dye-based photoinitiator systems has allowed for the use of visible light from DLP sources, having potential advantages of processes that are more

simple and safe to handle. Photoinitiating systems are often, in practice, highly elaborate mixtures of various compounds that provide optimum performance for specific applications. (Gibson et al., 2010)

### 3.5.1 Photopolymerization

Photopolymerization is a chain reaction in which unsaturated molecules are linked into macromolecules (polymers). The liquid mix of single molecules (monomers) is transformed into cross-linked, cured polymers. All processes in which the solidification of liquids is the fundamental mechanism are grounded in the concept of polymerization. (Gebhardt & Hötter, 2016) The general process contains fixing a batch of neat polymer with small amounts of photoinitiator, followed by selective radiation of light, resulting in a highly-cross-linked product. Many of these reactions do not require solvent which excludes termination path via reaction of initiators with solvent and impurities, in addition to decreasing the overall cost. (Cowie, 2008)

Photopolymeric systems basically consists of three components (Leonhardt et al., 2016):

- Monomers - Cross-linking agent: short- or long-chain molecules, which ensure the required mechanical properties
- Monomers - Reactive diluent: short-chain molecules, which reduce the viscosity
- Photoinitiators: molecules, which split into radicals after energy input and thus induce the curing reaction
- Additives: e.g. photo-stabilizers to prevent uncontrolled curing reactions

An example is shown in Figure 15 illustrating a combination of monomers, oligomers, and photoinitiators that result in a hardened polymeric material. This process is called curing.

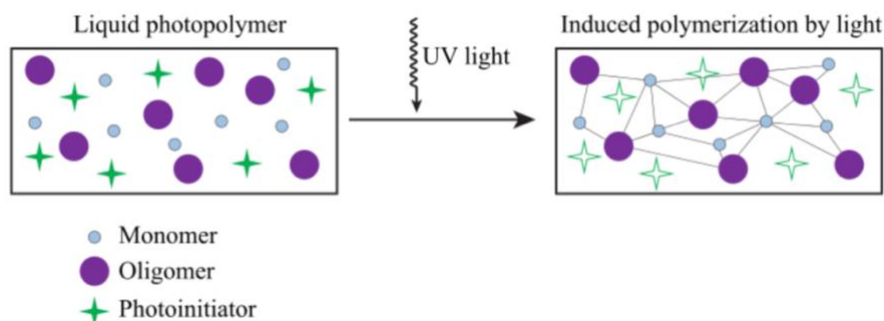


Figure 15: Schematic photo-polymerization process<sup>4</sup>

<sup>4</sup> <https://www.revolvy.com/page/Photopolymer> ; last visited on 18.10.2018

Essentially, there are two general routes for photo initiation that are commercially evident (Gibson et al., 2010):

- Free radical photo-polymerization – acrylate
- Cationic photo-polymerization – epoxy and vinyl ether

The molecular structures of these types of photopolymers are shown in Figure 16:

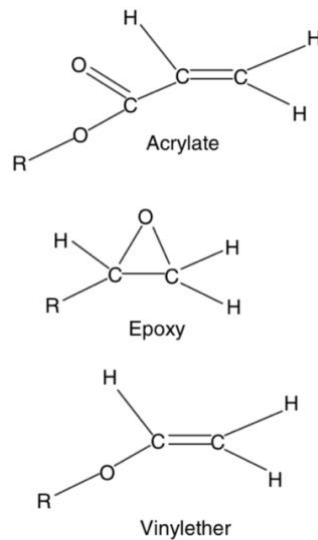


**Figure 16: Molecular structure of SL monomers (Orman, 2015)**

In Figure 16, symbols C and H indicate carbon and hydrogen atoms, while R indicates a molecular group which typically comprises one or more vinyl groups. A vinyl group is a molecular structure with a carbon–carbon double bond. It is these vinyl groups in the R structures that facilitate photopolymers to become cross-linked.

Free-radical photo-polymerization was the first type that was commercially developed with acrylates. Acrylates fuse to long polymer chains once the photo-initiator becomes “reactive”, building the molecule linearly by adding monomer segments. Cross-linking typically happens after the polymer chains grow enough so that they become close to one another. Acrylate photopolymers show high photo-speed, but have several drawbacks including significant shrinkage and a tendency to warp and curl. As a result, they are rarely used now without epoxy or other photopolymer elements.

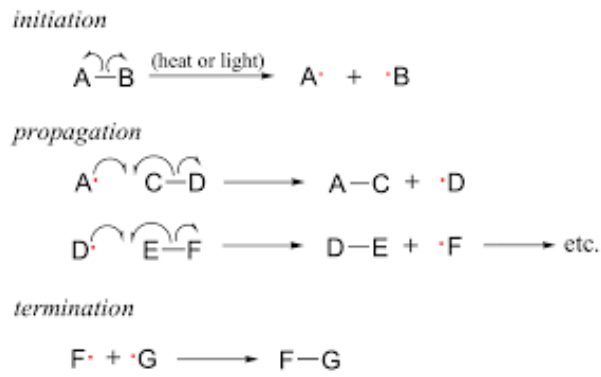


Figure 17: Free-radical polymerization process<sup>5</sup>

The most common cationic photopolymers are epoxies, although vinyl ethers are also commercially available. Epoxy monomers have rings, as shown in Figure 16. When reacted, these rings open, resulting in sites for other chemical bonds. Ring-opening is known to convey minimal volume change on reaction, because the number and types of chemical bonds are principally alike before and after reaction. As a result, epoxy resins typically have much smaller shrinkages and much lower tendency to warp and curl. Many commercially available stereolithography resins contain significant amounts of epoxies.

Schematically, the free radical-initiated polymerization process can be illustrated as shown in Figure 17. That radical can easily lead to the polymerization as shown in the transitional steps of the process, called propagation. Generally, longer polymer molecules are preferred, developing higher molecular weights. This indicates a more complete reaction. In Figure 17, the A–B term indicates a photo-initiated or thermally induced polymerization for a polymer.

Finally, photopolymerization ends due to one of three causes:

- Recombination
- Disproportionation
- Occlusion

Recombination occurs when two polymer chains merge by joining two radicals. Disproportionation essentially involves the elimination of one radical by another, without joining. Occlusion ensues when free radicals become “trapped” within a solidified polymer, meaning that reaction sites remain available, but are prevented from reacting with other monomers or polymers by the limited mobility within the polymer network. These occluded spots will ultimately react, but not with another polymer chain or monomer. Conversely, they will react with oxygen or another reactive species that

<sup>5</sup> [http://resscientiae.wikia.com/wiki/Vabad\\_radikaalid](http://resscientiae.wikia.com/wiki/Vabad_radikaalid) ; last visited on 14.11.2018

diffuses into the occluded region. This may be a cause of aging or other changes in mechanical properties of cured parts. (Gebhardt & Hötter, 2016)

### 3.5.2 Reactivity of photopolymers

Thus, reactivity is an important property that refers to the chemical stability of a polymer network in terms of reaction rate and equilibrium point. A parameter that indicates the reactivity of a polymer is its double bond conversion. The degree of conversion could be defined as the extent to which monomers react to form polymers or as the degree to which carbon double bonds ( $C = C$ ) are converted into carbon single bonds ( $C-C$ ). During the radical polymerization, the monomers polymerize to form a three-dimensional network containing double bonds and free radicals. It is known that residual double bonds in polymers make them less resistant to degradation reactions. Adequate curing of composite resins is of paramount importance to ensure optimal clinical performance. (Mautner, Steinbauer, Orman, et al., 2016)

## 4 Materials and methods

In this chapter, we will examine the different components of the formulations that are characterized and developed in this study and discuss the different measurement and fabrication methods utilized. The base matrix of the components in both fields of study includes these components. The material characterization by nanoindentation was done on the formulation MP3 (see Table 12), while the development of tough photopolymer was conducted on M3 (see Table 6).

### 4.1 Material components

Here, the most significant components of the chemical compounds that were used in the research and development of this thesis will be delineated. The vinyl esters in this section were all synthesised by Sandra Orman from the chemical department of macromolecules (Orman, 2018) if not stated otherwise.

#### 4.1.1 Divinyl Carbonate

Divinyl carbonate (DVC) is the long chain branching selected for material development to toughen vinyl ester-based formulations and is based off PCL. It distinguishes itself with high impact-resistance and tensile strength, which leads to toughness improvement for compounds. Hence it is highly viscous.  $C_{5}H_6O_3$  is the synthesised long-chain branch additive for M3\_DVC that is believed to improve overall toughness.

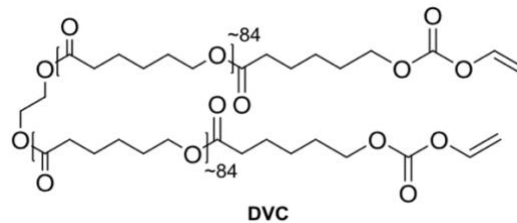


Figure 18: Divinyl carbonate structural formula (Orman, 2018)

#### 4.1.2 Divinyl Adipate

Divinyl Adipate (DVA) is a 2-fold functional monomer that has good reactivity. It can, however, be brittle in lower thermal regions.  $C_{10}H_{14}O_4$  is a chemical compound based on vinyl ester. It is the basis of both the MP3 and M3 formulations used. The monomer used in this thesis was synthesised by TCI-EP®.

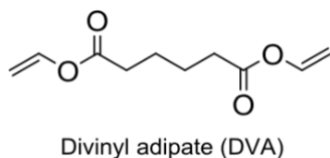


Figure 19: Divinyl Adipate structural formula (Orman, 2018)

#### 4.1.3 (Ethoxylated) Glycerol modified with Divinyl Adipate

GDVA is a base monomer for both formulations and is synthesised from DVA and Dianhydro-D-glucitol. Ethoxylated GDVA has a similar composition, except that ethylene oxide with the formula  $C_2H_4O$  is added. It is a vinyl ester monomer that is both biocompatible and –degradable.

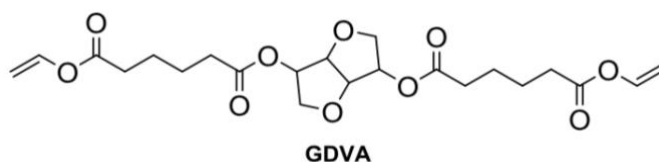


Figure 20: Glycerol modified with DVA (Orman, 2018)

#### 4.1.4 Pyrogallol®

Pyrogallol® is a benzenetriol. It is a white crystalline powder and a powerful reducing agent. Pyrogallol® is an organic compound with the formula  $C_6H_3(OH)_3$ . It is a water-soluble solid, although samples are typically brownish because of its sensitivity toward oxygen. It has a molar mass of 126.11 g/mol, boiling point of 309 °C, melting point between 131-134 °C and density of 1.45 g/cm<sup>3</sup>. (National Center for Biotechnology Information, 2018) The monomer used in this study stems from Sigma-Aldrich®.

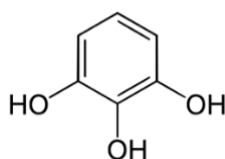


Figure 21: Pyrogallol® (National Center for Biotechnology Information, 2018)

#### 4.1.5 Trimethylolpropane tris(3-mercaptopropionate)

Trimethylolpropane tris(3-mercaptopropionate) (TMPMP) is used as a chain transfer agent in resins. In thermal or radiation cured thiol-ene systems, TMPMP can be used as the main binder in combination with acrylates or vinyl esters. Thiol-ene systems that react via radical initiation and step-growth polymerization do not show oxygen inhibition and result in lower shrinkage compared to standard UV cured systems reacting via

chain-growth polymerization. (Merck, 2018) The TMPMP used for our formulations was obtained by Bruno Bock®.

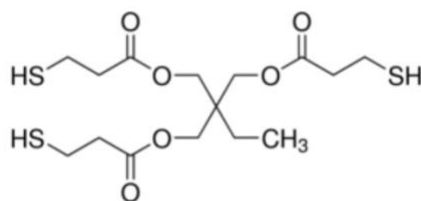
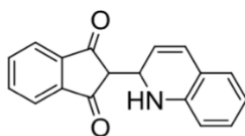


Figure 22: TMPMP (Merck, 2018)

#### 4.1.6 Quinoline Yellow

The light absorber used for UV curing in printing the biomaterial in L-AMT is quinoline yellow (Sigma-Aldrich®). Its job is to absorb excessive light and reduce over-polymerisation in non-irradiated areas. This must often be ensured for good printing performances of photopolymers. Evidently, this also reduces the amount of light the photoinitiator has available to initiate and cut the polymerization. Consequently, a balance must be found between upholding good resolution and preventing pores from closing during the printing process, applicable curing speed and conversion. (Orman, 2018) Quinoline Yellow SS is a bright yellow dye with green shade. It is insoluble in water, but soluble in nonpolar organic solvents. In this study, it functions as a photostabilizer and light absorber in printed M3\_DVC and MP3\_LA.



Quinoline Yellow SS (QY)

Figure 23: Quinoline Yellow (Orman, 2018)

#### 4.1.7 Ivocerin®

Ivocerin® is patented photoinitiator by Ivoclar Vivadent®. It has a deep yellow colour before polymerization, though it has good bleaching properties during polymerization. For visual purposes, its use is preferred in dental composites. Also, Ivocerin® has a good double bond conversion rate. Naturally, the high reactivity of Ivocerin® influences the shrinkage behaviour of the composite resin, however this depends on the amount of Ivocerin® used in the polymer. (Watts, 1984)

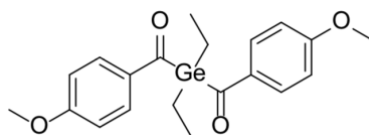


Figure 24: Chemical structure of Ivocerin® (Orman, 2018)

#### 4.1.8 10MV

Vinyl decanate (10MV) is a 1-fold functional monomer that reduces network density and creates therefore less brittle polymers than DVA. It has a bad reactivity, in contrast to DVA and GDVA. The formulation used here stems from Sigma-Aldrich®.

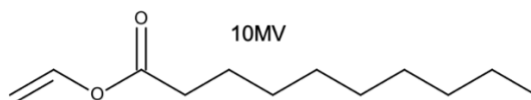


Figure 25: Structural formula for 10MV (Orman, 2018)

## 4.2 Applied Methods

In this thesis, we investigated the compounds with different measurement methods to examine mechanical properties. We examined material characterization on 3D printed compounds and material development on photopolymerized samples. Hence the applied methods and machines for material preparation and post-processing of the printed parts are discussed. The measurement methods utilized include tensile and Dynstat impact test, dynamic mechanical analysis (DMA) and nanoindentation. This chapter gives an overview over these methods.

### 4.2.1 Blueprinter 6

In this study, a DLP L-AMT system with an upside-down set-up was used termed Blueprinter 6. Furthermore, the light source was an InVision® WUXGA 1080p light engine with 460 nm LED. (Hofstetter, Orman, Baudis, & Stampfl, 2018) Moreover, the layers were cured with an irradiation intensity of  $84 \frac{\text{mW}}{\text{cm}^2}$  and a varying exposure time depending on cure depth analysis (see 6.1.3).

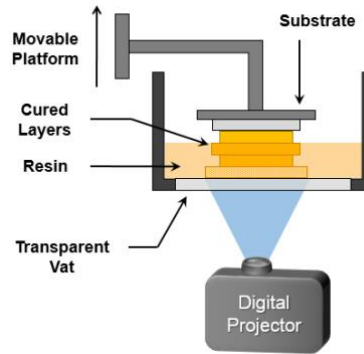


Figure 26: Working principle of DLP (Baudis, 2016)

## 4.2.2 UV-oven

A UV-oven exposes the sample to UV curing. This is an important procedure in post-processing as the product from the blueprinter is not completely cured. Only after post-processing in a UV-oven with timed and intensity-adjusted treatment can the material attain enhanced mechanical properties.

The UV-oven used in this study is Intelli-Ray 600 W from UViTRON International. The machine can be set up directly by manually configuring the desired intensity level of UV, as well as the desired exposure time. The intensity level can be set from 50-100 % (meaning 600 W or  $175 \frac{\text{mW}}{\text{cm}^2}$  and 320-390 nm UV light), while the exposure time in one run can be fixed to 1-9999 s. The set parameters for each study are mentioned in the respective process and field. The parameters are adjusted iteratively based on previous experience and reaction of the material to it.

## 4.2.3 $\gamma$ -sterilisation of cured photopolymers

A gamma ray is a penetrating electromagnetic radiation arising from the radioactive decay of atomic nuclei. It consists of the shortest wavelength of electromagnetic waves and so radiates the highest photon energy. Gamma rays are ionizing radiation and are consequently biologically dangerous. Due to their high penetration power, they can damage bone marrow and internal organs. Unlike alpha and beta rays, they pass easily through the body and thus are not easily protected against. Low levels of gamma rays cause a probable health risk, which may lead to cancer or genetic damage. High doses produce deterministic effects, which is the severity of acute tissue damage that is guaranteed to happen. (Dwyer & Smith, 2012)

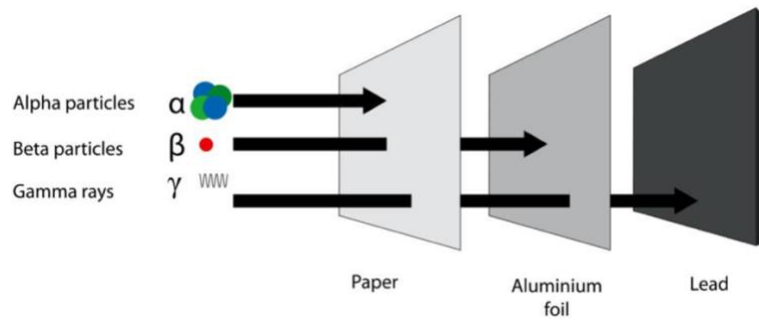


Figure 27: Sterilisation methods and materials (Saint-Denis, 2018)

Gamma irradiation provides several benefits in cost and sterility assurance. It can be applied under safe, well-defined and controlled operating parameters, and is not a heat- or moisture-generating process. Therefore, there is no heat stress and condensate drainage or outgassing. Most importantly, there is no residual radioactivity after irradiation. (Martin, 2012) This makes gamma-sterilization quintessential for materials that are used in medical application. The samples in this study were sterilized for both M3\_DVC and MP3\_LA by 18 kGy gamma exposure from a Kobalt-60 machine.

#### 4.2.4 Tensile test

Tensile testing is a key engineering measurement in which a sample is exposed to a controlled tension until failure. Properties that are directly measured via a tensile test are ultimate tensile strength, breaking strength, maximum elongation and area reduction. According to EN ISO 527-2:2012, the sample geometry 5B was used for all materials. For testing, a specimen is fixed between two clamps and a tensile load is applied, resulting in uniaxial elongation of the sample. Fixation was done with a parallel screw collet in our case. Due to the quasi-static nature of this method, the stress is distributed evenly across the whole cross-section, which is taken as constant throughout the measurement. Uniaxial tensile testing is frequently used for obtaining the mechanical characteristics of isotropic materials. (Davis, 2004) Figure 28 illustrates the mechanical structure of a typical tensile test.

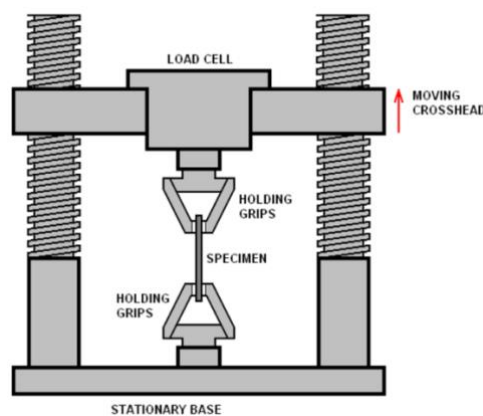


Figure 28: Schematic tensile test (Nguyen, 2012)

The tensile test results in a stress/strain-curve. Figure 29 shows the characteristic curve of a ductile material with elastic and plastic strain until fracture. Here, the most important properties are included in the diagram, because of the material's ductility. The already mentioned properties are derived from this curve. The y-axis shows the applied stress, whereas strain is represented on the x-axis.

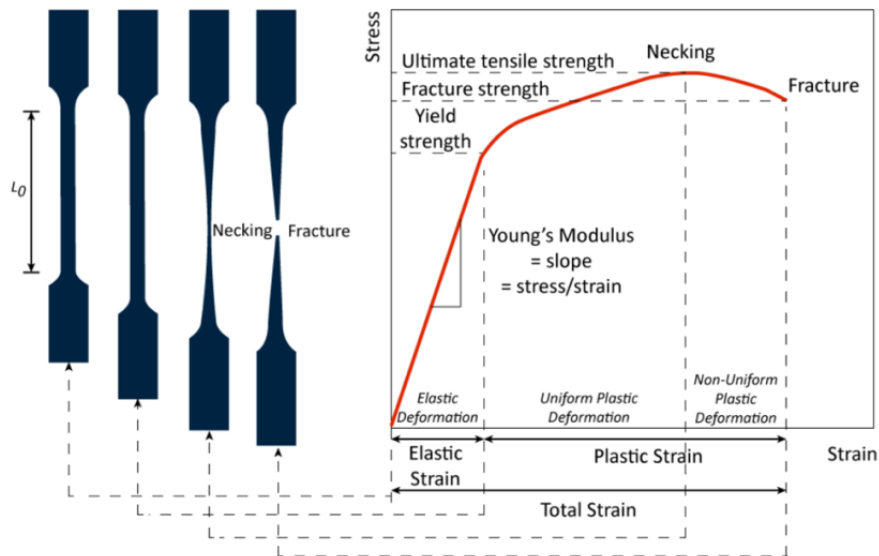


Figure 29: Shape of a ductile specimen during tensile testing (Yalcin, 2017)

The well-known Young's Modulus results from the relation from stress to strain in the elastic deformation area:

$$\sigma = \frac{F_n}{A}$$

Equation 1

$\sigma$  stress [MPa]

$F_n$  normal force [N]

$A$  cross-sectional area [m<sup>2</sup>]

$$\varepsilon = \frac{\Delta L}{L_0} = \frac{L - L_0}{L_0}$$

Equation 2

$\varepsilon$  strain [-]

$L$  length of specimen at break [m]

$L_0$  initial length of specimen [m]

$$E = \frac{\sigma}{\varepsilon}$$

Equation 3

The machines that were used for the conducted tests are Zwick Z050 and Zwick Z250. Both machines are electromechanical testing machines that have a broad application range and can be adjusted for several testing methods, temperatures, types of stress or microscope coupling. The required properties are easily analyzed using Zwick-Roell software and can be processed to other analytical softwares. For our purposes, the break (fracture) strength and elongation were retrieved. Finally, the parameter set used in our tests was unilaterally:

Table 3: Utilized parameter set for tensile testing

Parameter	Value
Preload	0.5MPa
Test speed	5mm/min
Force sensor	1kN

#### 4.2.5 Dynamic mechanical analysis

Dynamic mechanical analysis (DMA) is a method used to study and characterize materials. It is most useful for studying the viscoelastic behaviour of polymers. The specimen is applied in a 3-point-bend configuration and exposed to a sinusoidal stress under heat progression.

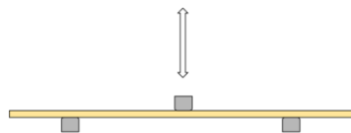


Figure 30: 3-point-bend setup

The strain in the material is measured, determining the complex modulus at a certain application temperature. The temperature of the sample or the frequency of the stress is typically speckled, leading to deviations in the complex modulus. This methodology may be used to find the glass transition temperature  $T_g$  of the material, as well as to detect changes consistent with other molecular motions.  $T_g$  is an area of reversible transition, where amorphous or semi-crystalline structures in the material emerge. Here it turns from hard and glassy material into a rubber-like material. (Stampfl & Degischer, 2010) As previously mentioned, a viscoelastic material is somewhere between an ideal viscous material, which shows a phase shift ( $\delta$ ) of  $\delta=\pi/2$ , and an ideal elastic material, with  $\delta=0.200$ . (Orman, 2018)

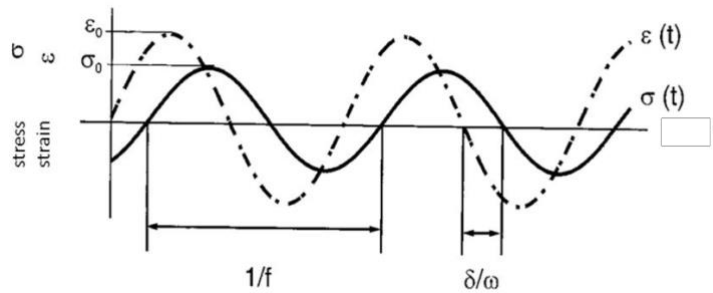


Figure 31: Stress and strain during DMA (Hess, 2018)

Figure 31 shows the phase shift between stress and strain during DMA. To obtain the complex modulus, we need to understand its composition. The storage modulus  $E'$  and loss modulus  $E''$  are important to determine it. From this, the viscoelastic behaviour and  $T_g$  can be determined using analysis software.

$$\sigma(t) = \sigma_0 \sin(\omega t)$$

Equation 4

$\sigma(t)$  stress at any given point in time [MPa]

$\sigma_0$  stress amplitude [MPa]

$\omega$  angular frequency [ $s^{-1}$ ]

$f$  frequency [Hz]

$t$  time [s]

$$\varepsilon(t) = \varepsilon_0 \cos(\omega t - \delta)$$

Equation 5

$\varepsilon(t)$  strain at any given point in time [MPa]

$\varepsilon_0$  strain amplitude [MPa]

$\delta$  phase shift [-]

$$E^* = \frac{\sigma(t)}{\varepsilon(t)} = \frac{\sigma_0 \sin(\omega t)}{\varepsilon_0 \sin(\omega t - \delta)}$$

Equation 6

$E^*$  complex modulus [MPa]

$$E^* = E' + iE''$$

Equation 7

$$\tan \delta = \frac{E''}{E'}$$

Equation 8

The tests conducted in this thesis were done by machine 2980 from TA-Instruments with the following parameter set:

Table 4: Utilized parameter set for DMA

Parameter	Value
Amplitude	10 $\mu\text{m}$
Force	0.05 N
Force track	125 %
Frequency	1 Hz
Start temperature	15 $^{\circ}\text{C}$ -> 5 min
Heating ramp	3 $^{\circ}\text{C}$ -> 80 $^{\circ}\text{C}$

This parameter set was used for all materials tested, regardless of whether the material is M3\_DVC or MP3\_LA. The test results are depicted in a diagram showing the development of the storage modulus, loss modulus and damping of the material in relation to heat progression. A typical result that was derived from DMA is presented in Figure 32. From this diagram, we derive the storage modulus  $E'$  of the sample at different temperatures to gain insights into the viscoelastic behaviour of the material, as well as its glass transition temperature. For our purposes, we determined the storage modulus at 20  $^{\circ}\text{C}$  (room temperature), 37.5  $^{\circ}\text{C}$  (body temperature) and  $T_g$  (glass transition temperature) with Universal Analysis software.  $T_g$  is at the peak of the damping ( $\tan \delta$ ) curve.

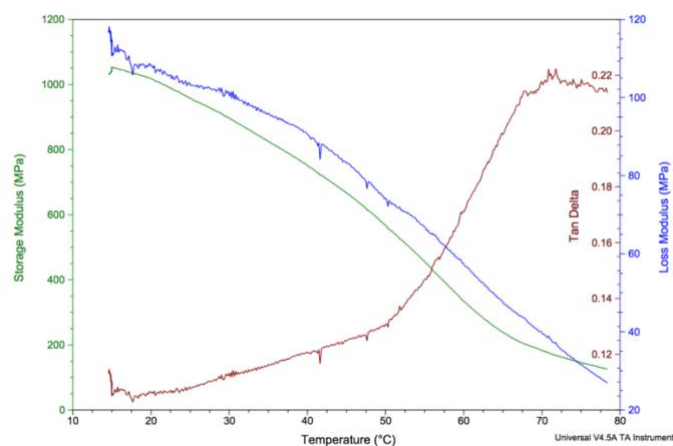


Figure 32: Typical DMA result showing  $E'$  (green),  $E''$  (blue) and  $\tan \delta$  (red) under temperature progression

## 4.2.6 Dynstat impact test

The impact test after Dynstat configuration is a standardized high strain-rate test, which establishes the amount of energy absorbed by a material during fracture. This absorbed energy is a measure of a given material's notch toughness and acts as a tool to study temperature-dependent ductile-brittle transition. It is widely applied in industry, since it is easy to prepare as well as conduct, and results can be obtained quickly and cheaply. A disadvantage is that some results are only comparative. (Stampfl & Degischer, 2010) Other related tests differ only in the configuration of the sample upon impact. The most significant of these is the Charpy configuration. Even so, the configuration used for these tests is Dynstat and presented in Figure 33.

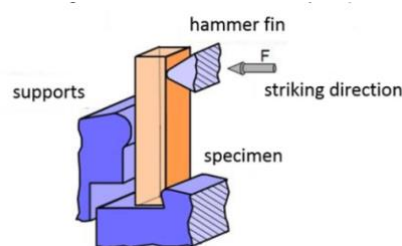


Figure 33: Dynstat configuration for impact test (Mueller & Oluschinski, 2018)

A specimen is placed on supports and the pendulum hammer is raised and fastened at a certain height, giving it a known potential energy. After activating the release mechanism, the hammer swings down and breaks the sample and the absorbed energy is recorded by a needle on a scale. Relating the displayed value with the geometry of the sample conveys the impact strength. The process is illustrated in Figure 34.

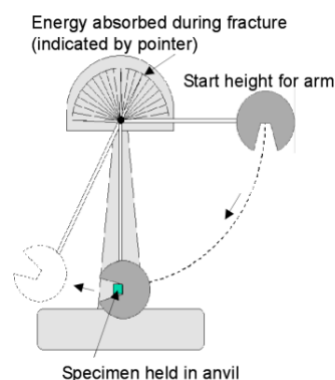


Figure 34: Schematic impact test (University of New South Wales, 2013)

The hammer energy can be retrieved from the displayed value on the machine and needs to be calculated with the dimensions of the sample to provide the impact resistance. In our tests, we worked with a 20 kpcm and 10 kpcm hammer depending on the impact resistance of the material. If the material showed less impact resistance for a sample, the 10 kpcm was taken for the next sample to get a more precise result.

Lastly, the tests were conducted on a manual device by Frank with a maximum working capacity of 4 J.

In the following, the equation for impact resistance is presented:

$$a_n = \frac{A_n}{h \cdot b}$$

$a_n$  impact resistance [ $\frac{\text{kJ}}{\text{m}^2}$ ]

$A_n$  hammer energy [kJ]

$h$  sample thickness [m]

$b$  sample width [m]

### 4.2.7 Nanoindentation

This is a complex but useful measurement because only small sample volumes are needed. The measurement proceeds as follows: A diamond-tipped probe indents the specimen with defined force and indenting rate. The displacement of the tip is measured and with the known shape of the indenter the contact area at full load is calculated from the cavity of penetration. A schematic nanoindentation test is shown in Figure 35.

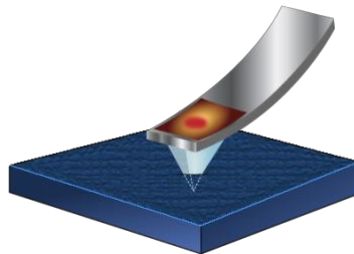


**Figure 35: Schematic nanoindentation test process**

A characteristic curve of a nanoindentation is illustrated in Figure 36. This recorded load-displacement curve can be used to calculate various mechanical properties of the material. The most important mechanical property that can be retrieved is a reduced Young's Modulus, which characterizes the hardness of the material.

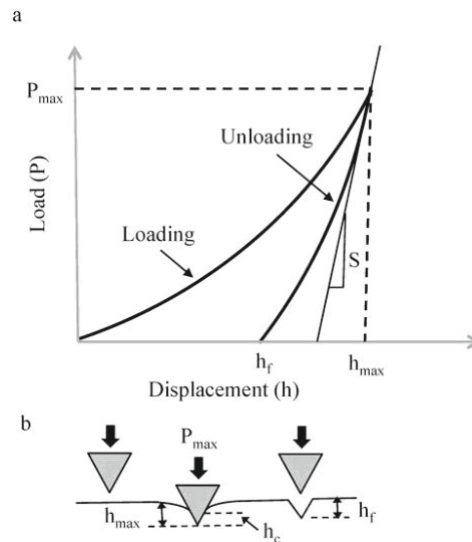


**Figure 36: a) load/displacement-curve; b) conforming indentation phase (Ladani, Harvey, Choudhury, & Taylor, 2013)**

The reduced Young's modulus ( $E_r$ ) is calculated by the stiffness ( $S$ ) of the contact which again can be calculated from the slope of the curve  $dP/dh$  upon unloading.

$$E_r = \frac{1}{\beta} \frac{\sqrt{\pi}}{2} \frac{S}{\sqrt{A_p(h_c)}}$$

**Equation 9**

$A_p(h_c)$  is the projected area of the indentation at the contact depth  $h_c$  and  $\beta$  is a geometrical constant.

The hardness ( $H$ ) relates the maximum load ( $P_{max}$ ) to the indentation area ( $A_r$ ) and is given by the following equation:

$$H = \frac{P_{max}}{A_r}$$

**Equation 10**

Lastly, the strain-rate sensitivity of the flow stress ( $m$ ) is defined as:

$$m = \frac{\partial \ln \sigma}{\partial \ln \dot{\epsilon}}$$

**Equation 11**

$\sigma$  symbolizes the flow stress and  $\dot{\epsilon}$  is the strain rate produced under the indenter.

For our nanoindentation experiments, we used a Hysitron Ubi 750 from XP with extended z-stage and Berkovich indenter tip. The Berkovich indenter is typically built with a face angle of  $65.03^\circ$ , which provides the identical actual surface area to depth ratio as a Vickers indenter. The tip radius is between 50-100 nm, which usually

increases to 200 nm with usage. (Fischer-Cripps, 2011) As nanoindentation is a very precise measurement, the cross-section must be smooth and scratch-free. This means accurate grinding and polishing of the sample. Moreover, the parameter set used for nanoindentation depends on the sample and its post-treatment or lack thereof. Harder samples with post-treatment were measured with a different set of parameters than green samples. The differentiation in setup comes mainly from the significant difference in hardness between green and post-treated samples. An overview of the parameter sets used in this study is given in Table 5.

**Table 5: Utilized parameter set for nanoindentation**

<b>Parameter</b>	<b>Green sample</b>	<b>Post-treated sample</b>
<b>Maximum load</b>	0.15 mN	1 mN
<b>Penetration depth</b>	1-1.5 $\mu\text{m}$	1-1.5 $\mu\text{m}$
<b>Measurement points</b>		
<b>Vertical measurement steps</b>	20 $\mu\text{m}$	20 $\mu\text{m}$
<b>Horizontal measurement steps</b>	20 $\mu\text{m}$	20 $\mu\text{m}$
<b>Horizontal measurement points for statistical validation</b>	3	3
<b>Measurement strategy</b>	Every 100 $\mu\text{m}$ layer to mid-cross-section	Statistical measurements with more layers on boundaries and fewer to mid-cross-section
<b>Surface extension on impression</b>	7x penetration depth	7x penetration depth
<b>Measurement control</b>	Force-controlled	Force-controlled
<b>Impression time</b>	2 min	2 min

## 5 Material development of tough photopolymers

One part of this study is focused on development of biomaterials towards higher toughness. An already developed vinyl ester-based photopolymer is enhanced with a carbonate monomer based on linear thermoplastic PCL. This carbonate-based additive divinyl carbonate (DVC) has a high molecular weight and can lead to network crosslink density-reduction. To specify the chemical compound in development, a symbol is assigned to it: M3\_DVC. The symbol is a combination of the main formulation M3 and the toughness agent DVC. Here, a generation-wise approach was conducted to optimise the material and deduct promising formulations of tough photopolymers that are both biocompatible and -degradable.

Polymers show distinct features depending on their physical properties. The characteristic curve of different polymer structures is presented in Figure 37. The red curve with strain hardening is the desired property of vinyl ester-based biomaterials with DVC since it would indicate high toughness.

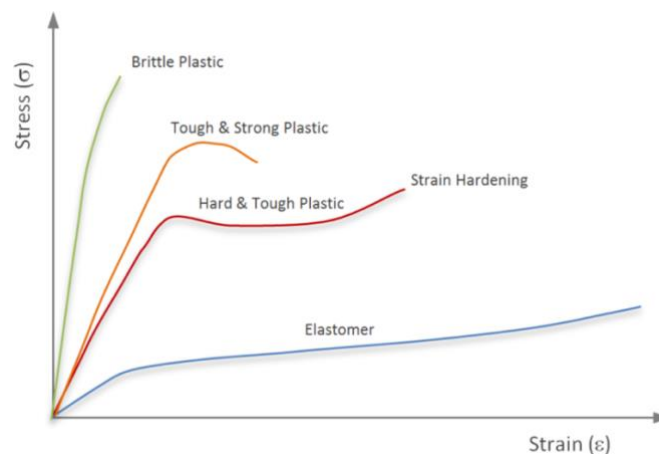


**Figure 37: Typical stress/strain-curves for duroplasts (green), thermoplasts (orange & red) and elastomers (blue) (Wu, 1992)**

This generational method can be divided into three phases. The first phase comprises the selection and feasibility of the molar mass of the additive. The effect of the molar mass of the DVC monomers on mechanical properties is investigated. The second phase comprises a statistical method that identifies the optimal weight distribution of the base matrix monomers in the compound in terms of toughness. This was achieved by a full factorial design. In the third phase, one formulation was selected for implementation tests and printability examinations. For this purpose, a tensile test, a Dynstat impact test and a dynamic mechanical analysis (DMA) were performed to determine the mechanical properties for. Moreover, a scaffold was printed via hot-lithography to showcase the printability of the developed material. Furthermore, gamma ray sterilization was conducted on printed parts to replicate the medical application requirements fully and to examine its effect on mechanical properties. This

chapter discusses the obtained results of material development towards tough photopolymers for bone tissue engineering.

## 5.1 DVC as toughness modifier

Divinyl carbonate (DVC) is a viscous and tough monomer that is believed to improve mechanical properties, especially the toughness. Consequently, we aim to blend this monomer into M3\_DVC to attain toughened photopolymers. To do so, the molecular weight and proportion of the monomer is decisive and needs to be analyzed. Therefore, we compare different compositions of M3\_DVC by analysing their mechanical properties.

### 5.1.1 Compound preparation

Table 6 shows the mix ratio of the formulation in weight proportion percentage. GDVA is the base monomer from which the other monomer weight shares are derived according to Table 6. This was based on previous work that displayed good biocompatibility and –degradability for such a vinyl ester-based photopolymer.

**Table 6: Chemical composition of M3\_DVC**

<b>M3_DVC</b>	<b>[wt%]</b>
<b>GDVA</b>	
<b>EGDVA</b>	6.2 %
<b>TMPMP</b>	2.8 %
<b>Pyrogallol</b>	0.02 %
<b>Ivocerin</b>	0.5 %

Added to the vinyl ester-based formulation is a vinyl carbonate additive with varying molecular weight and proportion. Two options are available: include DVC with a molar mass of either 25000 g/mol or 80000 g/mol. Furthermore, concentration of this additive may cause mechanical changes in the compound. Thus, we decided to test the material with 25000 g/mol with a 30 % and 20 % concentration, as well as the 80000 g/mol with a 5 % and 10 % concentration, respectively. A higher amount of DVC was due to its too high viscosity not possible. This means that four variations of the compound were tested to analyze and to identify the optimal combination.

The different components of M3\_DVC all have a specific function in the vinyl ester network. GDVA is a vinyl ester that functions as the base monomer for the compound. It distinguishes itself by its biocompatibility and –degradability in bone tissue engineering. Added to this is EGDVA to regulate the degradability further. TMPMP is a chain transfer agent that is added to delay gelation. At the gel point, a polymer loses its fluidity and forms a solid polymer network. Pyrogallol®, on the other hand, is an antioxidant that works as a radical scavenger in photopolymerization that is, in turn,

initiated by Ivocerin® in a free radical formation. Eventually, DVC is expected to be the component that improves the compound in terms of toughness as a carbonate-based additive.

The chemical compound was produced by blending the material to a desired batch size. The weight proportions of the respective monomers were derived from Table 6 and blended by using a precise scale. Then, the compound was exposed to heat treatment (60 °C) and mixing by magnetic stirring to complete blending. Afterwards, the viscous fluid was moulded to form the required shapes of the material tests. Subsequently, the moulded samples were cured in a UV-chamber by exposing them first to 60 s and 50 % intensity on each side. Then, intensity of UV was raised to 100 % for 300 s on each side. This ensures that the polymer cures gradually rather than rapidly as this would destroy its network. Lastly, the retrieved samples were manually grinded with abrasive paper to prepare it for mechanical testing.

In total, every configuration of M3\_DVC was tested with three tensile and Dynstat specimen each for statistical validation and one DMA specimen to determine storage modulus at room and body temperature, glass transition temperature, tensile strength, elongation at break and impact strength.

### 5.1.2 Mechanical properties of M3\_DVC with varying molar mass

After moulding the different compounds, we received four compositions that were named according to their molecular mass and their weight proportion in the compound. Table 7 explains the different descriptions:

**Table 7: Chemical composition of M3\_DVC**

DVC composition	Molar mass [g/mol]	Weight distribution [wt%]
M3_DVC25_20	25000 g/mol	20 %
M3_DVC25_30	25000 g/mol	30 %
M3_DVC80_5	80000 g/mol	5 %
M3_DVC80_10	80000 g/mol	10 %

Hence the samples were tested and the results evaluated to compare and analyze the effects of varying molar mass and amount of DVC shares on the mechanical properties of the compound.

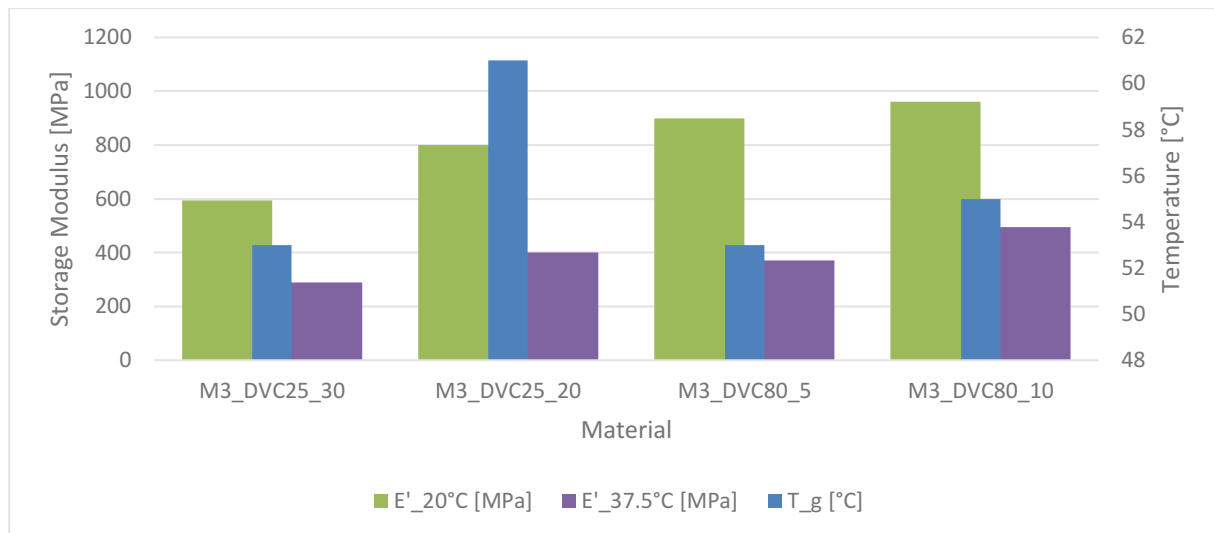


**Figure 38: DMA results for examination of molecular mass and amount of the carbonate additive**

The first test results of a DMA of material variations of the long-chain branch in Figure 38 show the storage modulus  $E'$  at different temperature settings. The y-axis is split into a primary and secondary axis representing  $E'$  and glass transition temperature  $T_g$ , respectively. The x-axis shows the four different material variations. The storage modulus and Young's modulus can be regarded as similar in terms of magnitude. Consequently, a high storage modulus indicates the ability of the compound to store deformation energy in an elastic manner. This is directly related to the extent of cross-linking; the higher the degree of cross-linking, the greater the storage modulus. Swelling is also directly related to the degree of cross-linking; the more cross-linking the more swelling will be restricted. Moreover,  $T_g$  should also be favourably high, so that there can be a broad range of usable temperature. It is notable that the storage modulus decreases steadily with higher temperatures. Remarkably,  $T_g$  is relatively high in M3\_DVC25\_20, so this should be investigated further and might be due to a measurement error. Omitting this compound, we see a gradual increase in  $T_g$  with an increase in DVC share and molecular mass. This trend is also observable in storage modulus over the compounds. All four compounds show a favourable visco-elasticity at room temperature (20 °C). However, the storage modulus decreases significantly at body temperature (37.5 °C), which is the application temperature and should, therefore, be taken as a reference for our biomedical purposes. Conclusively, M3\_DVC80\_10 shows the best mechanical properties compared to the other compositions.

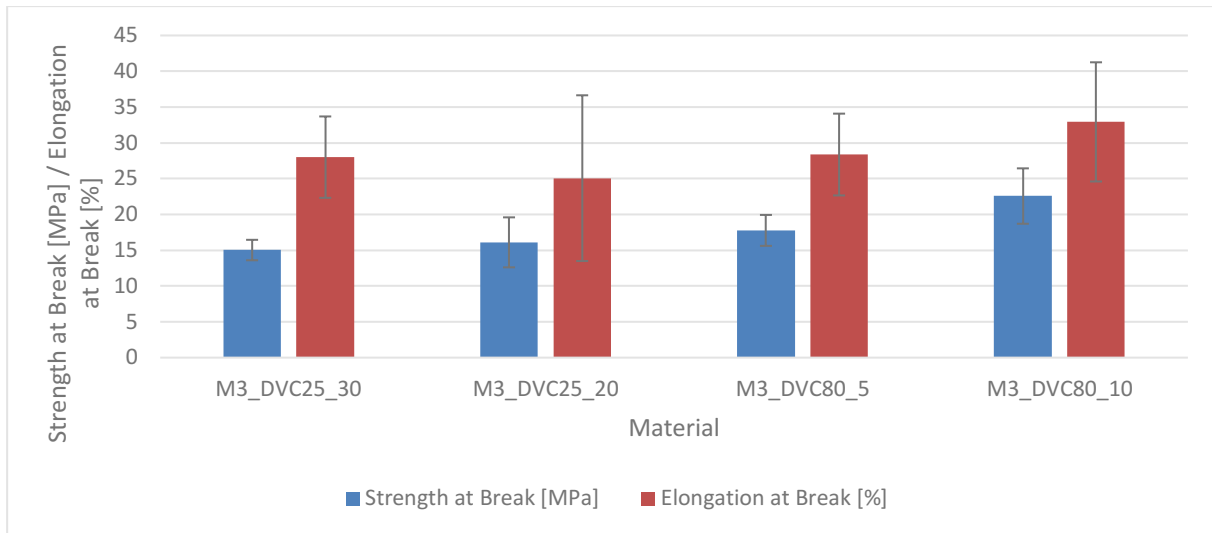


**Figure 39: Tensile test results for examination of molecular mass of the carbonate additive**

Next, the tensile test results for the four variations are shown in Figure 39. This bar graph shows the tensile strength in MPa and elongation at break in % of the different formulations. The bars show the standard deviation of the samples that were measured. Generally, the compound variations of DVC show distinguished mechanical properties in terms of elastic and plastic deformation and strength at break. The trends observed in DMA are coherent to the ones obtained by tensile test. Here, the variation M3\_DVC80\_10 is most favourable again.

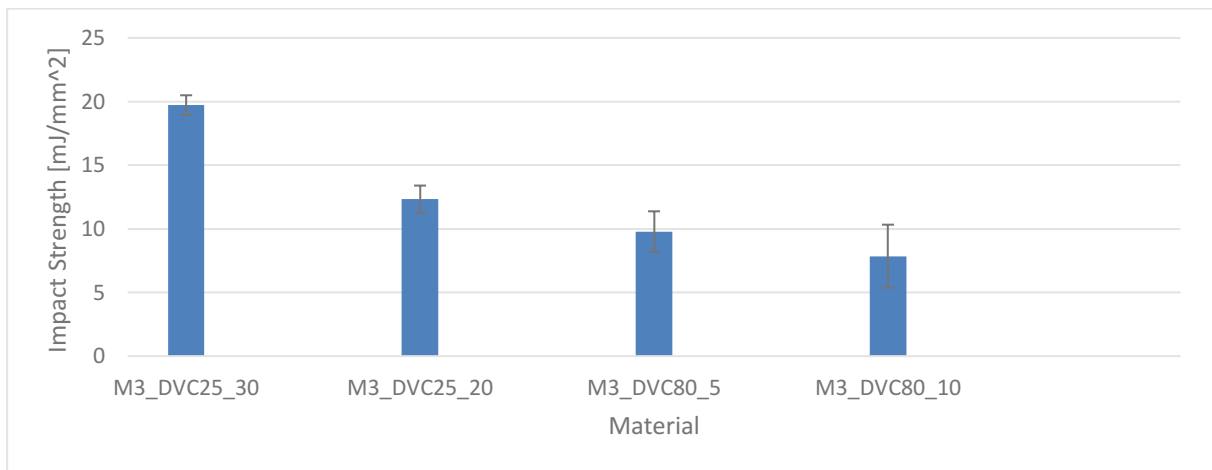


**Figure 40: Impact test results for examination of molecular mass of the carbonate additive**

The third mechanical examination on impact strength was conducted with a Dynstat configuration. High impact strength is required for bio-photopolymers to withstand sudden force change that happens in muscular activity. Figure 40 shows the results of the four variations. The y-axis shows the impact-strength of the respective material variations (x-axis). Conversely, the trend is reversed here and shows the compound with high molar mass DVC to have less impact strength. It can be seen, that here, the amount and less the molar mass is the critical parameter to increase the impact-

strength of the material, which leads to an optimized network structure with decreased crosslink density.

Summing up this section, it can be deduced that M3\_DVC offers a good starting point for the development of tough, biocompatible and -degradable photopolymers suitable for production of bone scaffolds. Compared to commercially available thermoplasts based on PLA, several benchmarks are already met while others need to be developed further. Succeeding material generations should focus on the increase of material toughness in terms of impact strength. Future experiments should focus on mixing different molar mass monomers (25000, 50000, 80000 g/mol and higher). Ultimately, the mechanical properties of the compounds with DVC80 show more favourable mechanical properties. Therefore, we decided to continue the material development with a long-chain branching of DVC80.

## 5.2 Base matrix analysis with factorial design

After analysing the effects of different high molar mass monomers on the mechanical properties of polymers, the base matrix of the selected compound was investigated via full factorial design (FFD). This reveals how the base components interact, which is important in order to optimize the mechanical properties along with enhancing them through post-processing.

A factorial experiment is a statistical concept to determine possible combinations of a set of factors; a design in which every setting of every factor appears with every setting of every other factor. A common experimental design is one with all input factors set at two levels each. These levels are called 'high' and 'low' or '+1' and '-1', respectively. As part of material development, a primary selection procedure for rudimentary formulation selection was done in FFD. The base matrix was altered to include a monofunctional vinyl ester monomer (10MV) for reduction of network density. The weight distribution of the vinyl ester monomers DVA, 10MV and vinyl carbonate DVC80 is presented in FFD in Table 8.

**Table 8: Full factorial design for base matrix**

	<b>-1</b>	<b>0</b>	<b>1</b>
<b>DVA</b>	10 %	15 %	20 %
<b>10MV</b>	15 %	20 %	25 %
<b>DVC80</b>	4 %	8 %	12 %

This outline of the factorial design is the basis for the weight distribution of the eight variations.

Table 9 displays the resulting variations from FFD. The base components DVA, 10MV and DVC80 (80000 g/mol) are varied according to FFD and filled up with GDVA. Added to this, is Ivocerin® with 0.5 wt% for curing the photopolymer through free radical polymerization.

**Table 9: Resulting wt% of Divinyl Adipate, Vinyl decanate and Divinyl carbonate from FFD**

Compounds wt% distribution	DVA	10MV	DVC80
M3_TS_DVC80_0	15 %	20 %	8 %
M3_TS_DVC80_1	10 %	15 %	4 %
M3_TS_DVC80_2	20 %	15 %	4 %
M3_TS_DVC80_3	10 %	25 %	4 %
M3_TS_DVC80_4	20 %	25 %	4 %
M3_TS_DVC80_5	10 %	15 %	12 %
M3_TS_DVC80_6	20 %	15 %	12 %
M3_TS_DVC80_7	10 %	25 %	12 %
M3_TS_DVC80_8	20 %	25 %	12 %

These different distributions are blended and moulded to test the materials. Specifically, impact strength, elongation at break and Young's modulus were analyzed. Still, the Young's modulus retrieved by tensile testing without suitable tensometer is not precise and should be evaluated with caution. The complex modulus from DMA is a more precise indicator of material stiffness. Nevertheless, this experiment is supposed to determine the optimal configuration of the base matrix towards toughness of the developed material and a tensile test suffices for this comparative examination.

Every compound variation was mixed to present a batch of 5 g each. From these batches, four samples of every variation for tensile test was moulded and post-processed by UV-chamber exposure. The used machine has a spectrum of 320-500 nm and an intensity of up to  $175 \frac{\text{mW}}{\text{cm}^2}$ . (Uvitron International Inc, 2018) Every sample was exposed at first to a 50 % light intensity for 60 s and afterwards inverted to repeat. Then, light intensity was increased to a 100 % ( $175 \frac{\text{mW}}{\text{cm}^2}$ ) for 300 s and inverted to repeat as well.

Subsequently, the samples were grinded manually on abrasive paper to eliminate incisions or notches that otherwise would adversely affect the results by premature fracture of the sample. Finally, the moulded samples were tested on tensile machine Zwick Z250.<sup>6</sup>

<sup>6</sup> [https://www.tuwien.ac.at/ausstattung/mechanische\\_charakterisierung/pruefmaschine\\_zwick\\_z250/](https://www.tuwien.ac.at/ausstattung/mechanische_charakterisierung/pruefmaschine_zwick_z250/) ; last visited 06.10.2018

### 5.2.1 Full factorial experiment

The eight configurations of the base matrix were examined via tensile testing. The formulations for the different DVC induced vinyl ester-based compounds were obtained by a full factorial design. The following diagram in Figure 41, Figure 42 and Figure 43 are accordingly the experiment results.

The x-axis in these diagrams represents the compound's eight variations developed by the full factorial design, while the y-axis shows, depending on the investigated parameter, a retrieved mechanical property. On the y-axis, the elongation at break, Young's modulus and tensile strength are presented in the respective units. The bar value consists of the mean value and standard deviation obtained by measuring four samples of each variation.

In comparison to previously developed vinyl ester-based bio-photopolymers the obtained results show promising mechanical properties, as they show higher toughness through an extended break elongation, good strength and Young's modulus. This speaks to the general applicability and suitability of this base matrix for biomedical application. The high standard deviation of the given values needs to be considered. However, this test's aim is to give comparative results that indicate the optimal base composition. Specifically, the Young's modulus obtained through tensile test on Z250 is known to be imprecise and is only practical as an indication. Therefore, the statistical quality of these results ultimately suffices for our purposes.

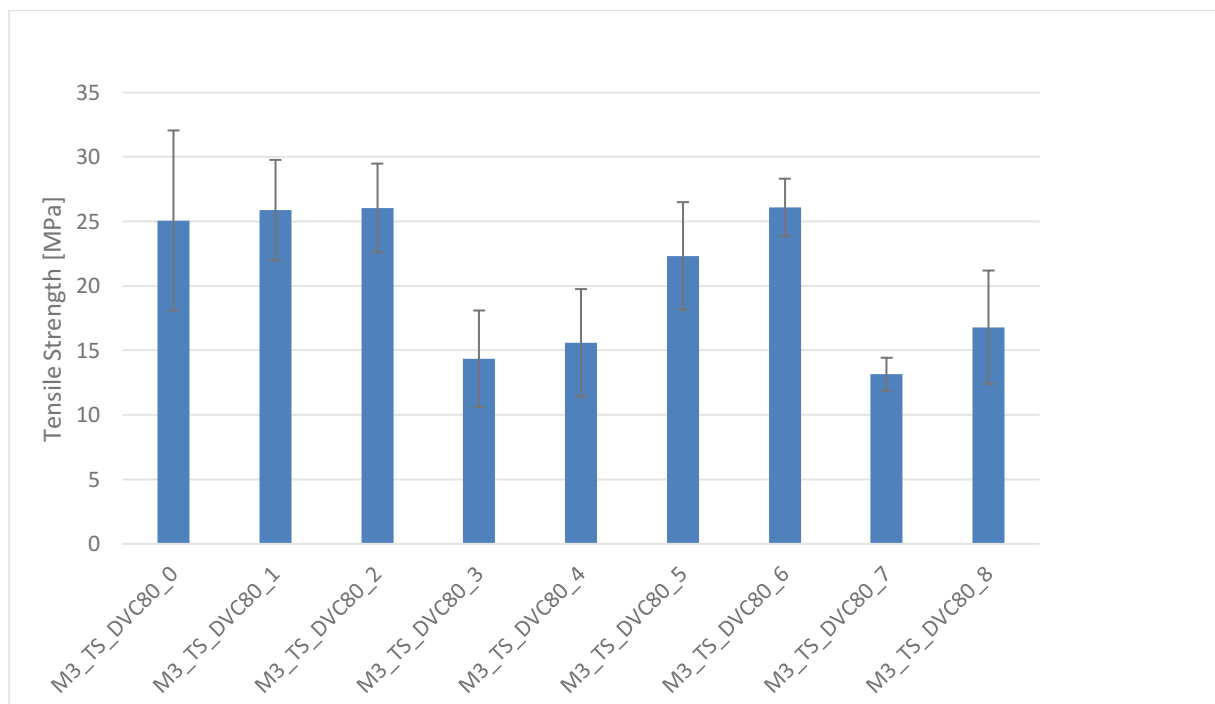
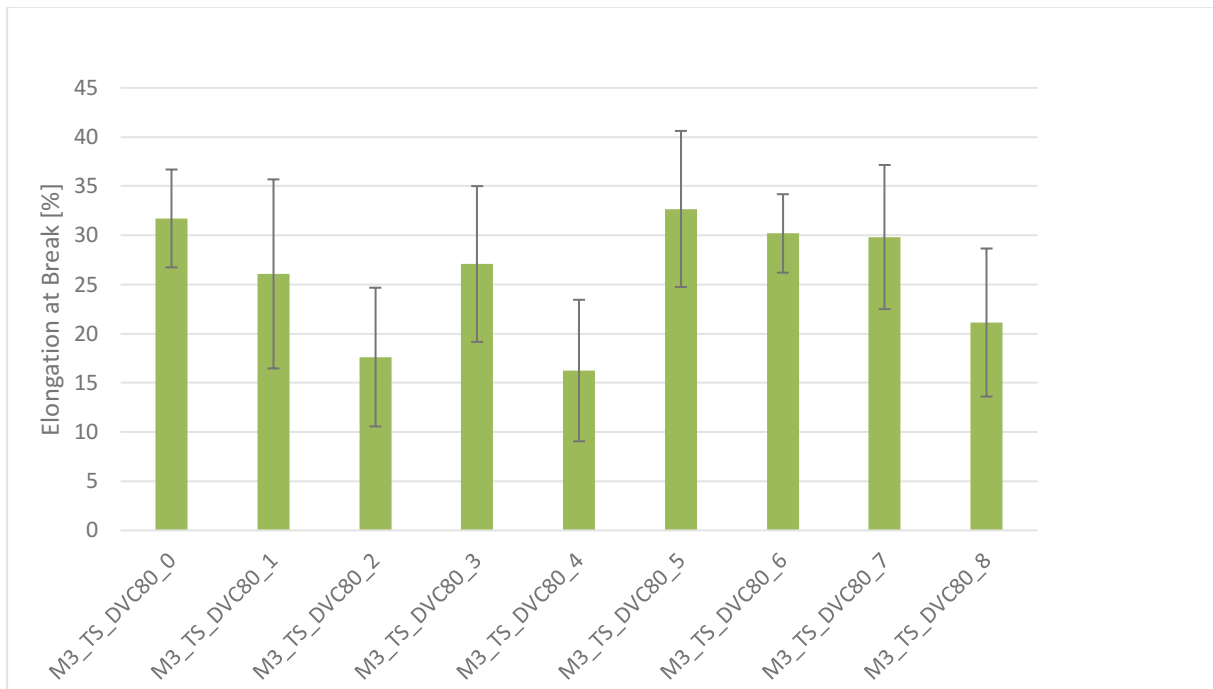


Figure 41: Tensile strength from factorial experiment

The results of tensile strength variation in Figure 41 show good, but also typical, tensile strength for vinyl ester-based materials. The first three formulations along with variation

M3\_TS\_DVC80\_6 show the strongest properties. The first three formulations distinguish themselves with relatively low ratios of DVC80, which is the toughening additive and thus, in larger portions, diminishes the strength somewhat. The exception to this is clearly M3\_TS\_DVC80\_6 with high strength values, despite 12 % of DVC80 in the compound. Moreover, it shows a low standard deviation, which further speaks to the quality of the result. As expected, the higher the amount of monofunctional 10MV monomer reduces the tensile strength of the polymer tendentially.



**Figure 42: Elongation at break from factorial experiment**

The strain values shown in Figure 42 generally indicate excellent values for biophotopolymers signaling the efficacy of divinyl carbonate. Considering the proportion ratios of 10MV, DVC80 and DVA in the different formulations, the formulations with higher ratios of DVC80 show higher elongation at break values, emphasizing this hypothesis.

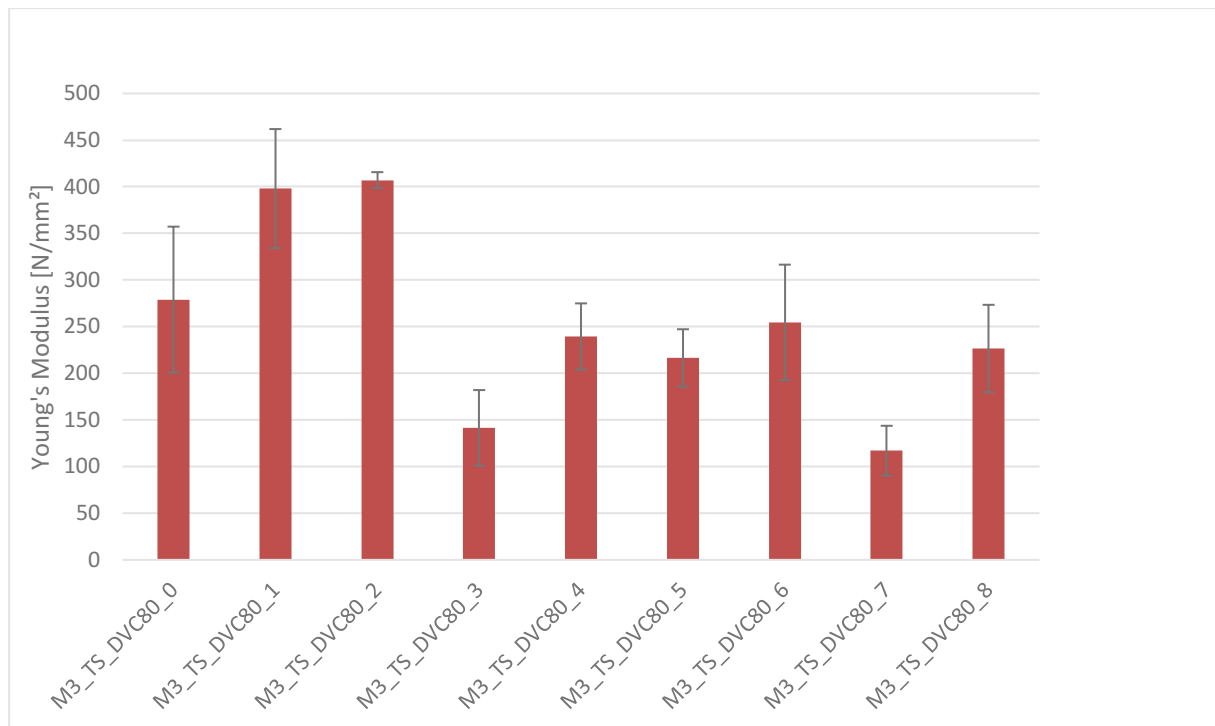


**Figure 43: Young's modulus from factorial experiment**

The Young's modulus shown in Figure 43 must be critically analyzed, as the parameter is better obtained from more reliable tests like DMA. However, the parameter was included in the full factorial experiment, as the objective was to optimize a base matrix and select a resulting formulation for further development. Having said that, M3\_TS\_DVC80\_2 shows the highest E with a low standard deviation. Moreover, even more distinct as at the tensile strength values, the softening effect of 10MV monomers to the polymer is visible. Nonetheless, a conclusive trend is difficult to derive from these results.

The aim was to improve all three parameters, which means to increase elongation at break and strength simultaneously, without losing too much of the stiffness of the material. Through these tests, we identified three interesting formulations that qualify for further development. These are M3\_TS\_DVC80\_0, M3\_TS\_DVC80\_5 and M3\_TS\_DVC80\_6. However, only one formulation was selected for further experiments. Overall, the material M3\_TS\_DVC80\_6 showed the most potential along with low standard deviations. A low standard deviation promises a stable range for the actual characteristic values. Moreover, the formulation combines a high Young's modulus with break strength and elongation; the most from all variations.

### 5.2.2 M3\_TS\_DVC80\_6

As a result, we analyzed the rest of the properties of M3\_TS\_DVC80\_6 based on the first-generation measurements. The results are shown in Table 10. This vinyl ester-based material shows promising properties in terms of toughness and can be

commercially viable for certain medical applications. A full description of mechanical properties of the developed biopolymer is presented in the following.

**Table 10: Mechanical properties of M3\_TS\_DVC80\_6**

<b>M3_TS_DVC80_6</b>		
<b>Parameter</b>	<b>Unit</b>	<b>Value</b>
<b>Tensile strength</b>	[MPa]	22.697
<b>Elongation at Break</b>	[%]	24.73
<b>Young's Modulus</b>	[MPa]	250.45
<b>Impact Strength</b>	[mJ/mm <sup>2</sup> ]	9.0215
<b>Glass Transition Temperature</b>	[°C]	72
<b>Storage Modulus at 20°C</b>	[MPa]	775
<b>Storage Modulus at 37.5°C</b>	[MPa]	512.5

In Figure 44, Figure 45 and Figure 46, the developed toughened bio-photopolymer is related to the benchmark compound M2 (GDVA based bio-photopolymer, Dissertation Hofstetter 2019). The base matrix of M2 resembles M3\_DVC and is distinguished by its biocompatibility and –degradability as well. It does not, however, have vinyl carbonate additive that enhances toughness.

The diagrams show the mechanical properties of both compounds to emphasize the increase in toughness achieved by the addition of DVC. The compared properties are: glass transition temperature, elongation at break, tensile strength, storage modulus at body temperature and impact strength. The x-axis consists of the two compounds: the reference formulation from previous research and the developed toughened photopolymer.

The clear increase in the values of the properties can be observed in all parameters except impact strength. However, the addition of a vinyl carbonate additive leads to increased cross-linking which leads, in turn, to increased strength of the polymer network. The results in elongation at break compare favourably to the well-established thermoplastic PLA in biomedical applications, which directly links to material toughness favourably. Ultimately, M3\_TS\_DVC80\_6 has improved roughly in +64 % in  $\sigma_B$ , +88 % in  $\epsilon_B$ , +26 %  $E'_{37.5^\circ\text{C}}$ , +25 % in  $T_g$  and declined -22 % in  $a_n$  compared to the benchmark M2.

DVC demonstrates photoreactivity on a level or even above (meth)acrylates. Furthermore, much lower cytotoxicity as well as degradation via a surface erosion mechanism qualifies it for medical use. (Mautner, Steinbauer, Russmüller, et al., 2016)

Thus, the hypothesis that the addition of carbonate-based additive leads to an increase of material elongation in vinyl ester-based photopolymers can be confirmed.

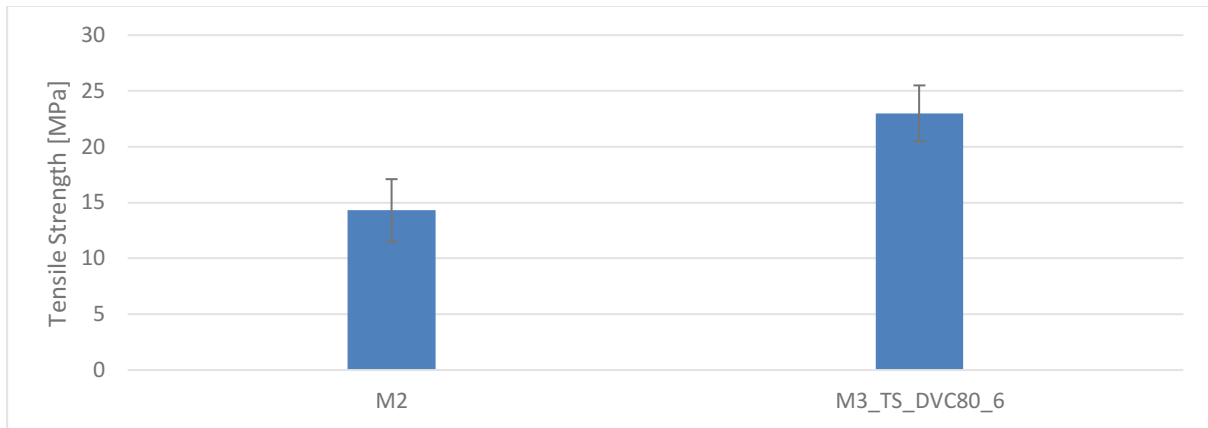


Figure 44: Benchmark and developed material – Tensile Strength

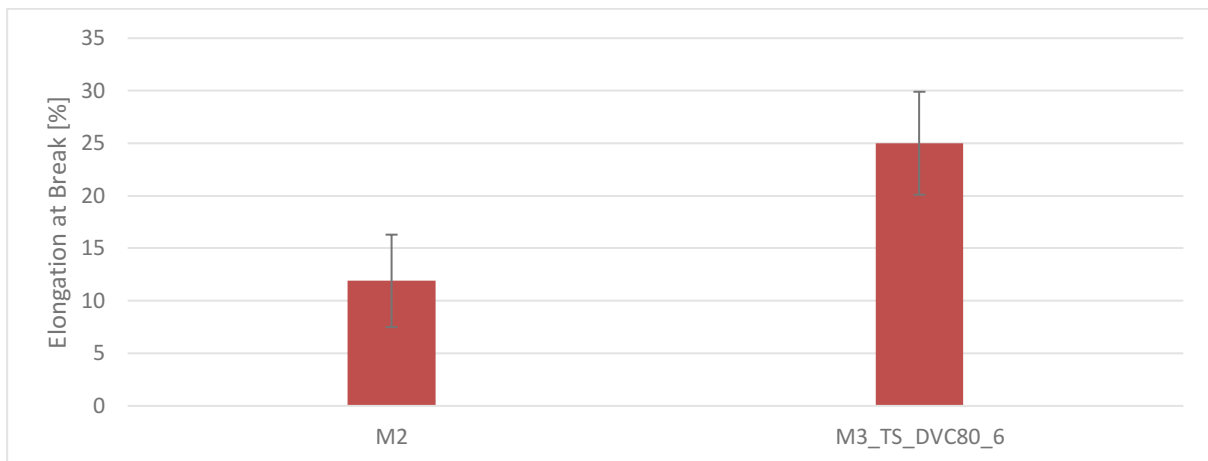


Figure 45: Benchmark and developed material - Elongation at Break

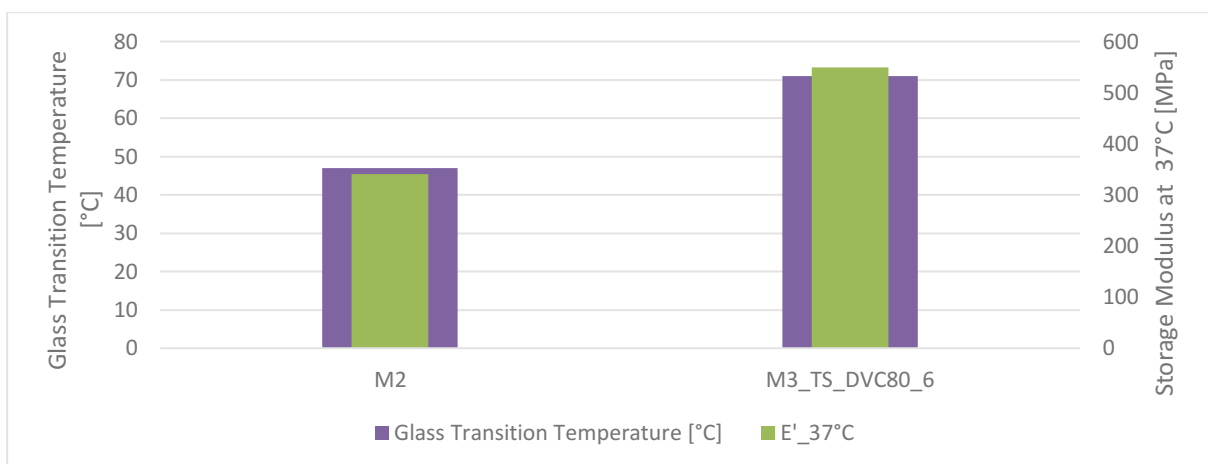
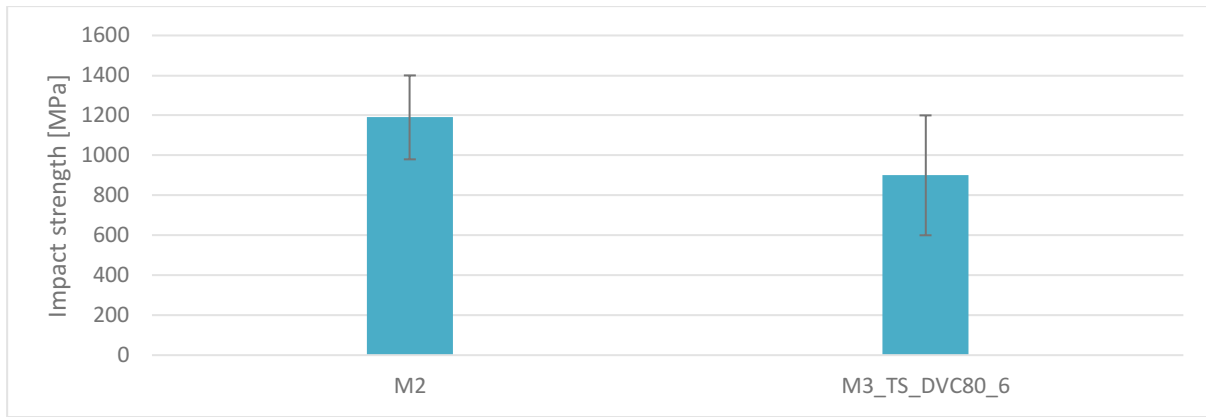


Figure 46: Benchmark and developed material -  $T_g$  &  $E'_{37^\circ\text{C}}$



**Figure 47: Benchmark and developed material - Impact Strength**

If we analyze the compound in relation to state-of-the-art biopolymers things change. In our case, we determine the toughness of the material in terms of its elongation capability and impact strength. In comparison with mechanical properties of an established thermoplast, the compound does not quite reach the level of established biopolymers like PLA (see Table 1). (Wang, Gramlich, & Gardner, 2017) Even acrylate based polymers show significantly tougher properties, but lack the prerequisites defined in this thesis. Acrylate based biomaterials are fast curing and show better reactivity leading to better properties in strength compared to vinyl ester-based compounds. (Hofstetter et al., 2018) However, they are often brittle due to their reactivity and do not have the same biocompatibility as the developed formulation. Most importantly, the main shortcoming of these acrylate resins is the high cytotoxicity of residual unreacted acrylate groups. (Heller, Schwentenwein, Varga, Liska, & Stampfl, 2009)

### 5.3 Application perspective of developed material

The third and final phase of the material development consists of a two-level analysis: the effect of post-processing, specifically gamma sterilisation, on mechanical properties as well as buildability via digital light processed lithography-based additive manufacturing technology (DLP L-AMT). Hence, the consistence of the chemical compound M3\_TS\_DVC80\_6 was amalgamated again to have a batch for a new iteration of material testing and rapid prototyping. Thus, the material is printed in a process that is thermally treated due to the high viscosity of the vinyl ester-based photopolymer. This “hot-lithography” technology ensures the fluidity and even distribution of the resin in the vat during the printing process. In the following, preparation methods that went into the material and the mechanical properties of gamma sterilised and printed components are discussed.

### 5.3.1 Material preparation

To compare moulding and printing methods and their effects on mechanical properties and buildability, we mixed two batches of formulation M3\_TS\_DVC80\_6. The compound formula requires an additional light absorber to ensure printing of parts with overhanging structures with L-AMT. A high amount of LA in a compound leads to increased mechanical properties at a constant curing depth. (Hofstetter et al., 2018) For printing methods, we decided to integrate Quinoline Yellow as a light absorber with a 0.12 % share. The batch was harmonised by magnetic stirring for an hour at 65 °C.

The mould batch has the same identical composition as the previous generation and its specimen moulded accordingly via UV chamber. The prepared samples for the different mechanical tests were exposed to post-processing that leads to gamma sterilization. The proceedings for material preparation can be derived from 5.1.1.

### 5.3.2 Mechanical properties of gamma-sterilized material

Following the formulation development towards toughness, the mechanical properties are examined in comparison to their reference material and to non-sterilized material. The gamma sterilization of material leads to further cross-linking in the material, which in turn leads to tougher materials. The developed material M3\_TS\_DVC80\_6 was sterilized after printing and then tested under the specification name M3\_TS\_DVC80\_6\_sterile. The most important findings are summarized in Table 11.

**Table 11: Mechanical properties of the sterilized, toughened compound**

<b>M3_TS_DVC80_6_sterile</b>		
<b>Parameter</b>	<b>Unit</b>	<b>Value</b>
<b>Tensile strength</b>	[MPa]	38.6
<b>Elongation at Break</b>	[%]	21.8
<b>Impact Strength</b>	[mJ/mm <sup>2</sup> ]	10.04
<b>Glass Transition Temperature</b>	[°C]	>80
<b>Storage Modulus at 20 °C</b>	[MPa]	1250
<b>Storage Modulus at 37.5 °C</b>	[MPa]	900

In Figure 48 to Figure 51, the development of the mechanical properties of the printed, sterilized compound is shown in comparison to related compounds to illustrate the improvement towards toughness. Here, the most important parameters of the tests are given. The y-axis shows  $\sigma_B$  and  $a_n$  in MPa and  $\frac{\text{mJ}}{\text{mm}^2}$ ,  $\epsilon_B$  in %, while  $T_g$  in °C and  $E'_{37.5^\circ\text{C}}$  in MPa on a secondary axis of the materials is given in the x-axis, respectively. The materials presented are, on the one hand, the reference photopolymer M2 and, on the other, the developed M3\_DVC formulation. Both their properties are presented alongside their gamma sterilized counterparts. Therefore, the effect of gamma sterilization can be observed along the overall development of tough vinyl ester-based photopolymers.

The developed M3\_TS\_DVC80\_6\_sterile shows significant improvement of strength and elongation at break in comparison to reference photopolymer M2, which goes back to the introduction of DVC into the formulation.  $T_g$  is with above 80 °C significantly above body temperature. The absolute value for the sterile compound could not be determined as the heat ramp during DMA was set to a maximum of 80 °C. Consequently, this illustrated bar for  $T_g$  indicates that it is above this temperature. Furthermore, the storage modulus at body temperature is quite high, although not reaching entirely the heights of M2\_sterile. A clear trend is visible where a decrease in network crosslinking density leads to a lower  $E'_{37.5^\circ\text{C}}$ . Moreover, the impact strength is significantly lower than in normal and sterilized M2 despite a significantly higher elongation at break. This aligns to the trend of previous generations of M3\_DVC that showed improved ductility but poorer impact strength. This could be the result of inaccuracies resulting from an exceedingly heavy hammer (20 kpcm). Interestingly, the test speed has that much influence on the mechanical behaviour of the material.

Chances were, that the sterilisation process might have adverse consequences on brittleness of the compounds, but the opposite was the case. The results illustrate the overwhelming positive impact of  $\gamma$ -radiation on mechanical properties of the printed samples. The final conversion and strength of the whole volume of the part can be reached with radiation treatment alone. Therefore, sterilization is deemed a necessary part of the post-processing routine to guarantee best mechanical properties. A detailed investigation of the restrictions of curing depth of light at the post-curing process was done in the second part of the thesis.

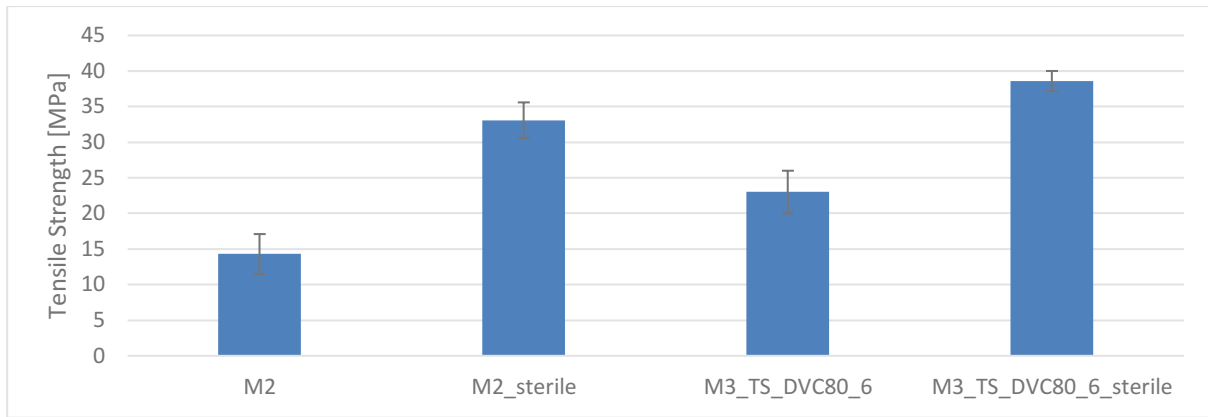


Figure 48: Tensile strength development

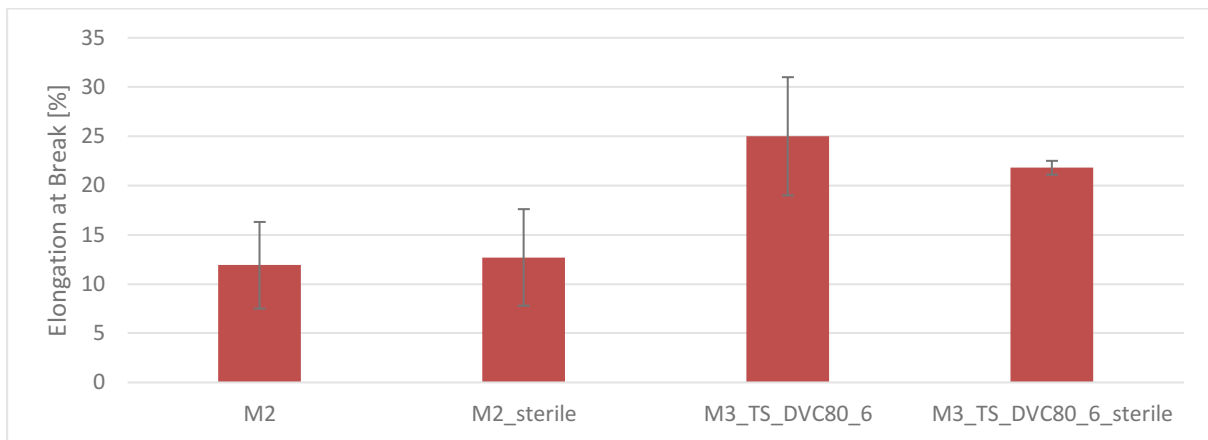


Figure 49: Elongation at break development

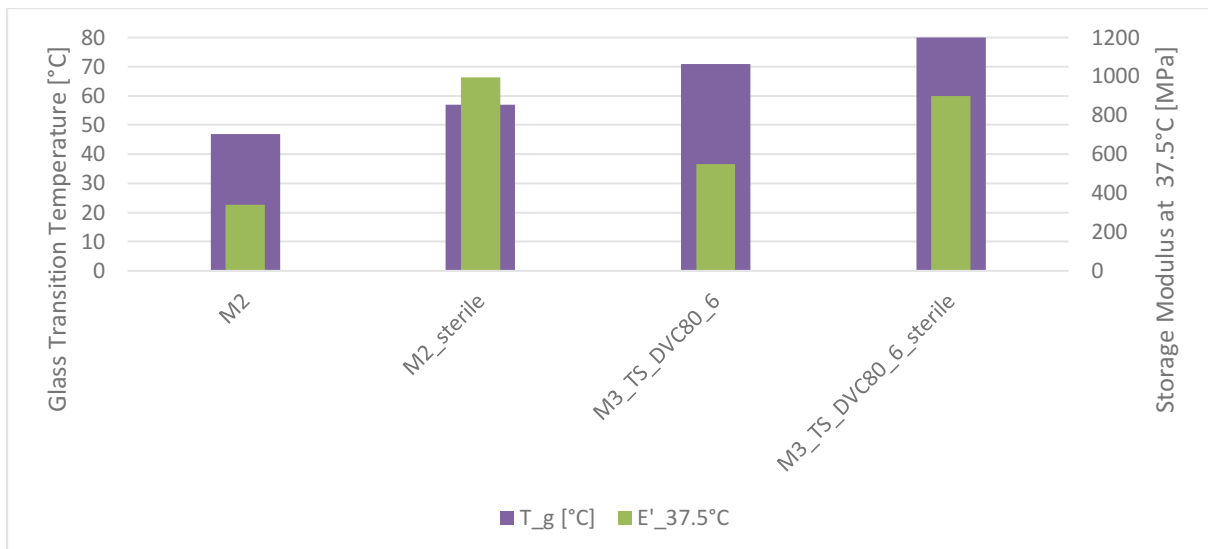


Figure 50: T<sub>g</sub> and Storage Modulus development

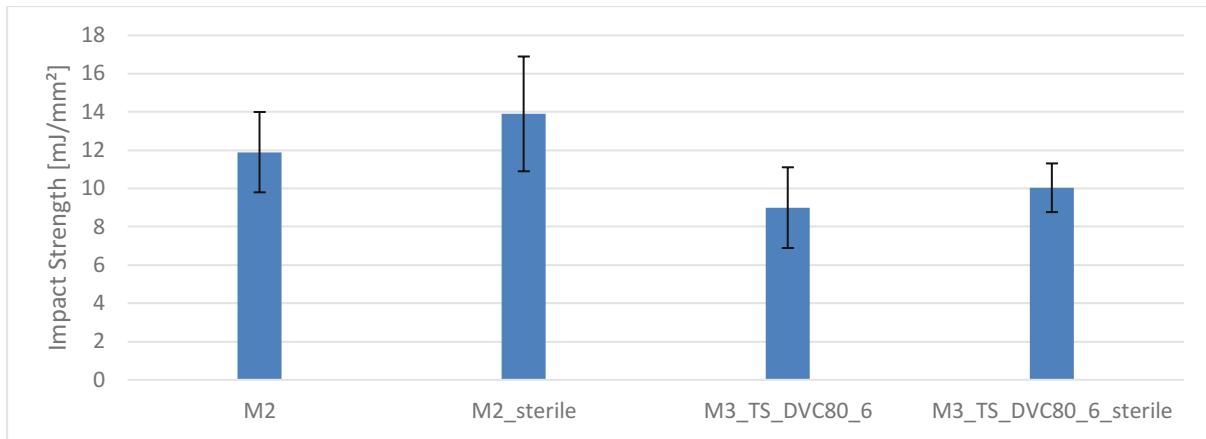


Figure 51: Impact strength development

### 5.3.3 Printability of tough photopolymers with hot lithography

To develop material that is manufactured by rapid prototyping, a model was built to showcase the printability of the material and its functionality for bone tissue engineering. A practical part was, thus, developing a scaffold for bone tissue engineering.

Due to the high viscosity of the developed compound, printing was a challenge. The model tended to detach from the building plate after contact to the vat was lost. This occurs when the surface adhesion of the resin does not suffice and the interlaminar bonding between the printed layers is not strong enough to withstand the detachment stress. Moreover, the small nature of the model made such a porous and detailed scaffold prone to over-curing in unintended areas.

As we used the same resin as for the measurement samples, the light exposure time was set to 15 s, which represents a curing depth of 75  $\mu\text{m}$  at a 25  $\mu\text{m}$  layer height. The exposure duration was derived from the resins' Jacobs working curve. The method is described in more detail in 6.1.3. For this structure, a foundation plate was added to the CAD model in the configuration process to improve the adhesive force during the printing process and function as a support to the scaffold. Due to the high viscosity of the resin formulation, the vat was constantly heated to 60  $^{\circ}\text{C}$  to ensure fluidity and even distribution in the vat during the print job. Moreover, the alignment of the object on the building plate was chosen in a way to improve its adhesive bond and decrease detachment stress. Ultimately, the printing process for a print job took approximately six hours. Yet, the printed scaffold is relatively small in scale (0.4x0.4x0.4  $\text{mm}^3$ ), which speaks to the slow curing speed of vinyl ester-based formulations.

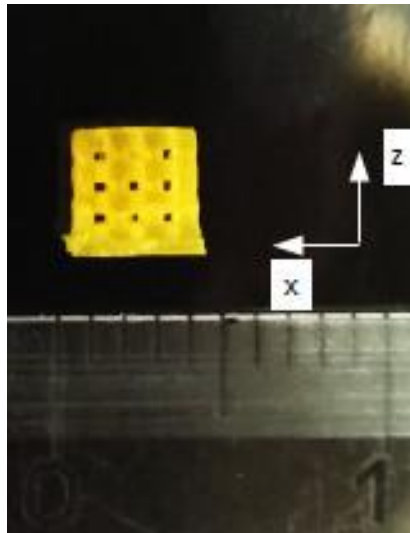


Figure 52: Scaffold printed from M3\_DVC80\_6

Figure 52 shows the printed scaffold with theoretical pore size of 500  $\mu\text{m}$ . The coordinate system shows the z-stage which was the building direction of the part; whereas the x-axis indicates the direction of coating during printing. Such a scaffold is a challenge to print, due to its requirements of high resolution and the interconnecting porous system. The porosity of the printed scaffold was observable, with minor over-polymerization. However, to remove unnecessary resin manually posed a challenge, especially because of the high viscosity of the uncured resin which is present in the pores of the scaffold direct after printing. The degree of porosity directly affects other properties of the scaffold such as mechanical stability. Therefore, its value should always be adjusted to the mechanical needs of the tissue that is going to be replaced. (Salgado et al., 2004). What is more, the quality of the print can be massively improved by further adjusting cure depth and exposure time iteratively. Also, by replacing the transparent, glass building plate with an opaque, aluminium plate the bond between the printed part and the building platform can be improved massively. Yet, improving the printing quality of the material was not the focus of this study.

## 5.4 Conclusions for results of material development

The material development conducted in this study attempted to improve mechanical properties of already established biocompatible and –degradable compounds in terms of toughness. Specifically, vinyl ester-based biopolymers for additive manufacturing were developed and printed with DLP L-AMT. In this section, the most important findings of the development of these materials are discussed.

The challenge of developing material for bone tissue engineering lies in the saturation of three vital variables: biocompatibility, -degradability and mechanical properties. All three variables are sought after in bone replacements but are rarely found in a material. For example, acrylate based photopolymers have fast curing speed and thus are easier

to print. On the other hand, vinyl ester-based photopolymers show less cytotoxicity by a factor of 100. (Heller et al., 2009) Consequently, the right formulation that adheres to bio-responsiveness and printability is difficult to find. The approach in this study was a vinyl ester-based photopolymer that was developed towards higher toughness in an iterative approach.

During the development of the compound M3\_TS\_DVC80\_6, GDVA based photopolymer with high molar mass vinyl carbonates blend showed a significant increase in mechanical properties in comparison to reference vinyl ester compounds. The addition of a high molar mass monomer to the compound that is characterized by toughness has proven to increase toughness of the entire material. Nevertheless, the mechanical properties can be improved further by variable modification, i.e. reducing network density. The results of the comparison of the two molecular masses of DVC (80000 and 25000 g/mol) show that DVC 80000 g/mol might provide higher values in strength and elongation at break. However, the 25000 g/mol of DVC suggest enhanced impact strength. Perhaps a combination of the molecular masses can retrieve further improvement towards overall mechanical properties due to a heterogenic polymer network.

Furthermore, it was shown that the base matrix of a vinyl ester-based compound (GDVA, DVA, 10MV and DVC) also plays an important role in the mechanical features. The base matrix configuration via full factorial design resulted in an optimized ratio distribution of the monomers in the compound that supports toughness.

Moreover, the application of vinyl ester-based bio-photopolymers in bone tissue engineering was demonstrated by printing an exemplary bone scaffold with pore size of 500  $\mu\text{m}$  via hot lithography AMT. The highly viscous resins lead to a difficulty in the printing process due to delamination, where the part breaks off the vat. Also, the porous structure contained residual resin that is difficult to remove post-curing due to the small scale and precision of the model. In its extreme form, too much exposure to UV curing and temperature can lead to the evaporation of 1-functional monomers, which, in turn, leads to brittleness. Hence, the printing process for hot lithography AMT of viscous photopolymers and especially the cleaning process must be optimized further to improve the quality of the part. Nonetheless, the developed material adheres to the requirements of biocompatibility and –degradability, as well as improved mechanical properties and can be printed for application.

Lastly, the positive influence of gamma sterilization on mechanical properties on vinyl ester based photopolymers was demonstrated, signaling the importance of this process in terms of improvement of mechanical properties, independent of wall thickness and part volume.

## 6 Material characterization via nanoindentation

In this study, a layer analysis of DLP L-AMT printed parts was performed. Therefore, measurements of the cross-sections of layers were conducted to evaluate the effect of Light Absorber (LA) and post-curing treatment on mechanical properties of vinyl ester-based photopolymers. Preliminary tests showed a possible heterogeneity of mechanical properties of the single layers of a printed part and as well as a gradient from surface to the inner volume, which are, both, supposed to be strongly influenced by the amount of Light Absorber.

Vinyl ester-based monomers are both biodegradable and –compatible and, thus, can be amalgamated to a polymer network suitable for application in bone tissue engineering. However, the mechanical properties must be developed in terms of strength and toughness. Also, vinyl ester-based photopolymers lack reactivity and show slow curing speed in comparison to acrylates. Consequently, vinyl ester-based bio-photopolymers are rather difficult to print. This is mainly due to insufficient interlaminar bonding, which may lead to the part breaking from the building plate. (Hofstetter et al., 2018) Moreover, heterogeneous mechanical properties of the printed layers obstruct part quality.

This assumed heterogeneity of layers has a gradient that transpires due to the penetration of irradiance into previously printed layers. It is assumed that this layer behaviour can be homogenized by adequate LA weight and adjusted post-processing with light or gamma radiation. Consequently, to improve the printing quality and understanding of DLP L-AMT printed bio-photopolymers, an investigation of layer heterogeneity via nanoindentation is conducted.

In this section, a compound is investigated via nanoindentation as a new approach to characterize photopolymers based on cure depth. In the following, we will consider the material preparation conducted, specifically targeting cure depth. Afterwards, we will discuss the results of nanoindentation testing on the material and the characteristic behaviour of the compound. Lastly, we will reiterate the conclusions from the measurements.

### 6.1 Material preparation

Precise and diligent material preparation is arguably one of the most important steps in material science. Planning and outlining the experimental steps in the lab is fundamental for the validation of measurements. In the following, we will look at the blending and composition of the material, cure depth ( $C_d$ ) and print job conditions. The print job defines one sample manufacturing run and its conditions like .STL-file, parameters and print speed.

### 6.1.1 Material blending

A chemical compound consists of several components and must be mixed together to show new, enhanced mechanical properties. The chemical compound that was used for these measurements was developed with my direct supervisor Dipl.-Ing. Christoph Hofstetter. Liquid (DVA, 10MV TMPMP) and solid components (Pyrogallol®, Ivocerin®) are mixed under 70 °C with the required weight distribution. It has been found that this heat range does not harm vinyl ester-based photopolymers and maintains its structural and mechanical properties. The basic components of the formulation with their weight distribution are outlined in Table 12.

**Table 12: Compound composition of MP3\_LA**

MP3_LA	
Monomer	[wt%]
DVA	66.66%
10MV	33.33%
TMPMP	11.16%
Pyrogallol®	0.02%
Ivocerin®	0.5%

Four different mixtures are produced with a dilution method to attain batches with 0 %, 0.04 %, 0.08 % and 0.12 % light absorber proportion (LA-0 % ...). This method is done with two batches, one with a 0.12 % distribution of light absorber, and the other batch without light absorber altogether. The blend of the different compounds is shown below in Table 13.

**Table 13: Dilution method via cross-over rule for LA-wt%**

LA-wt%	Target		Actual	
	0.12 % [g]	0 % [g]	0.12 % [g]	0 % [g]
LA-0.12%	12	0	12.8862	X
LA-0.08%	8	4	8.0101	4.0027
LA-0.04%	4	8	4.004	8.0065
LA-0%	0	12	X	18.45663

### 6.1.2 Cure depth

To print the model from a photopolymer resin, the right exposure configuration for the print process must be determined. Hence, we defined the desired cured depth of a layer we aimed for and determined the exposure duration at a certain irradiance intensity. Cure depth represents the height of solidified photopolymer after exposure of a photopolymerization without restrictions. To ensure sufficient interlaminar bonding during printing, the actual cure depth must be higher than the layer height. A possible

method to avoid delamination is to increase the exposure and subsequently the cure depth. (Lee et al., 2001) This leads to increased polymerization, which in turn, improves the adhesion and mechanical properties of the solidified layer. However, that harms the printing resolution because of over-curing, predominantly in the building direction. Thus, increasing the cure depth is not an option, especially when printing complex scaffold structures or patient specific implants for biomedical applications. (Hofstetter et al., 2018)

The relationship of cure depth to irradiance of DLP stems from the working curve of a photopolymer. Numerous parameters are found to influence the final monomer-to-polymer conversions of these systems, such as temperature, light intensity, monomer functionality and reactivity, and photoinitiator concentration. Though, the roles of these parameters on cure depth, as opposed to overall bond conversion, have not been fully examined. (Lee et al., 2001)

At SLA, which is similar to DLP, a beam is scanned across the resin surface, it cures a line of photosensitive resin to a depth. The shape of the cured line depends on resin characteristics, laser energy characteristics, and the scan speed (which is equivalent to the exposure time at DLP).

This is based on three key assumptions (Jacobs, 1992):

- The resin conforms to the Beer-Lambert law of exponential absorption
- The SLA irradiance scattering is Gaussian
- At gel-point, the resin moves from the liquid phase to the solid phase

Consequently, the relationship between cure depth  $C_d$  [ $\mu\text{m}$ ] and exposure  $E_{\text{max}}$  [ $\frac{\text{mJ}}{\text{cm}^2}$ ] is expressed through the working curve equation:

$$C_d = D_p \ln\left(\frac{E_{\text{max}}}{E_c}\right)$$

Equation 12

Creating the Jacobs working curve has become the basis for testing and characterizing new photocurable resins by generating a semi-logarithmic diagram with  $C_d$  in y-axis and  $E_{\text{max}}$  in x-axis results in a straight line. The intersection of the x-axis and the Jacobs working curve is the critical exposure  $E_c$  - seen in Figure 53 - which is related to the gel point of the resin. As the photosensitive resin is exposed with light, it solidifies to a cure depth  $C_d$  when the total energy exceeds  $E_c$ . If the energy was insufficient, no solidification takes place, which means exposure is less than  $E_c$ . Moreover, the penetration depth  $D_p$  is derived from the slope of the curve. Since  $D_p$  and  $E_c$ , are purely resin parameters, the slope and intercept of the working curve are independent of power. (Gibson et al., 2010)

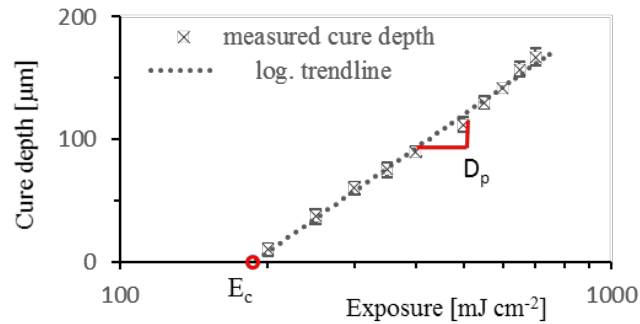


Figure 53: Typical Jacobs working curve (Hofstetter et al., 2018)

### 6.1.3 Defining $C_d$ via working curve

To determine the exposure duration for constant  $C_d$  in the printing process of the different compounds of the measurement batch MP3\_LA, the cure depth is examined in relation to time while the irradiance intensity was constant at  $84 \frac{\text{mW}}{\text{cm}^2}$ . To create the Jacobs working curves for the different mixtures, a vat was filled (3 mm fill height) with photopolymer formulation. Square geometries ( $5 \times 5 \text{ mm}^2$ ) with a hole of 1 mm diameter in the center were cured without constraints. Every square was cured with the same intensity of  $84 \frac{\text{mW}}{\text{cm}^2}$ , whilst the exposure times were varied. Residual resin was removed from the vat and the surface of the cured squares was cleaned with compressed air and solvent (ethyl lactate). Afterwards, the thickness of cured material was measured with a Kroeplin C110T (5 mm radius contact size) external thickness gauge. Hence, the exposure duration for the three formulations was determined from the Jacobs working curve illustrated in Figure 54.

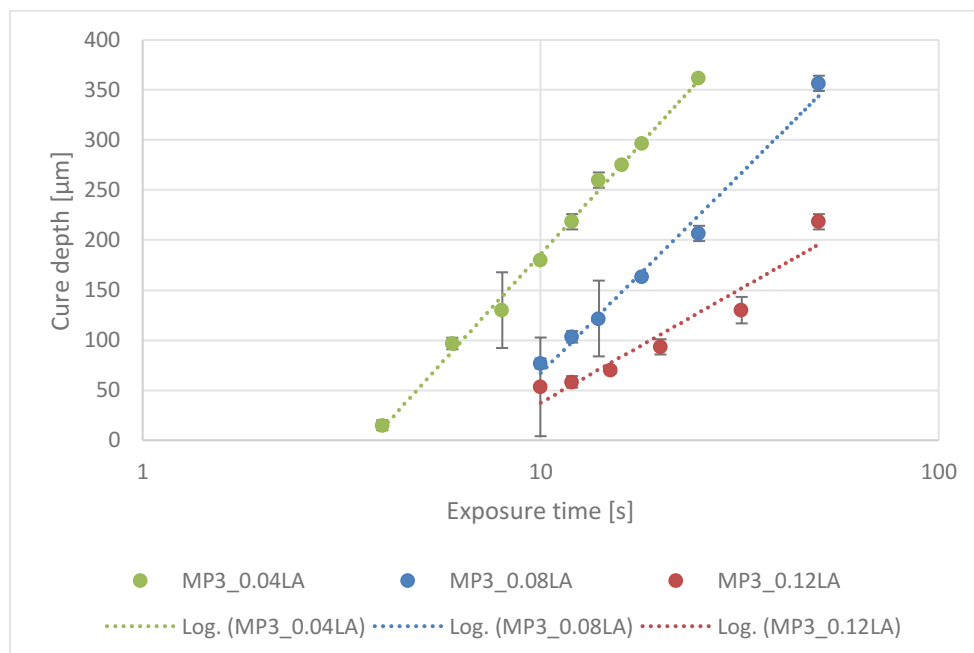


Figure 54: Cure depth of MP3\_LA with 0,5wt% Ivocerin®

The created working curves shows the cure depth in relation to exposure time. Cure depth  $C_d$  is measured in [ $\mu\text{m}$ ] and exposure time in [s], whilst presented in a semi-logarithmic scale. This is because the x-axis is logarithmic, while the y-axis is not. Clearly, the cure depth increases logarithmically with more exposure. The different colour markings of the scatter plot represent the different compounds. The standard deviation is also indicated, as for each point and exposure duration three samples were measured. These are the results for materials with a photoinitiator proportion of 0.5 %. A previous examination with PI 0.25 % did not achieve the targeted  $C_d = 200 \mu\text{m}$  for printing procedure for these light absorber shares. Based on this, the material taken for nanoindentation tests were polymerized with Ivocerin® 0.5 wt%.

The measurement supports the theory that penetration depth of photopolymers is inversely correlated to the weight proportion of light absorber in the compound. That's means, higher light absorber ratio means less penetration depth.

Thus, we calculated the needed exposure duration from the working curve equation (Equation 12). To achieve the targeted layer height of  $100 \mu\text{m}$  in the printing process, we exposed the compound to light for a duration that retained a cure depth of  $200 \mu\text{m}$ , to ensure a sufficient interlaminar bonding between the single layers. In Table 14, the exposure time and penetration depth are calculated representatively for each formulation and given in seconds and  $\mu\text{m}$ . This retrieved exposure duration was set in the parameter settings for the printing process of each compound. Evidently, the duration increased for the compounds with more light absorber weight.

**Table 14: Exposure duration and penetration depth for  $C_d = 200 \mu\text{m}$**

Compound	Working equation	Exposure duration [s]	$D_p$ [ $\mu\text{m}$ ]
MP3_0.04LA	$y = 190\ln(x) - 251.57$	10.679	190
MP3_0.08LA	$y = 172.18\ln(x) - 329.3$	21.631	172.18
MP3_0.12LA	$y = 98.364\ln(x) - 189.06$	52.212	98.364

Obviously, the exposure duration of the compound without light absorber is omitted from the list. MP3\_0LA is expected to cure very rapidly and over-polymerize, which leads to imprecisions in the model. In experiments conducted to determine the required duration of UV light processing of these materials, the high cure depth was evident. In Figure 55, the high penetration depth which resulted in high rate of polymerization can be observed. To establish the cure depth analogous to the procedure for the material with light absorber, liquid solvent was printed to form square geometries that help establish the Jacobs working curve. The height of the square geometries should vary depending on exposure time. With experiments for the compound without light absorber, a variation in height was not observable due to the high degree of polymerisation. The variation would have been needed to derive the Jacobs working

curve. Ultimately, the compound is solidified but unsuitable for accurate printing due to over-polymerization. This confirms the need of light absorber in formulations that are printed via DLP L-AMT.

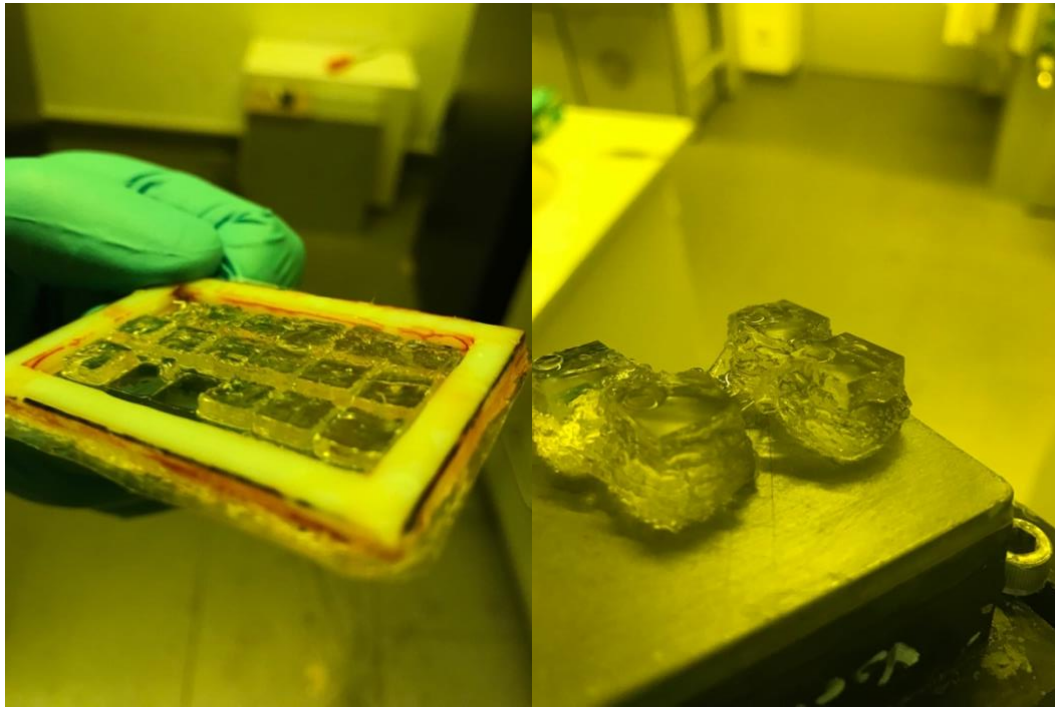


Figure 55: High polymerization of photopolymers without light absorber component

#### 6.1.4 3D-printing of test structure

To print a part via L-AMT, a CAD model has to be designed (cube 10x10x10 mm<sup>3</sup>) and converted into a .STL-file. The aim was, to investigate differences of hardness between printing layers along the building direction (z), and thus the proper sectional plane is significant. Hence the placement and position of the sample in the vat needs to be considered. Therefore, markings were added for better orientation as seen in Figure 56. The model was designed with CATIA V5 and converted to a .STL-file for the printer software to process.

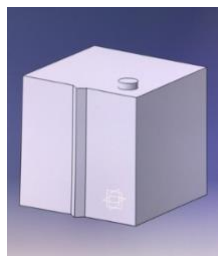
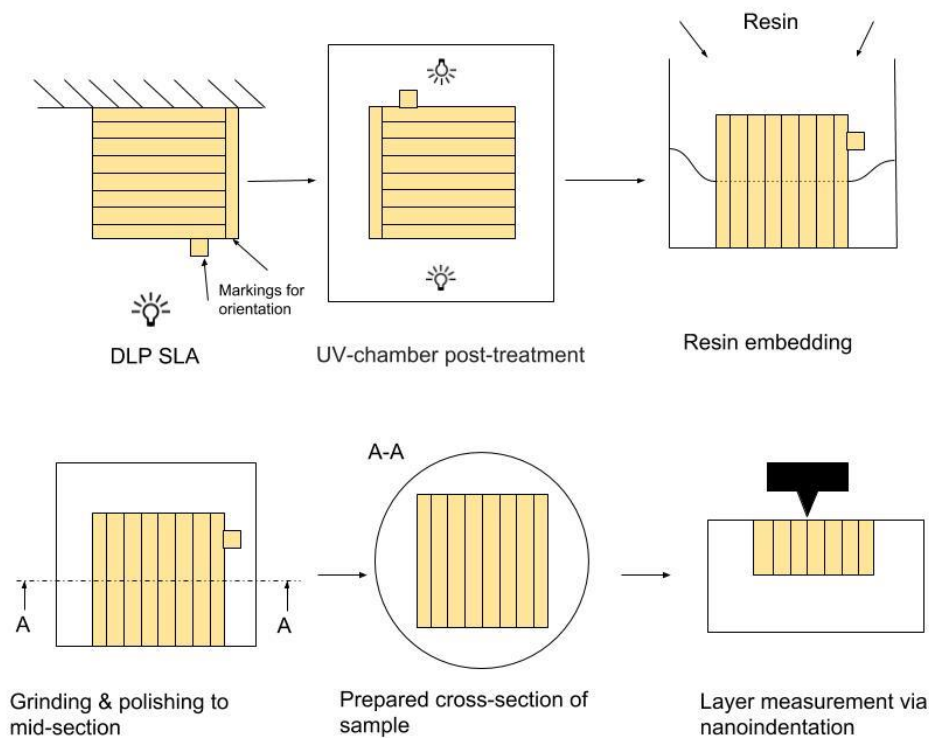


Figure 56: CAD model for printing process

Subsequently, the parameter set was configured with the light intensity and calculated exposure duration. The entire printing job was then completed under room temperature. On average, one printing process printed six models simultaneously and

had a print duration of about three to four hours depending on exposure time per layer retrieved from the Jacobs' working curve. Although the process was automatic, a continuous observance of the machine was important as complications may have occurred. The contact-removal of building plate and resin vat could have especially lead to difficulties that would have necessitated premature termination of the job.

The formulations of MP3\_LA have a liquid consistency at room temperature making scraper and thermal heating unnecessary during printing. The liquid spread evenly in the vat after a layer was printed and a separate coating step was not necessary, which significantly reduced the whole job duration. Figure 57 shows the schematic process from printing to nanoindentation in terms of sample preparation.



**Figure 57: Schematic preparation process for layer hardness examination**

### 6.1.5 Post-processing

After the print process of the samples was successfully completed, the post-processing step began. The first step entailed removing extra material that was built along the printed object by manual tools like pliers or razor blades. Then the probes were further photopolymerized by broad band light exposure in a UV chamber. Here, the first exposure with 50 % intensity for a minute was conducted to introduce mild exposure. After that, a more intense and longer exposure was steered with 100 % intensity for 300 s. This was repeated after inverting the sides of the sample to guarantee a constant exposure and full polymerization over the built layers.

To ensure practicality and handling, the sample was embedded in a resin as shown in Figure 58. The resin was an epoxy resin 37-127, along with hardener 37-615 from Farben Wolf®. This epoxy resin reacted with the polyfunctional hardener and formed a thermosetting polymer with high strength as well as high thermal and chemical resistance. The liquid mixture had to be treated in a vacuum to ensure that no air bubbles remain in the resin. The epoxy resin adhered to polishing procedure pressures for our purposes. It did not necessarily have to be transparent, as these samples were only used for testing. Nonetheless, the used resin was transparent and presented overall adequate hardness.

To analyze the differences in compound indentation modulus layer-by-layer, the cube had to be positioned in a way that ensured all layers were apparent. Then grinding and polishing were conducted until the mid-section of the cubicle in the resin as shown in Figure 57. As the cubicle has 10x10x10 mm<sup>3</sup> dimensions, grinding and polishing was done to 5 mm height of the cube in the resin to reach the mid-sectional pane. Grinding and polishing is an extremely important step to achieve a surface that adheres to nanoindentation criteria. A surface should be flat, scratch-free and smooth. An elaborate program with several steps was developed to realise the required surface form. The better the surface is prepared, the better and more precise the measurement is possible. Grinding and polishing of the sample was done with a TegraDoser-5 machine from Struers. The semi-automatic machine prepared samples using silicon carbide abrasive paper and had a disc diameter of 300 mm and speed up to 300 rpm, as well as a water in- and outlet. The program for our cross-section is presented in Table 15.

**Table 15: Program for grinding and polishing cross-section; DP-P: DP-Suspension P is a very high performing diamond product containing exclusively polycrystalline diamonds**

Process	Granulation/ Suspension	Lubricant	Time [min]	Disc Velocity [rpm]	Single Sample Force [N]	Sample Holder Force [N]
1	1000	Water	2	150	10	60
2	2400	Water	1	150	10	30
3	4000	Water	1	300	10	30
4	DP-P 15µm	Lubricant	6	150	10	60
5	DP-P 3µm	Lubricant	6	150	10	60

The resin embedded sample was then ready for nanoindentation measurements. A sample is shown in Figure 58. The scratches and cracks on the cross-section were not caused from grinding and polishing but likely emerged during the printing process or detachment of the vat due to the brittleness of the material. These surface errors had to be avoided during nanoindentation measurements to retain accurate results.



Figure 58: Embedded and polished sample

### 6.1.6 Microscopic images

After post-processing, the samples were analyzed under the microscope to examine the cross-section, particularly on a layer basis. Furthermore, the images of the measured series made it possible to locate suitable measurement points that were scratch- and crack-free on the cross-section during the nanoindentation measurement when linear measurement along the building direction was not possible. They also served to assign the correct formulation of the measurement series MP3\_LA to its associated sample.

Due to additional light induction in the UV chamber, the surface of the sample was expected to show an increased hardness and indentation modulus in contrast to inner regions. In contrast, a green sample theoretically leads to an increase of hardness in the centre of the digital light processor on the photopolymer surface. It decreases along the direction away from its centre. (Xu, Imamura, & Nakagawa, 1997b) A green sample refers to cross-sections that have been directly embedded in resin after the print job without irradiation treatment and thus not exposed to post-processing.

The microscopic images of the tested cross-sections of the batch show similarities regarding surface composition: all have major or minor scratches and cracks filled by resin after embedding. This might be a result of post-process treatment and high inner stresses of the material after UV-light exposure. More importantly, the composition of the material MP3\_LA and its physical properties suggest high brittleness. However, the characterization of layer heterogeneity did not require the development of the mechanical properties towards application during L-AMT and are, thus, not the focus of this study.

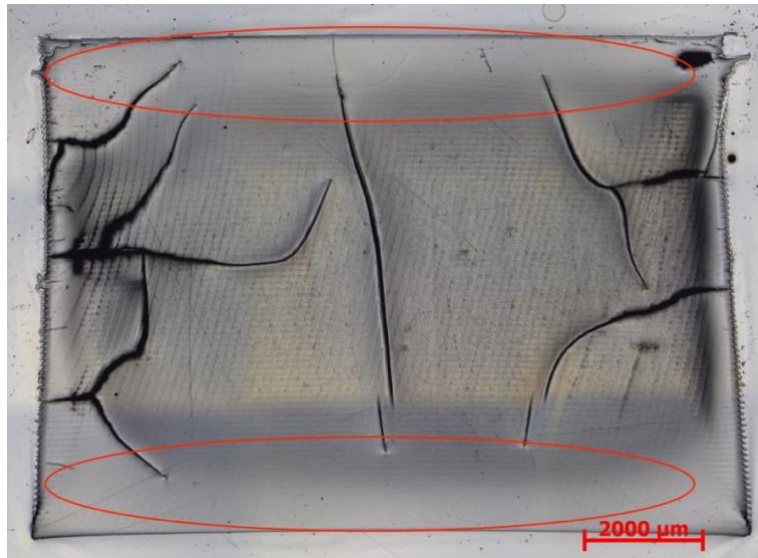


**Figure 59: Peripheral homogeneity of UV-induced photopolymers; example: MP3\_0.12LA\_2x300s**

In Figure 59, a sample microscopic image of the batch is presented. The homogenous boundaries in Figure 59 are encircled to emphasize the visual disparity from UV light post exposure. On the bottom-right side of Figure 59, the scale of the image is noted. The microscopic image shows the cross-section of MP3\_0.12LA\_2x300s (sample nr. 18). The homogeneity of the boundaries, on which the UV light was introduced on, is strongly visible. This probably stems from the refractive index heterogeneity of the compound, which describes how light propagates through it. The density of the material varies over the compound due to different polymerisation state (double bond conversion) and is higher on the boundary due to post light hardening. Another possibility is, that due to different polymerisation state in the polished area, the surface morphology is aligned to hardness, which results in the heterogenic visible effect. Furthermore, a material shrinkage of the part is also visible, which goes back to the to the warping mechanism inherent to L-AMTs. As photopolymers are printed, they initially expand somewhat but contract as they cool down. (Gibson et al., 2010) Moreover, the singular layers that comprise the sample together are visible on the vertical outline of the cross-section (spikes at the outer edge). Here, the layer principal of AMTs can be remarkably observed that is, otherwise, hidden to the naked eye.

## 6.2 Layer heterogeneity of cross-section

To investigate the research question, we look at the indentation modulus of the prepared samples, which also indicates the hardness of the material. Through this procedure, it will be evaluated whether the indentation modulus increases on the peripheries of a printed model via L-AMT and if layer heterogeneity varies depending on LA wt% in the compound.

### 6.2.1 Principal of the nanoindentation measurement

Figure 60 shows the principal scheme of the nanoindentation measurement of our 3D printed parts that were embedded in resin along with its representative measurement results. The yellow cross-section is lined to illustrate the layer-by-layer concept inherent to AMT. The black dots represent measurement points that are condensed representatively and indicate that every layer (100  $\mu\text{m}$ ) has 10 measurement points along the build pane (every 10  $\mu\text{m}$ ), with three horizontal measurements for each of these indents done for statistical validation. Scratches and cracks are represented as well as the starting position of the measurement on the boundary.

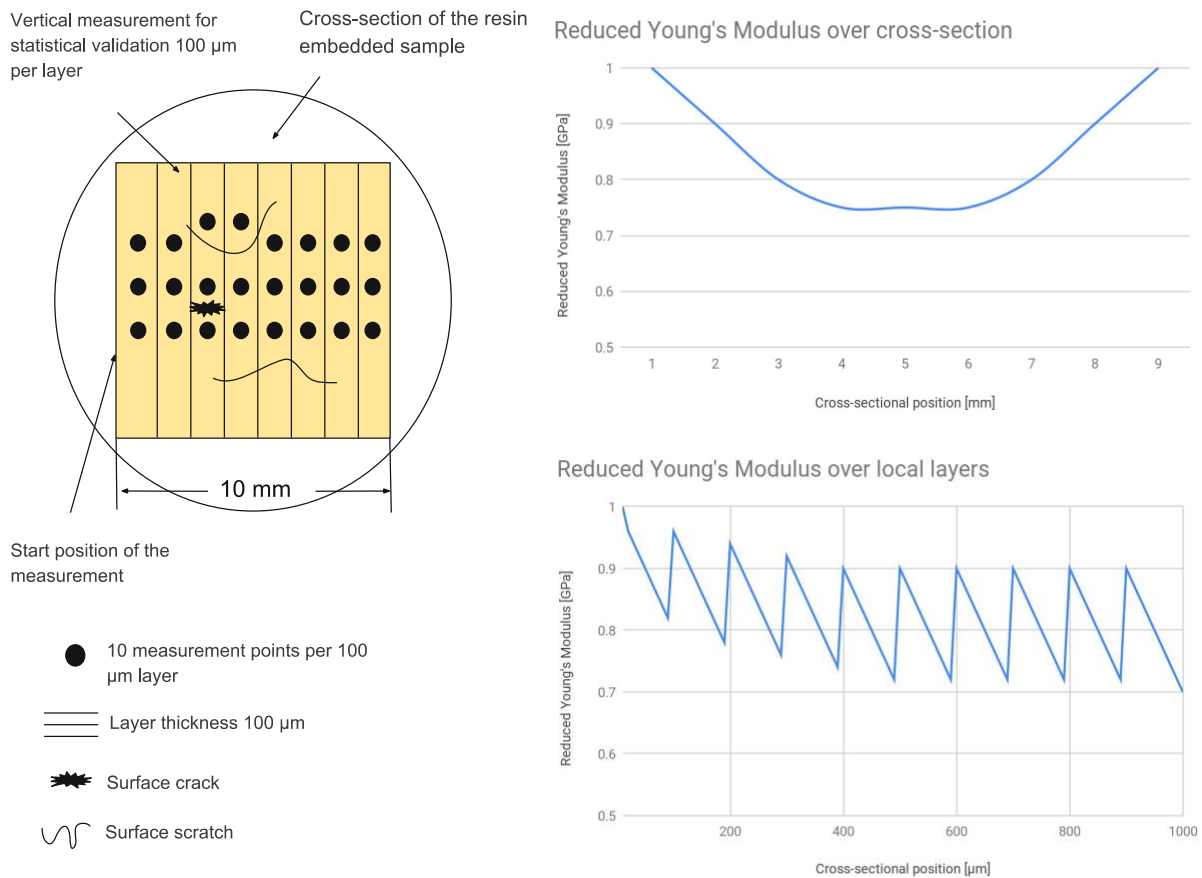


**Figure 60: Schematic view of measurement process & expected  $E_r$  behaviour over cross-section**

As our layer thickness for the print job was 100  $\mu\text{m}$ , the 10 mm cube was built with a total of 100 layers. Conversely, the inner indentation differences in one layer (local gradient) were to be investigated, which means that several points were measured within one layer to show if indentation modulus is influenced in one layer. It was assumed, due to indentation module decrease with layer height, that the indentation module per layer will result in a so-called sawtooth slope. Therefore, we decided to measure three points vertically (same layer height) to get an average with standard deviation. This was recommended for every indentation measurement and was adjusted in the parameter set accordingly. The measurement starting point was on one

boundary of the sample in the center pane with 20  $\mu\text{m}$  distances in horizontal direction unless scratches and cracks necessitated different distances between the measurement points.

The diagrams in Figure 60 show the expected indentation modulus over the cross-section. The first diagram shows the expected global gradient of the curve, while the second one shows the expected indentation modulus behaviour over the first 10 layers of a post-cured sample. The results of the nanoindentation deliver a lot of variables such as indentation depth but are omitted for the indentation modulus that designates hardness of the compound.

### 6.2.2 Global layer behaviour

In this section, we will discuss the results of the nanoindentation measurement of printed cross-sections. The results of the formulation MP3\_0.12LA\_2x300s are shown as an example. The measurement results of the other formulations are also discussed to derive general conclusions of light absorber impact and post-processing on layer heterogeneity. These diagrams can be found in the appendix.

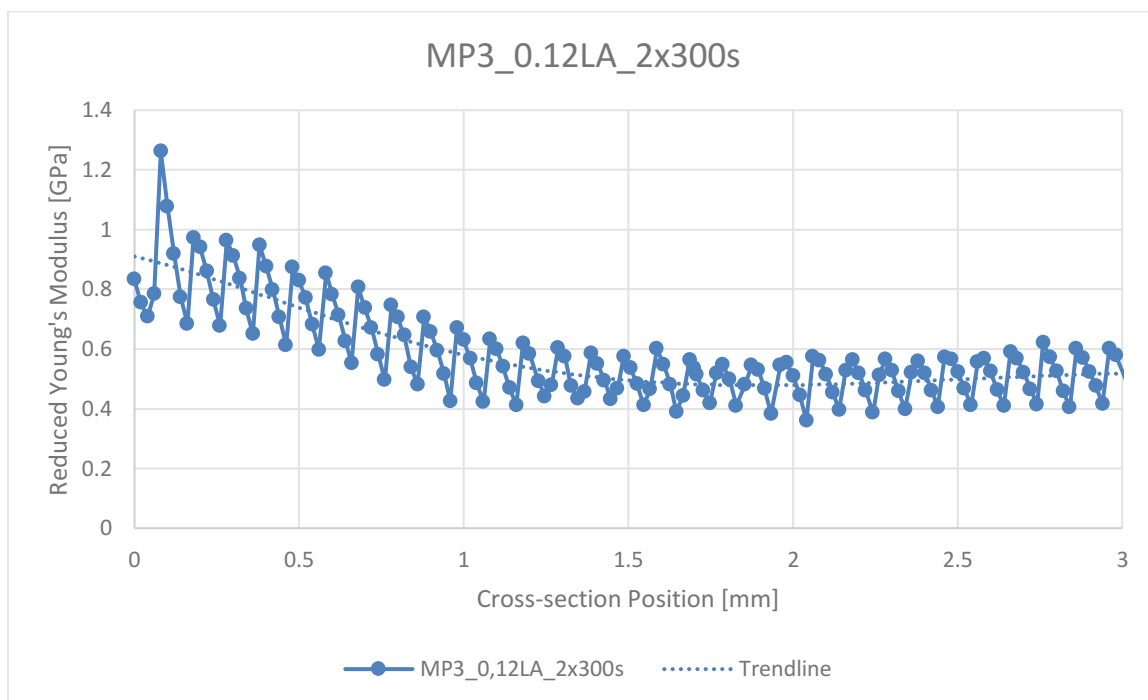


Figure 61: Cross-section hardness over layers

In Figure 61, an exemplary nanoindentation of the measured photopolymer MP3\_0.12LA\_2x300s is shown. The abscissa represents the value of the cross-section position in mm, meaning the position of the measurement point along the print direction. The full cube would lead to 10 mm, but this specific measurement was only conducted to half of the cube because of the symmetry of the problem in terms of part geometry, post-curing and resulting  $E_r$ . The UV post-curing was done on both areas

that lay in printing direction of the samples evenly. Measurements on other samples that measured the whole cube confirm the symmetry in indentation modulus. Even so, the ordinate represents the indentation modulus, or reduced Young's modulus,  $E_r$  in GPa, which correlates with hardness as has been previously discussed. The blue graph shows the indentation modulus in relation to layer position, while the dotted curve is the sixth polynomial order of the blue graph and indicates the global gradient of the indentation curve.

As expected, a single layer is cured through 460 nm exposure and the indentation modulus decreases with the layer height, due to decreased light intensity caused by light absorbance based on Beer-Lambert law:

$$E_{\lambda} = \log\left(\frac{I_0}{I_1}\right) = \varepsilon_{\lambda} \cdot c \cdot d$$

Equation 13

$I_0$ ...Intensity before the medium [ $\frac{\text{mW}}{\text{cm}^2}$ ]

$I_1$ ...Intensity behind the medium [ $\frac{\text{mW}}{\text{cm}^2}$ ]

$T = \frac{I_0}{I_1}$ ...Rate of transmission

$\varepsilon_{\lambda}$ ...Decadic extinction coefficient (material property for specific wave length) [ $\frac{\text{L}}{\text{mol}\cdot\text{cm}}$ ]

$c$ ...Substance concentration [ $\frac{\text{mol}}{\text{L}}$ ]

$d$ ...Layer thickness [cm]

This phenomenon is visible in the complete layer. After coating, the plate moves back to printing position and the next layer prints atop the former one. This explains the decline of the indentation modulus within a layer itself. The spike in the curve before the next round number is because the reference point at the beginning of the measurement was not precise. The highest indentation modulus value indicates that a new layer starts at this point and should be treated as such.

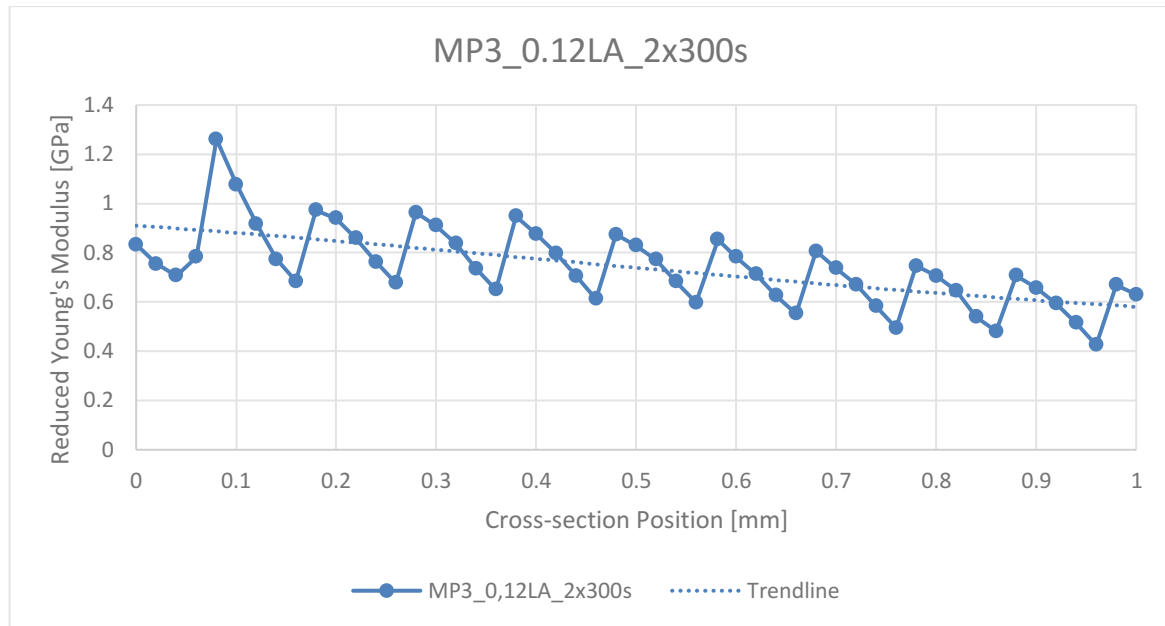


**Figure 62: Detailed indentation curve over 10 layers**

Figure 62 presents the same results of MP3\_0.12LA\_2x300s, but for ten peripheral layers this time, to illustrate and emphasize the local gradient. This is essentially a zoomed-in version of the previous diagram in Figure 61. In this illustration, the actual measurement points are more visible and show an overall decline of hardness with every layer, barring minor increases along the overwhelming trend. These minor spikes occur due to a small scale of measurement in  $\mu\text{m}$  range. Ultimately, this is the so-called sawtooth curve, which results from the decreased light intensity with layer height

Moreover, the dotted trendline decreases with progression towards the cross-section center. This effect can be explained with the post-curing treatment that increases global hardness. However, also the post curing intensity decreases with penetration depth, which results in the shown global decrease of indentation modulus. At some point the global indentation modulus trend remains relatively constant. This is due to post-UV-curing that does not penetrate the centre of the cube because of the high LA amount.

In contrast to a post-cured printed part, green parts did not show the global layer heterogeneity. Figure 63 presents the green compound with 0.12 wt% LA and shows continuous global layer behaviour. This confirms the assumption that post-curing leads to more controlled layer printing globally for slow curing compounds in L-AMT. Green parts showed global deviations from the trend in contrast to post-cured parts that showed continuous layer behaviour beyond the cure depth. All post-cured samples showed the same trend with a higher indentation modulus on the boundary and a lower, but global homogenous layer indentation modulus near the center of the cross-section. However, the local gradient within a  $100 \mu\text{m}$  layer was still apparent in all tested samples.

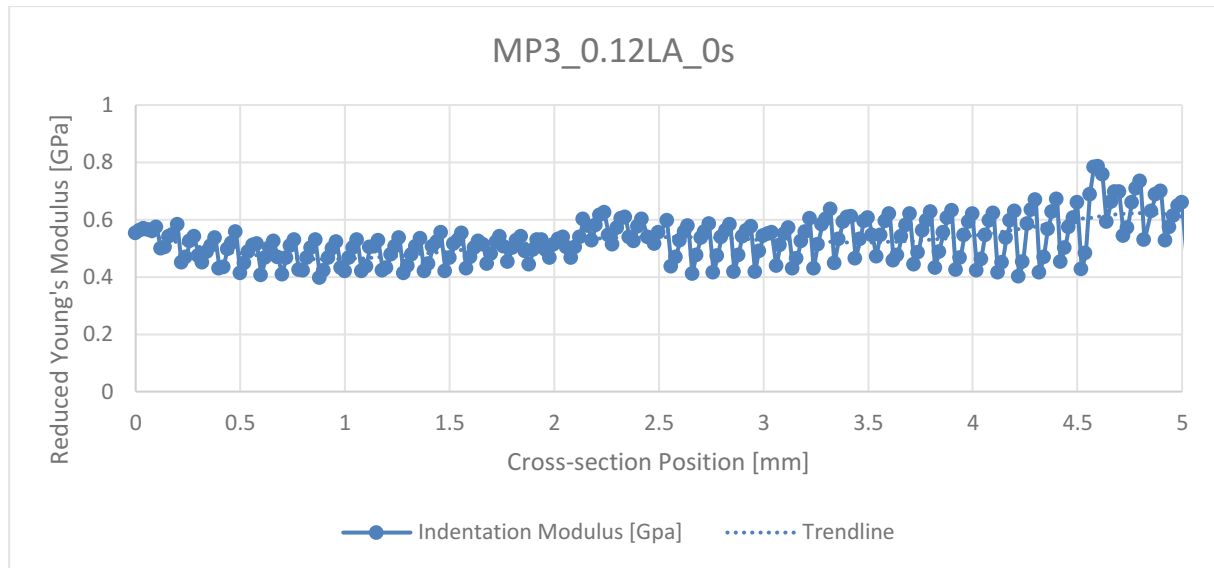


**Figure 63: Green part with global layer heterogeneity**

Finally, the values of  $E_r$  are derived from the average of all the measurement points and the average of the constant layer hardness that was not affected by LA post-curing in terms of hardening. This was mostly in 2/3 range of the overall cross-section position (between 3-5 mm from the starting point). The global hardness was, thus, slightly higher than the mean of the layer hardness beyond UV-light penetration depth. This did not apply to the green samples, however. Here, the trend was reversed because no post-curing was undertaken that could harden the boundary of the object. Conversely, the mean layer hardness slightly increased towards the center of the cross-section. Moreover, the layer hardness was notably lower in green samples, indicating the necessity of post-curing following 3D printing. As the light absorber protects the object from excessive light and over-polymerization it does not hinder the hardening, but is necessary for controlling the printing process.

### 6.2.3 Post-processing curing depth

To investigate the local trend of the indentation modulus, we analyzed the post-processing curing depth  $ppC_d$ . After a certain layer, specifically at 1.3 mm depth in the case of MP3\_0.012LA\_2x300s, the global layer behaviour remains relatively constant. The post-processing curing depth was determined by the intersection of the linear trendlines of boundary and central nanoindentation of the cross-section. Figure 64 illustrates how this intersection point was found exemplary for the sample MP3\_0.12LA\_2x300s. At this layer level, post-curing does not impact layer heterogeneity.

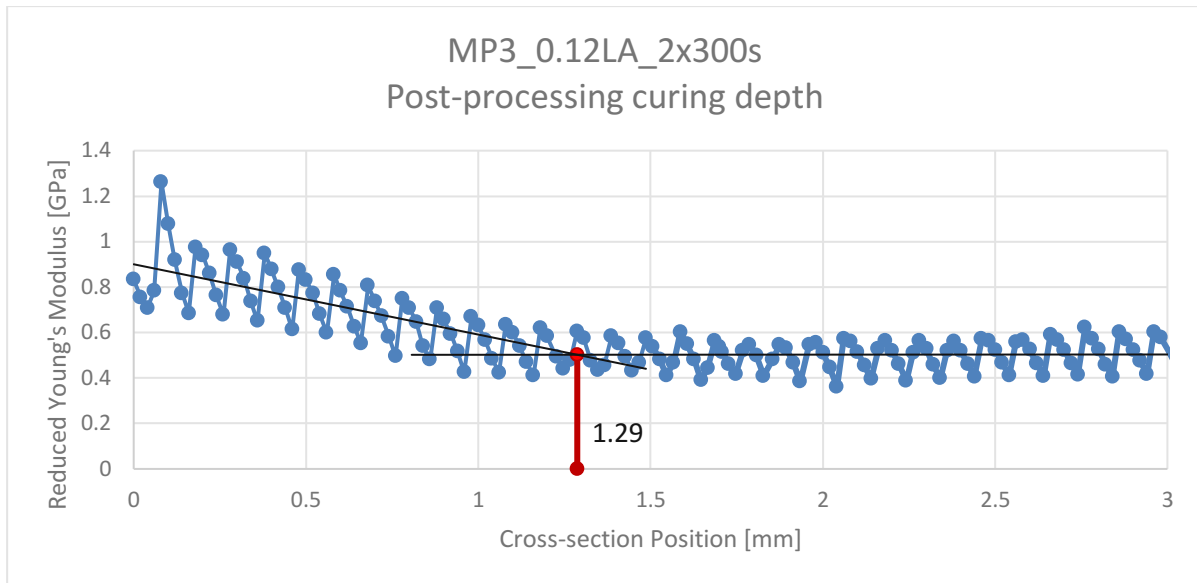


**Figure 64: Exemplary determination of post-processing curing depth**

This post-processing curing depth is affected by the post-curing duration and the LA wt%. Post-treatment finalizes residual cross-linking of the compound, but only increases hardness on the periphery. Interestingly, this correlates with the homogeneity observed on the periphery of the corresponding microscope sample. The post-processed cross-section visually showed more homogeneous and transparent areas on the boundary and darker and coarse areas in the center of the analysed cross-sections.

In Figure 65, the results of the analysis of post-processing curing depth are presented for some tested samples. Evidently, MP3\_0.04LA\_2x300s with LA wt% has a relatively high post-processing curing depth. As LA protects a compound from over-polymerization and excessive irradiance, lower levels of LA result in higher irradiation impact post-curing. It is clear from these results that LA impacts the post-processing curing depth considerably. This sample has more than a two-fold penetration depth compared to triple light absorber weight. Though the difference between 0.08 and 0.12 wt% can be discarded, as  $ppC_d$  stays relatively the same. Light absorber weight possibly has a threshold regarding its effect on  $ppC_d$ . Furthermore, Figure 65 shows that extended irradiation leads to a higher  $ppC_d$ , as compound MP3\_0.12LA\_2x300s triples MP3\_0.12LA\_2x100s in post-processing curing depth. Still elongated irradiation that exceeds 2x300s post-curing would be needed to determine  $ppC_d$  saturation for these vinyl ester-based formulations.

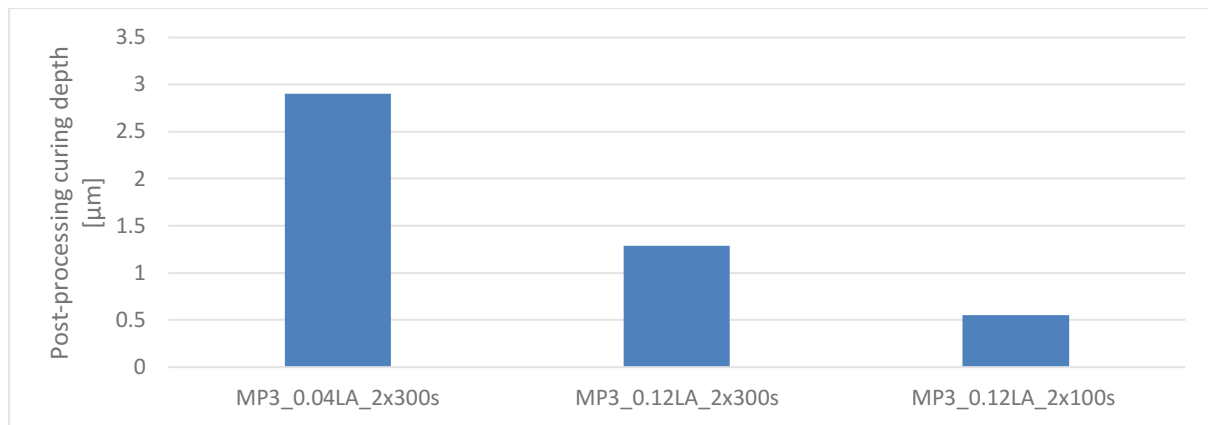


Figure 65: Post-processing curing depth of different samples

### 6.2.4 Local layer behaviour

As observed in previous results of nanoindentation, all parts have a local gradient within a printed layer. Unfortunately, the post-processing did not remove this gradient and homogenize the printed layers, which would considerably improve the quality and speed of the printing process of vinyl ester compounds in DLP L-AMT. To investigate this local heterogeneity further, we analyzed five periphery layers and five central layers for each tested part. Here we calculated the mean local gradient  $\Delta E_r$  and normalized this to exclude the effect of post-curing on the local gradient, as periphery layers have higher indentation modulus peaks.

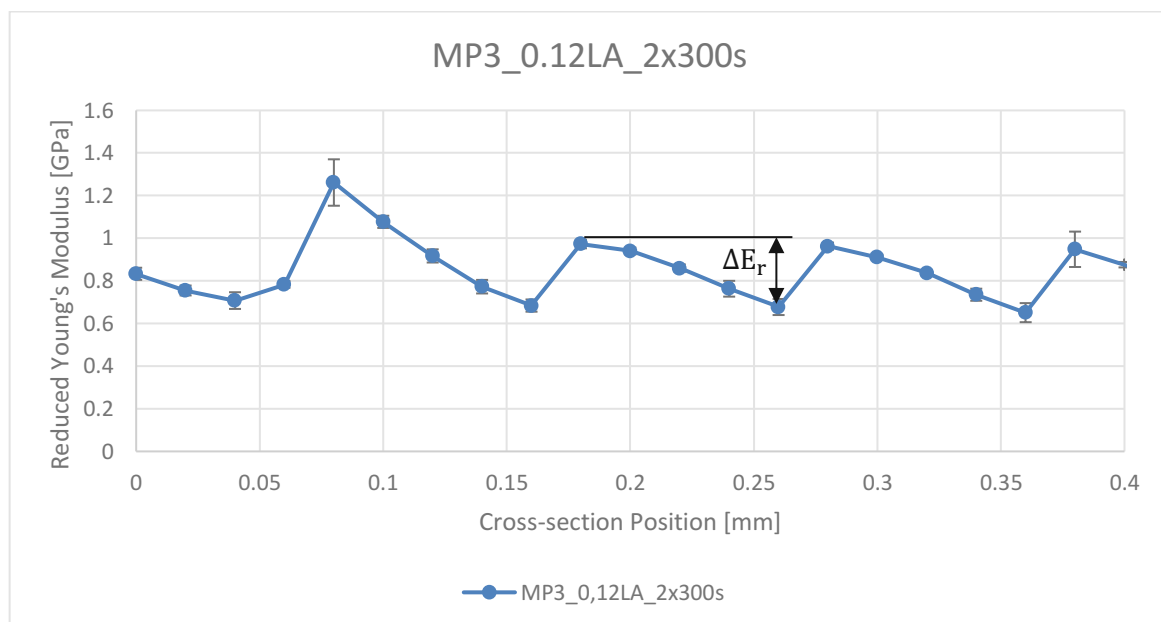
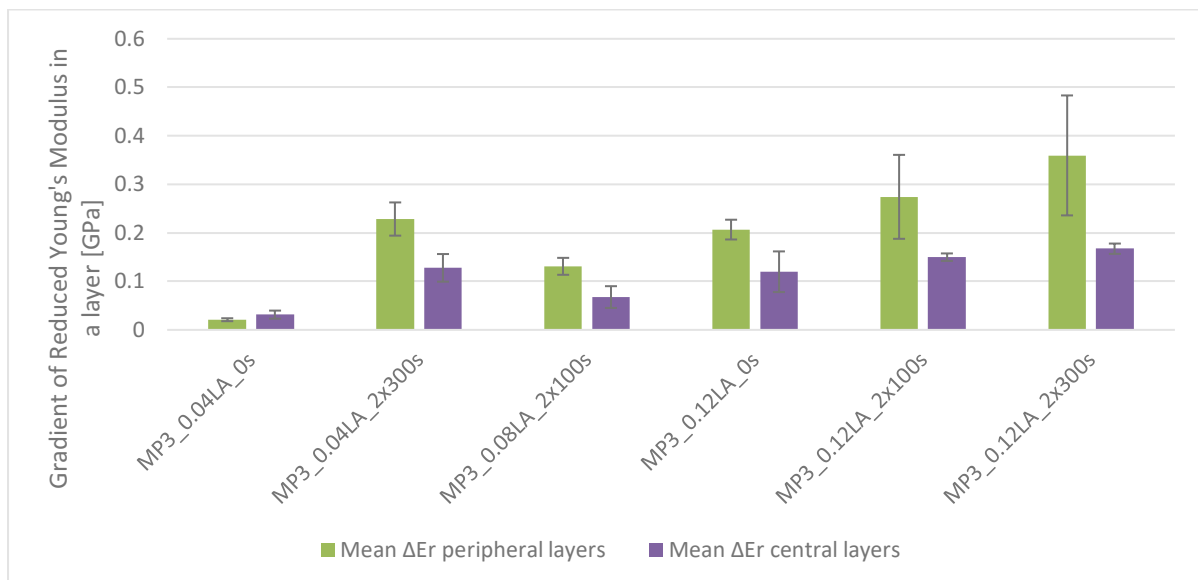


Figure 66: Detailed indentation curve over 4 layers with standard deviation

The compound MP3\_0.12LA\_2x300s and the corresponding layer heterogeneity for three different layers are depicted in Figure 66. The standard deviation of every measurement point is shown in this diagram, as every cross-section position was measured with three perpendicular points for statistical validation. The decreasing

global trendline is not visible in this representation, because of the small number of layers. Furthermore, the local gradient  $\Delta E_r$  is emphasized on the second depicted layer.

Moreover, the results for the local gradient analysis are presented in a bar diagram, in Figure 67. On the y-axis, the local gradient of reduced Young's modulus is shown in GPa, while the x-axis depicts the tested part. The local gradient increases with post-processing and higher LA wt%. The not post-cured samples show a more homogenous layer behaviour with considerable lower  $\Delta E_r$  than the other post-cured samples, which makes it more favourable in terms of printing. Regrettably, printed parts from vinyl ester resins have repeatedly shown to be impractical without post-processing due to inferior mechanical properties. Post-processing is necessary to cure residual resin in the compound. Furthermore, a considerable difference in indentation moduli between periphery and central layers can be observed. This deviation can be traced back to the residual cross-linking effect of post-curing that hardens periphery layers but unfortunately simultaneously increases the local gradient within a layer. As post-curing leads to an increase in global indentation modulus, the drop that occurs in a layer nearing the end of the 100  $\mu\text{m}$  is higher in absolute terms. This explains the considerably higher gradient that is seen in Figure 67 for all post-processed parts.



**Figure 67: Local gradient between peripheral & central layers**

Therefore, the absolute local gradient was normalized through dividing it by the mean indentation modulus of the respective layer. Statistical normalization refers to value adjustment that harmonizes measurement points to a common scale and exhibits values between 0 and 1. In this case:

$$\Delta E_{r_{n_i}} = \frac{\Delta E_{r_i}}{\bar{E}_{r_{m_i}}} \quad , \quad i = 1, \dots, n$$

Equation 14

$\Delta E_{r_{n_i}}$ ...normalized indentation modulus of particular layer [-]

$\Delta E_{r_i}$ ...indentation modulus of particular layer [GPa]

$\bar{E}_{r_{m_i}}$ ...mean indentation modulus of particular layer [GPa]

Consequently, the results of the mean normalized  $\Delta E_r$  are depicted in Figure 68. Evidently, the gradient bar of green MP3\_0.04LA\_0s is now in the same range with the other tested parts. The differences between the local gradient of the different samples are negligible and suggest that the light absorber wt% and post-curing do not harmonize the layer gradient locally. The vinyl ester compounds abide by the Beer-Lambert law and have too much transmittance for homogenous layer behaviour. Interestingly, the difference between the layers exposed to post-curing on the periphery and the ones beyond post-processing penetration depth is not visible with lower light absorber wt%. Decisively, the local gradient was visible in all samples even after post-curing, concluding that post-processing fails to reduce layer heterogeneities in terms of indentation moduli regardless of post-treatment schemes discussed in this study.

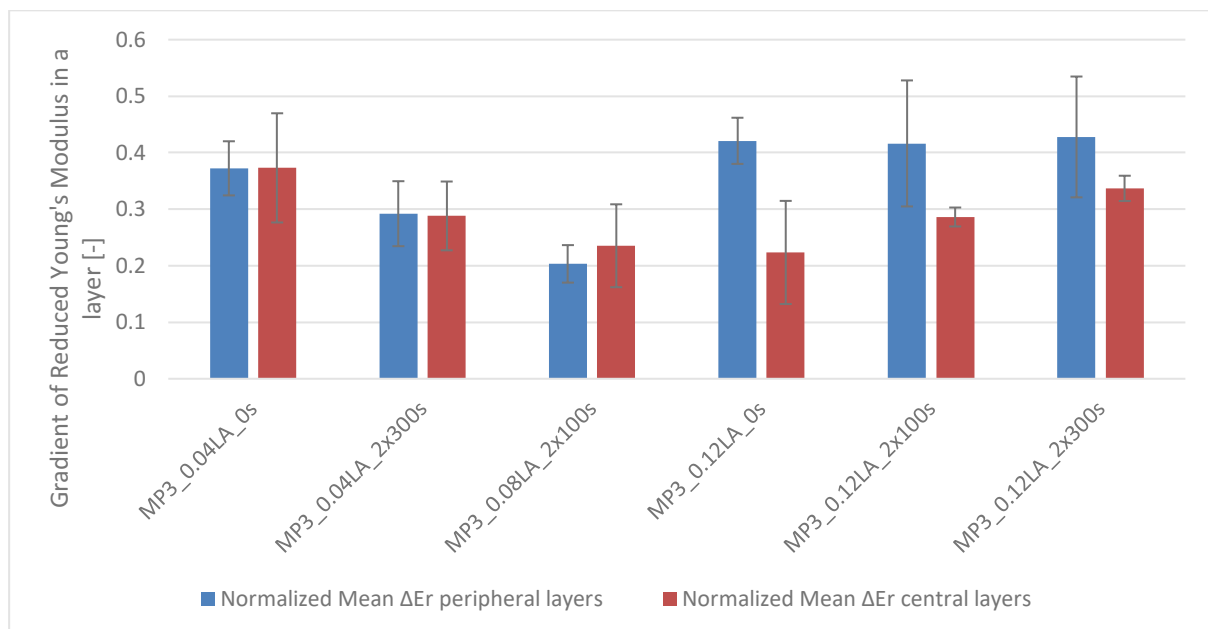
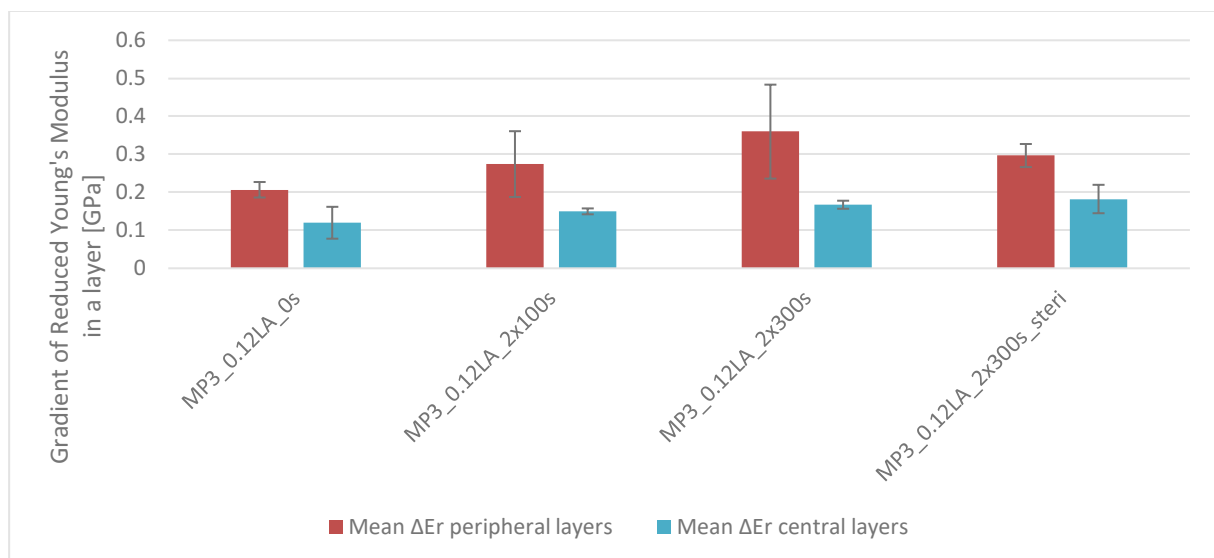


Figure 68: Normalized local gradient between peripheral & central layers

### 6.2.5 Sterilization effect on layer heterogeneity

The effect of  $\gamma$ -sterilization was expected to increase the post-processing curing depth along with the global and local layer homogenization. Unfortunately, this was not the

case as the layer behaviour showed very similar characteristics to the rest of the measured series. Figure 69 shows the layer gradient of the compound with 0.12 wt% and varying post-processing, while Figure 70 shows the normalized layer gradients accordingly. The left bars are indicating the peripheral, while the right bars are displaying central layer gradients for the respective compounds. The same general trend is observable that peripheral layers have a higher gradient compared to central ones, but show more global homogeneity after normalization. Moreover, the post-processing curing depth did not increase as expected. This might be due to oxygen inhibition after the part was embedded in resin, although the part surface was polished (approximately 100  $\mu\text{m}$  was removed) after sterilization again to reduce a possible oxygen inhibited zone. Thus, gamma radiation did not change the indentation modulus of the tested material. Possibly, the sterilization effect merely becomes evident deeper in the part or nanoindentation fails to display its effect. However, the sterilization did not have, or only minor the desired impact on layer homogeneity of the measured series.



**Figure 69: Sterilization effect on layer gradient**

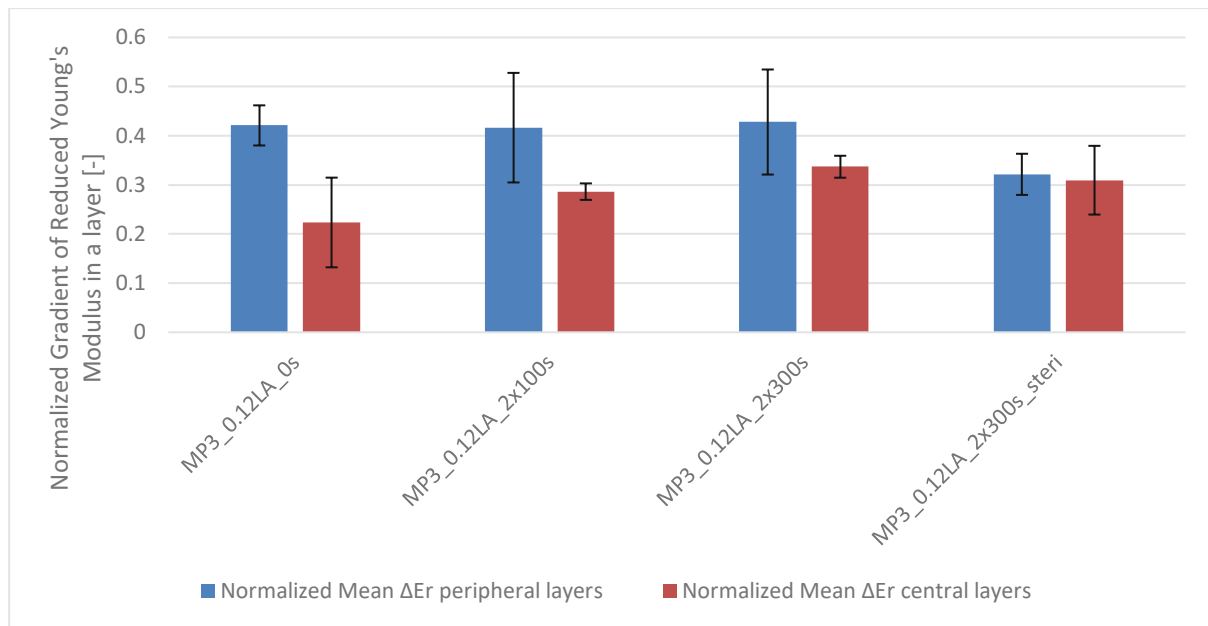


Figure 70: Sterilization effect on normalized layer gradient

## 6.3 Conclusions for results of material characterization

This study utilized nanoindentation as a novel characterization method of cross-sections to optimize the light absorber content and post-curing of vinyl ester compounds printed via DLP SLA. This was done by investigating the difference of a cross-section's indentation modulus.

The investigations were based on constant cure depth, which was evaluated with the Jacobs working curve. The Jacobs working curve is necessary to determine the right amount of exposure time for curing a defined height. The Jacobs working curve gives information about how much exposure a certain layer needs to cure, the critical exposure to material gelation and the penetration depth for a tested compound. It is a valuable tool and suitable to fully characterize highly crosslinked photopolymers with fast curing behavior. This behavior can be called a digital curing behavior and effectively has only two states: not crosslinked (fluid) and highly crosslinked (fully cured). (Hofstetter et al., 2018)

Unfortunately, the Jacobs working curve is insufficient to characterize photopolymers with decreased cure speed, where the polymer network and the resulting mechanical properties of the cured layer need more time to build up. Therefore, MP3\_LA photopolymer mixtures with different amounts of light absorber (0.04, 0.08 and 0.12 wt%) and photoinitiator (0.25 and 0.5 wt%) were investigated to analyze the differences of mechanical properties in the single layers and as well, after post curing.

The nanoindentation of printed cross-section samples showed the big heterogeneity of indentation modulus of cured layers, which strongly depends on the amount of light absorber. Furthermore, the global hardness distribution was found to show parabolic

behavior in post-cured resins. After post-curing in a UV oven, the hardness of post-cured material was higher on the periphery and constant in the center. This global deviation of the layers' reduced indentation modulus was improved by post-curing, but still showed a local gradient within the layers themselves. In contrast, green parts without post curing showed no global parabolic behavior, but also very low indentation modulus, leading to the conclusion that post-curing is necessary. Unfortunately, the local gradients were still traceable in all measured samples, which goes back to the vinyl esters slow curing speed. However, gamma sterilization performed not as expected on improving layer homogeneity, showing that different homogenizing technological processes should be investigated to improve printing quality for vinyl esters.

Moreover, the post-processing curing depth was decreased by more than half due to its protective effect against over-polymerization with higher light absorber weight in the vinyl ester-based compounds.

## 7 Conclusions

This chapter summarizes the results of this work and deduces the most important findings with a critical evaluation. The conclusions are split up and reiterate the findings discussed previously in the respective chapters.

### 7.1 Conclusions for material development of tough photopolymers

The development of tough vinyl ester based photopolymers showed that:

- Biocompatible and –degradable long-chain additives, like divinyl carbonate, considerably improve toughness of vinyl ester based compounds
- A bone scaffold was successfully printed, demonstrating the printability of the highly viscous resin via hot-lithography
- Heterogenic polymer network combining different molecular weights of divinyl carbonate indicates optimized mechanical properties leading to even tougher 3D printed material
- Gamma sterilization strengthens the biomaterial, while marginally reducing elongation at break and impact strength
- Vinyl ester based formulations are viable materials for biomedical application

#### 7.1.1 Limitations of approaches and results

The developed formulation of vinyl ester based bio-photopolymers show significant improvement in terms of mechanical properties. However, the impact strength of the developed resin does not align with the values of elongation at break that were measured, suggesting a necessary validation for this. Moreover, the sample size for tensile and Dynstat impact test was relatively small per batch to statistically validate the results, though a mean value and standard deviation was obtainable. Furthermore, the printability of the M3\_DVC formulation was showcased but the resolution of the bone scaffold must be improved in terms of full porosity and precision in order to function as biomaterial. This can be achieved by adjusting layer thickness and cure depth via Jacobs working curve and as well by improving the cleaning process of highly viscous resins.

#### 7.1.2 Outlook

The developed biomaterial shows great promise to function as a viable bone scaffold in terms of mechanical properties. A looming challenge will be to find balance between enhanced better double bond conversion and reactivity against inferior mechanical properties due to networks with less cross-linking. Furthermore, the immunogenicity of

the compound should be validated with the introduction of divinyl carbonate along with the degradation behavior of the compound before application. Moreover, the toughness of these resins can be optimized even further by additives and base matrix optimization based on vinyl esters. However, it must be said that several other factors affect the degradation behavior and mechanical properties of photopolymers upon implantation, too. These include crystallinity, molecular weight and distribution and double bond conversion, which should be determined for a complete material characterization.

Moreover, it would be interesting to conduct in vivo studies on animals to determine the applicability of the developed resin as the mechanical properties possibly deviate during environmental exposure. Eventually, when vinyl ester-based photopolymers are successfully printed with mechanical properties like PLA or other synthetic polymers and implanted in vivo for cell proliferation, it will be a revolution in bioengineering.

## 7.2 Conclusions for material characterization via nanoindentation

The characterization of materials via nanoindentation showed that:

- Combined with the Jacobs working curve, nanoindentation is a reliable information source, along with cure and penetration depth that describe the material
- Assumed layer heterogeneity was observable via nanoindentation and cannot be eliminated via post-curing
- High amount of light absorber in the compound is crucial at constant cure depth for good mechanical properties of green samples
- The low toughness of printed samples leads to cracks and scratches on the surface that hinder nanoindentation
- Post-processing curing depth into vinyl ester compounds is cut in half when the light absorber amount exceeds a threshold
- Gamma sterilization does not prevent hardness gradients within the layers

### 7.2.1 Limitations of approaches and results

Nanoindentation measurement of the cross-section has shown the effects of light absorber share and post-curing parameters. However, the nanoindentation does not enable a full characterization of the material with toughness, strength and rigidity also being important parameters for that. For further studies, a broader range of measurements including Dynstat impact strength and tensile test, as well as dynamic mechanical analysis is required.

## 7.2.2 Outlook

The nanoindentation of printed biomaterials verified the assumed layer heterogeneity of printed parts. However, the brittleness of the parts showed that the current formulation is not practical for implantation. Consequently, a material with higher toughness should be investigated for implementation. Optimizing the printing process of slow curing photopolymers could significantly decrease the printing time and increase homogeneity of the printed part. Longer irradiation times were needed to cure the desired layers, which would significantly extend processing time when bigger parts with more layers are built. Consequently, it should be considered to further increase the reactivity and double bond conversion of vinyl ester-based systems to reduce printing time. Hence other homogenizing treatments or additives should be investigated to develop a printable compound with homogenous layers.

## 8 References

- Awad, H. A., O'Keefe, R. J., Lee, C. H., & Mao, J. J. (2014). Chapter 83 - Bone Tissue Engineering: Clinical Challenges and Emergent Advances in Orthopedic and Craniofacial Surgery. In R. Lanza, R. Langer, & J. Vacanti (Eds.), *Principles of Tissue Engineering (Fourth Edition)* (pp. 1733–1743). Boston: Academic Press. <https://doi.org/10.1016/B978-0-12-398358-9.00083-5>
- Bak, D. (2003). Rapid prototyping or rapid production? 3D printing processes move industry towards the latter. *Assembly Automation*, 23(4), 340–345. <https://doi.org/10.1108/01445150310501190>
- Baudis, S. (2016). Knochen, Knorpel und Gefäße maßschneidern mit Licht. *Nachrichten Aus Der Chemie*, 64(4), 406–410.
- Bose, S., Roy, M., & Bandyopadhyay, A. (2012). Recent advances in bone tissue engineering scaffolds. *Trends in Biotechnology*, 30(10), 546–554.
- Daniels, A. U., Chang, M. K., Andriano, K. P., & Heller, J. (1990). Mechanical properties of biodegradable polymers and composites proposed for internal fixation of bone. *Journal of Applied Biomaterials*, 1(1), 57–78.
- Dwyer, J. R., & Smith, D. M. (2012). Deadly Rays from Clouds. *Scientific American*, 307, 54–59. <https://doi.org/10.1038/scientificamerican0812-54>
- Dzobo, K., Thomford, N. E., Senthebane, D. A., Shipanga, H., Rowe, A., Dandara, C., ... Motaung, K. S. C. M. (2018). Advances in Regenerative Medicine and Tissue Engineering: Innovation and Transformation of Medicine. *Stem Cells International*, 24. <https://doi.org/10.1155/2018/2495848>
- Fan, Y., Fan, Y., Li, Z., Loan, M., Lv, C., & Bo, Z. (2011). Optimal principle of bone structure. *PloS One*, 6(12), e28868.
- FDM vs SLA: Direct Comparison Guide. (2018). [WordPress]. Retrieved October 19, 2018, from <http://apm-designs.com/fdm-vs-sla-3d-printer-tech-comparison/>
- Feng, B., Jinkang, Z., Zhen, W., Jianxi, L., Jiang, C., Jian, L., ... Xin, D. (2011). The effect of pore size on tissue ingrowth and neovascularization in porous bioceramics of controlled architecture in vivo. *Biomedical Materials*, 6(1), 7–15.
- Fischer-Cripps, A. C. (2011). Nanoindentation Testing. In A. C. Fischer-Cripps, *Nanoindentation* (pp. 21–37). New York, NY: Springer New York. [https://doi.org/10.1007/978-1-4419-9872-9\\_2](https://doi.org/10.1007/978-1-4419-9872-9_2)
- Garlotta, D. (2001). A literature review of poly (lactic acid). *Journal of Polymers and the Environment*, 9(2), 63–84.

- Gebhardt, A., & Hötter, J. S. (2016). *Additive Manufacturing - 3D Printing for Prototyping and Manufacturing*. Munich: Hanser Publishers.
- Gibson, I., Rosen, D. W., & Stucker, B. (2010). *Additive manufacturing technologies: rapid prototyping to direct digital manufacturing*. London ; New York: Springer.
- Heller, C., Schwentenwein, M., Varga, F., Liska, R., & Stampfl, J. (2009). Biocompatible and biodegradable photopolymers for microstereolithography. In *LAMP2009* (p. 5). Kobe.
- Hess, M. (2018). *Dynamic-Mechanical and calorimetric properties of polymers*. Presented at the Polychar 22 - short course. Retrieved from <https://slideplayer.com/slide/7649534/>
- Hofstetter, C., Orman, S., Baudis, S., & Stampfl, J. (2018). Combining cure depth and cure degree, a new way to fully characterize novel photopolymers. *Additive Manufacturing*, 24, 166–172.
- Jacobs, P. F. (1992). Fundamentals of stereolithography. In *1992 International Solid Freeform Fabrication Symposium* (pp. 196–211). Valencia, California.
- Kawamura, N., Kugimiya, F., Oshima, Y., Ohba, S., Ikeda, T., Saito, T., ... Hoshi, K. (2007). Akt1 in osteoblasts and osteoclasts controls bone remodeling. *PLoS One*, 2(10), 10–58.
- Ladani, L., Harvey, E., Choudhury, S. F., & Taylor, C. R. (2013). Effect of varying test parameters on elastic–plastic properties extracted by nanoindentation tests. *Experimental Mechanics*, 53(8), 1299–1309.
- Lee, J., Aksay, I., & Prud'homme, R. (2001). Cure depth in photopolymerization: Experiments and theory. *Materials Research Society*, 16(12), 3536–3544.
- Leonhardt, S., Klare, M., Scheer, M., Fischer, T., Cordes, B., & Eblenkamp, M. (2016). Biocompatibility of photopolymers for additive manufacturing. *Current Directions in Biomedical Engineering*, 2(1), 113–116. <https://doi.org/10.1515/cdbme-2016-0028>
- Martin, J. M. (2012). Understanding Gamma Sterilisation. *Pharmaceutical Technology Europe*, 24(2), 3.
- Mautner, A., Steinbauer, B., Orman, S., Russmüller, G., Macfelda, K., Koch, T., ... Liska, R. (2016). Tough Photopolymers Based on Vinyl Esters for Biomedical Applications. *Journal of Polymer Science*, (54), 1987–1997.
- Mautner, A., Steinbauer, B., Russmüller, G., Lieber, R., Koch, T., Stampfl, J., & Liska, R. (2016). Vinyl carbonate photopolymers with improved mechanical properties

- for biomedical applications. *Designed Monomers and Polymers*, 19(5), 437–444. <https://doi.org/10.1080/15685551.2016.1169378>
- Merck, Kg. (2018). Trimethylolpropane tris(3-mercaptopropionate) [Company Page]. Retrieved October 19, 2018, from <https://www.sigmaaldrich.com/catalog/product/aldrich/381489?lang=de&region=AT>
- Mueller, H., & Oluschinski, A. (2018). Impact test and notched impact test. Retrieved October 19, 2018, from <https://www.polymerservice-merseburg.de/en/plastics-testing/mechanical-tests/impact-testing/schlagbiegeversuch-und-kerbschlagbiegeversuch.html>
- Murphy, C. M., Haugh, M. G., & O'Brien, F. J. (2010). The effect of mean pore size on cell attachment, proliferation and migration in collagen–glycosaminoglycan scaffolds for bone tissue engineering. *Biomaterials*, 31(3), 461–466.
- National Center for Biotechnology Information. (2018). *Pyrogallol*. US Department of Health & Human Services. Retrieved from <https://pubchem.ncbi.nlm.nih.gov/compound/pyrogallol#section=Top>
- Nguyen, N. T. (2012). A Conductivity Testing System Coupled with a Tensile Testing Machine to Measure the Surface Properties of Polymer Specimens, 134.
- Orman, S. (2015). *Biodegradable Polymers for 3D print* (Master thesis). Vienna University of Technology, Vienna.
- Orman, S. (2018). *Toughening of Photopolymers for Additive Manufacturing of Bone Replacements* (PhD thesis). Vienna University of Technology, Vienna.
- Palermo, E. (2013a). Fused Deposition Modeling: Most Common 3D Printing Method. Retrieved October 18, 2018, from <https://www.livescience.com/39810-fused-deposition-modeling.html>
- Palermo, E. (2013b). What is Selective Laser Sintering? Retrieved October 18, 2018, from <https://www.livescience.com/38862-selective-laser-sintering.html>
- Palermo, E. (2013c). What is Stereolithography? Retrieved October 18, 2018, from <https://www.livescience.com/38190-stereolithography.html>
- Pina, S., Oliveira, J. M., & Reis, R. L. (2015). Natural-based nanocomposites for bone tissue engineering and regenerative medicine: A review. *Advanced Materials*, 27(7), 1143–1169.

- Raghunath, J., Rollo, J., Sales, K. M., Butler, P. E., & Seifalian, A. M. (2007). Biomaterials and scaffold design: key to tissue-engineering cartilage. *Biotechnology and Applied Biochemistry*, 46(2), 73–84.
- Raposo-Amaral, C. E., Bueno, D. F., Almeida, A. B., Jorgetti, V., Costa, C. C., Gouveia, C. H., ... Alonso, N. (2014). Is bone transplantation the gold standard for repair of alveolar bone defects? *Journal of Tissue Engineering*, 5, 2041731413519352.
- Redl, M. (2016). *Biokompatible Photopolymere auf Basis neuer Vinylester* (Bachelor thesis). Vienna University of Technology, Vienna.
- Rowe, J. W., Fried, L., Jackson, J., Novelli, W., & Stone, R. (2016). A Vital Direction for Health and Health Care. *DISCUSSION PAPER*, 9.
- Saint-Denis, M. (2018). What is gamma ray sterilisation? [Buerkle homepage]. Retrieved October 19, 2018, from <https://www.buerkle.de/en/knowhow/gamma-ray-sterilisation>
- Salgado, A. J., Coutinho, O. P., & Reis, R. L. (2004). Bone tissue engineering: state of the art and future trends. *Macromolecular Bioscience*, 4(8), 743–765.
- Schnürer, S. M., Gopp, U., Kühn, K. D., & Breusch, S. J. (2003). Bone substitutes. *Der Orthopade*, 32(1), 2–10.
- Sheikh, Z., Najeeb, S., Khurshid, Z., Verma, V., Rashid, H., & Glogauer, M. (2015). Biodegradable Materials for Bone Repair and Tissue Engineering Applications. *Materials*, 8(9), 5744–5794. <https://doi.org/10.3390/ma8095273>
- Stampfl, J., & Degischer, H. P. (2010). *Grundlagen der Werkstoffwissenschaft Vorlesungsskriptum*. TU Wien.
- University of New South Wales. (2013). Charpy Impact test [University homepage]. Retrieved October 19, 2018, from <http://www.materials.unsw.edu.au/tutorials/online-tutorials/1-charpy-impact-test>
- Uvitron International Inc. (2018). INTELLIRAY 400 / 600 UV Flood Curing System | PN: UV0338 / UV0832. Uvitron International Inc. Retrieved from <https://www.uvitron.com/pdf/brochures/brochure-floods-intelliray.pdf>
- Vallet-Regí, M., Colilla, M., & González, B. (2011). Medical applications of organic–inorganic hybrid materials within the field of silica-based bioceramics. *Chemical Society Reviews*, 40(2), 596–607.

- Van de Velde, K., & Kiekens, P. (2002). Biopolymers: overview of several properties and consequences on their applications. *Polymer Testing*, 21(4), 433–442. [https://doi.org/10.1016/S0142-9418\(01\)00107-6](https://doi.org/10.1016/S0142-9418(01)00107-6)
- Varotsis, A. (2016). 3D Hubs [Wiki]. Retrieved October 18, 2018, from <https://www.3dhubs.com/knowledge-base/introduction-sla-3d-printing#author>
- Wang, L., Gramlich, W. M., & Gardner, D. J. (2017). Improving the impact strength of Poly(lactic acid) (PLA) in fused layer modeling (FLM). *Polymer*, 114, 242–248. <https://doi.org/10.1016/j.polymer.2017.03.011>
- Watts, D. C. (1984). Characteristics of visible-light-activated composite systems. *Br Dent J*, 156, 209–215.
- Willems, N., Everts, V., Langenbach, G., & Zentner, A. (2013). (PDF) The microstructural and biomechanical development of the condylar bone: A review [Wiki]. <http://dx.doi.org/10.1093/ejo/cjt093>
- Wu, S. (1992). Secondary relaxation, brittle–ductile transition temperature, and chain structure. *Journal of Applied Polymer Science*, 46(4), 619–624.
- Xu, Y., Imamura, M., & Nakagawa, T. (1997a). MICRO-HARDNESS MEASUREMENT OF PHOTOPOLYMER IN STEREOLITHOGRAPHY. *Journal of Photopolymer Science and Technology*, 10(2), 181–186.
- Xu, Y., Imamura, M., & Nakagawa, T. (1997b). Micro-hardness measurement of photopolymer in stereolithography. *Journal of Photopolymer Science and Technology*, 10(2), 181–186.
- Yalcin, D. (2017). Effect of Specimen Geometry on Tensile Testing Results [Brochure]. Retrieved October 19, 2018, from <https://www.admet.com/effect-specimen-geometry-tensile-testing-results/>

## 9 Table of Figures

Figure 1: Criteria for material in bone tissue engineering.....	2
Figure 2: Ideal degradation time of a scaffold in relation to regenerative tissue (Raghunath, Rollo, Sales, Butler, & Seifalian, 2007).....	10
Figure 3: Chemical structures of biocompatible and -degradable polymers.....	11
Figure 4: Cortical and cancellous bone in human femur (Willems, Everts, Langenbach, & Zentner, 2013).....	13
Figure 5: Types of transplants.....	15
Figure 6: Pillars of tissue engineering.....	16
Figure 7: Schematic process of bone tissue engineering (Redl, 2016).....	17
Figure 8: Principle of layer technology (Gebhardt & Hötter, 2016).....	18
Figure 9: Schematic process.....	18
Figure 10: Selection of AMTs.....	19
Figure 11: FDM vs. SLA (“FDM vs SLA: Direct Comparison Guide,” 2018).....	20
Figure 12: Schematic principle of SLA printer (Varotsis, 2016).....	21
Figure 13: Schematic principle of SLS (Palermo, 2013b).....	22
Figure 14: Materials paradigm.....	23
Figure 15: Schematic photo-polymerization process.....	25
Figure 16: Molecular structure of SL monomers (Orman, 2015).....	26
Figure 17: Free-radical polymerization process.....	27
Figure 18: Divinyl carbonate structural formula (Orman, 2018).....	29
Figure 19: Divinyl Adipate structural formula (Orman, 2018).....	30
Figure 20: Glycerol modified with DVA (Orman, 2018).....	30
Figure 21: Pyrogallol® (National Center for Biotechnology Information, 2018).....	30
Figure 22: TMPMP (Merck, 2018).....	31
Figure 23: Quinoline Yellow (Orman, 2018).....	31
Figure 24: Chemical structure of Ivocerin® (Orman, 2018).....	32
Figure 25: Structural formula for 10MV (Orman, 2018).....	32
Figure 26: Working principle of DLP (Baudis, 2016).....	33
Figure 27: Sterilisation methods and materials (Saint-Denis, 2018).....	34
Figure 28: Schematic tensile test (Nguyen, 2012).....	34
Figure 29: Shape of a ductile specimen during tensile testing (Yalcin, 2017).....	35
Figure 30: 3-point-bend setup.....	36

Figure 31: Stress and strain during DMA (Hess, 2018).....	37
Figure 32: Typical DMA result showing E' (green), E'' (blue) and tan $\delta$ (red) under temperature progression .....	38
Figure 33: Dynstat configuration for impact test (Mueller & Oluschinski, 2018) .....	39
Figure 34: Schematic impact test (University of New South Wales, 2013) .....	39
Figure 35: Schematic nanoindentation test process.....	40
Figure 36: a) load/displacement-curve; b) conforming indentation phase (Ladani, Harvey, Choudhury, & Taylor, 2013).....	41
Figure 37: Typical stress/strain-curves for duroplasts (green), thermoplasts (orange & red) and elastomers (blue) (Wu, 1992) .....	43
Figure 38: DMA results for examination of molecular mass and amount of the carbonate additive.....	46
Figure 39: Tensile test results for examination of molecular mass of the carbonate additive .....	47
Figure 40: Impact test results for examination of molecular mass of the carbonate additive .....	47
Figure 41: Tensile strength from factorial experiment .....	50
Figure 42: Elongation at break from factorial experiment.....	51
Figure 43: Young's modulus from factorial experiment .....	52
Figure 44: Benchmark and developed material – Tensile Strength .....	54
Figure 45: Benchmark and developed material - Elongation at Break .....	54
Figure 46: Benchmark and developed material - T <sub>g</sub> & E' 37 °C.....	54
Figure 47: Benchmark and developed material - Impact Strength.....	55
Figure 48: Tensile strength development.....	58
Figure 49: Elongation at break development.....	58
Figure 50: T <sub>g</sub> and Storage Modulus development.....	58
Figure 51: Impact strength development .....	59
Figure 52: Scaffold printed from M3_DVC80_6.....	60
Figure 53: Typical Jacobs working curve (Hofstetter et al., 2018) .....	65
Figure 54: Cure depth of MP3_LA with 0,5wt% Ivocerin® .....	65
Figure 55: High polymerization of photopolymers without light absorber component	67
Figure 56: CAD model for printing process.....	67
Figure 57: Schematic preparation process for layer hardness examination.....	68
Figure 58: Embedded and polished sample .....	70

Figure 59: Peripheral homogeneity of UV-induced photopolymers; example: MP3\_0.12LA\_2x300s .....71

Figure 60: Schematic view of measurement process & expected Er behaviour over cross-section.....72

Figure 61: Cross-section hardness over layers .....73

Figure 62: Detailed indentation curve over 10 layers .....75

Figure 63: Green part with global layer heterogeneity.....76

Figure 64: Exemplary determination of post-processing curing depth.....77

Figure 65: Post-processing curing depth of different samples .....78

Figure 66: Detailed indentation curve over 4 layers with standard deviation .....78

Figure 67: Local gradient between peripheral & central layers .....79

Figure 68: Normalized local gradient between peripheral & central layers .....80

Figure 69: Sterilization effect on layer gradient .....81

Figure 70: Sterilization effect on normalized layer gradient .....82

## 10 List of Tables

Table 1: Natural bone tissue compared to other degradable and non-degradable materials and their application (Sheikh et al., 2015).....	7
Table 2: Sample of characteristic values of materials .....	24
Table 3: Utilized parameter set for tensile testing .....	36
Table 4: Utilized parameter set for DMA .....	38
Table 5: Utilized parameter set for nanoindentation .....	42
Table 6: Chemical composition of M3_DVC .....	44
Table 7: Chemical composition of M3_DVC .....	45
Table 8: Full factorial design for base matrix .....	48
Table 9: Resulting wt% of Divinyl Adipate, Vinyl decanate and Divinyl carbonate from FFD.....	49
Table 10: Mechanical properties of M3_TS_DVC80_6 .....	53
Table 11: Mechanical properties of the sterilized, toughened compound.....	56
Table 12: Compound composition of MP3_LA .....	63
Table 13: Dilution method via cross-over rule for LA-wt% .....	63
Table 14: Exposure duration and penetration depth for Cd = 200 $\mu\text{m}$ .....	66
Table 15: Program for grinding and polishing cross-section; DP-P: DP-Suspension P is a very high performing diamond product containing exclusively polycrystalline diamonds.....	69

# 11 List of Equations

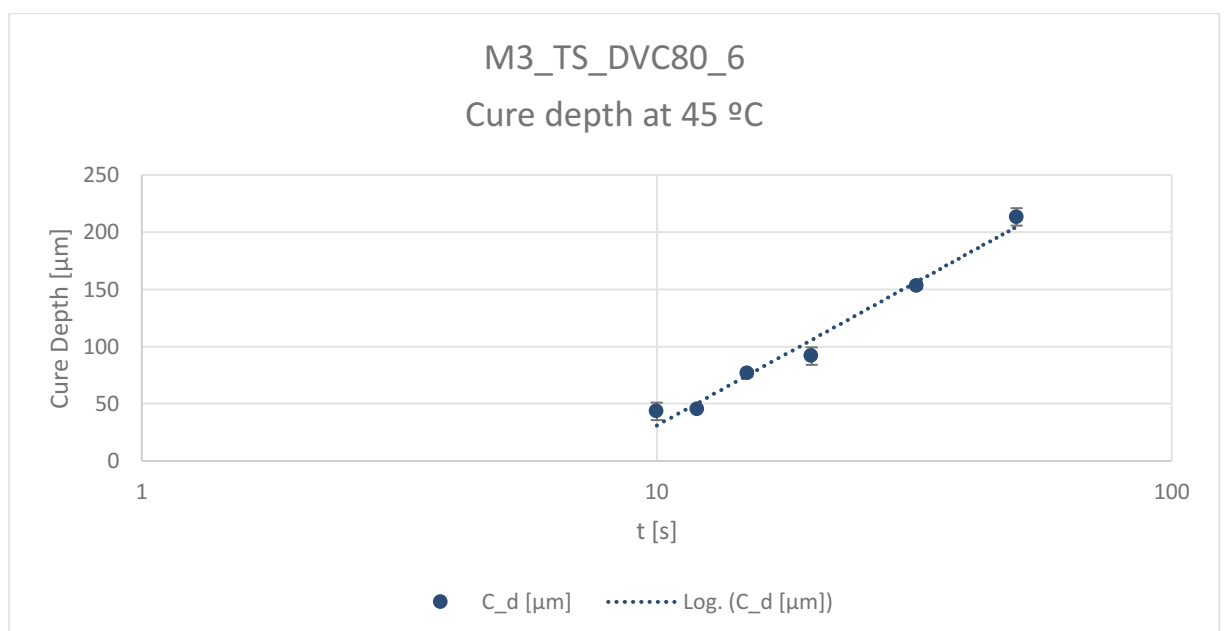
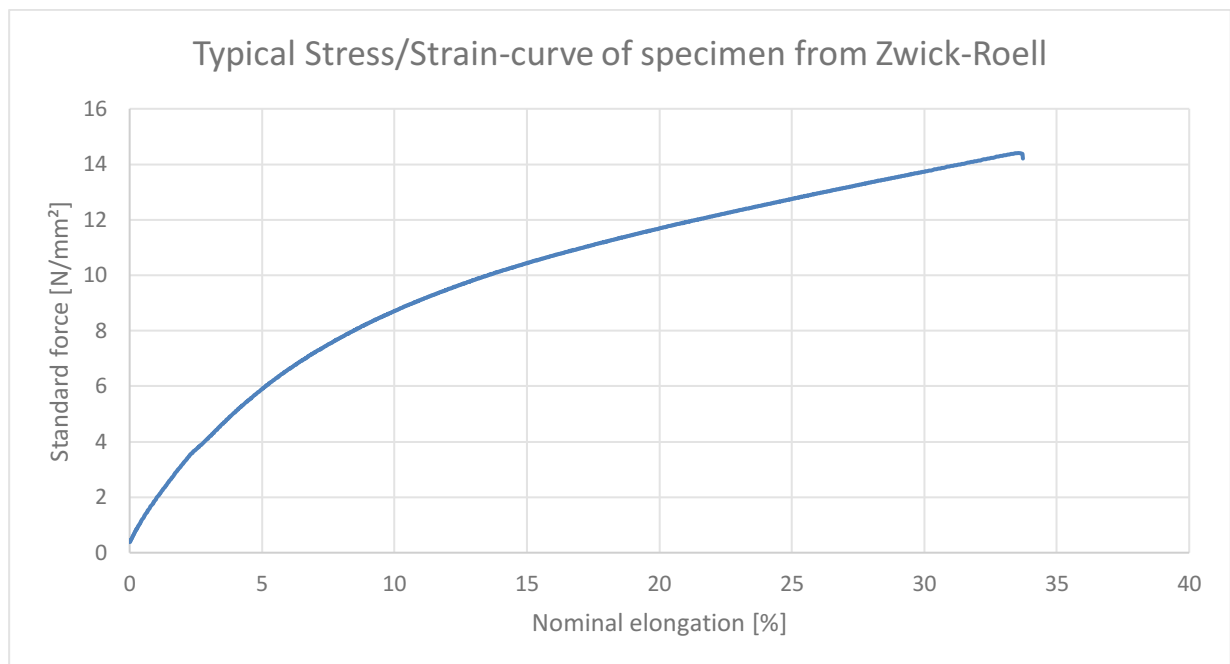
Equation 1 .....	35
Equation 2 .....	35
Equation 3 .....	36
Equation 4 .....	37
Equation 5 .....	37
Equation 6 .....	37
Equation 7 .....	37
Equation 8 .....	38
Equation 9 .....	41
Equation 10 .....	41
Equation 11 .....	41
Equation 12 .....	64
Equation 13 .....	74
Equation 14 .....	80

Die approbierte gedruckte Originalversion dieser Diplomarbeit ist an der TU Wien Bibliothek verfügbar  
The approved original version of this thesis is available in print at TU Wien Bibliothek.

## 12 Appendix

This chapter encloses data and diagrams that are supplementary to the achieved results in this study. It is presented without further explanation and is to be understood in its associated chapter.

### 12.1 Appendix for material development of tough photopolymers



## 12.2 Appendix for material characterization

